MACROLAMINATE PARTICLE COMPOSITE MATERIAL DEVELOPMENT

May 1965

Prepared Under U. S. Navy Bureau of Weapons
Contract NOw 64-0194-f

Summary Report

1 April 1964 to 1 May 1965

THE BOEING COMPANY
Aero-Space Division

MACROLAMINATE PARTICLE COMPOSITE MATERIAL DEVELOPMENT

May 1965

Prepared Under U. S. Navy Bureau of Weapons
Contract NOw 64-0194-f

Summary Report

1 April 1964 to 1 May 1965

Authors: F. H. Simpson
L. M. Stejskal

THE BOEING COMPANY
Aero-Space Division
P. O. Box 3707
Seattle, Washington 98124

ABSTRACT

A study has been made of the effect of particle geometry, forming methods, sintering and metal-to-ceramic ratio on the strength, ductility and oxidation resistance of a refractory laminate particle composite material, 93.1 HfO_2 · 4.9 CeO_2 · 2 MgO-Mo.

Knife coating techniques were developed capable of producing laminates having individual metal and ceramic layer thicknesses of from 20 to 25 microns. Experimental results indicate thinner layers would be desirable. Cutting and sizing techniques were developed to produce different sizes and shapes of laminate particles. Highest flexural strength was achieved from elongated particles and smaller particles produced higher strength than larger particles. There were indications that ductility increases with increasing laminate particle size. Oxidation resistance and ductility are more subject to variation due to impurities than to particle geometry.

Flexural strength was found to increase at a decreasing rate with metal content; while ductility increased at an increasing rate. Compressive strength and oxidation resistance both increased at increasing rates with increasing ceramic content.

Isostatic pressing produces very random orientation of laminae. Warm pressing in steel dies produces some orientation while hot pressing produces the highest degree of orientation. Warm extrusion was found to orient laminae at the exterior of specimens with the direction of extrusion and to reduce the laminate particle size by shear during reduction of the cross section. Orientation of laminae parallel to the direction of tensile stress increased flexural strength.

Atmosphere, temperature, time at temperature and heating and cooling rates were evaluated. Differential shrinkage between the metal and ceramic phases was found to be critical. When the ceramic shrinks more than the metal during sintering, microcracks occur in the ceramic phase reducing its tensile strength. Greater shrinkage in the metal phase places the ceramic in compression increasing the flexural strength of the composite. Two to four percent difference in shrinkage appears to be optimum; at higher difference the increased stress reduces strength. Heating rate is critical, as is surface activity and particle packing during forming.

CONTENTS

ILLUSTRATIONS

TABLES

I. INTRODUCTION

A. Background

W. J. Knapp [1] and F. R. Shanley developed the concept of a ductile metal-ceramic composite system made from randomly oriented particles consisting of alternate thin layers of a ductile metal phase and a brittle ceramic phase. Their schematic representation of this system is shown in Figure 1. Slip resulting from loading parallel with or normal to the laminate cannot occur, as shown in Figure 1a. Figure 1b shows the type of loading expected to produce slip. Accordingly, random distribution of the laminate particles can produce slip and a limited amount of plastic deformation.

Using the above concept, the following method has been used by this contractor to fabricate test specimens of a number of refractory metal and ceramic compositions. Metal and ceramic powders are suspended in a solvent with an organic binder to form paints. These paints are applied to a backing sheet in alternate layers to build up a laminate. The laminate is stripped from the backing sheet, cut and screened to form macrolaminate particles. These particles are then compacted and sintered by powder metallurgy techniques to form a finished part or a blank from which a finished part can be ground. Figure 1 also shows a polished section of a composite system made by this process.

B. Objectives

The ultimate objective of this program is to develop macrolaminate particle composite materials which have sufficient tensile ductility and strength to permit their use in structural members operating in an oxidizing environment at temperatures in excess of 2000°F.

This program was established to investigate the effects of particle geometry, forming method and sintering on the strength, ductility and oxidation resistance of a refractory-metal-based composite material. The information obtained will then be used to point out the significance of different variables and to direct future work in the development of macrolaminate particle composites.

1 U.S. Patent No. 3,089,796 - May 1963 "Process for Making Laminated Materials"

II MATERIAL SYSTEM

Preliminary work by this contractor on the development of refractory metal based macrolaminate composites for use above 3000°F under entry conditions indicated greatest promise in a composition $HfO_2 \cdot 5CeO_2$ -Mo. When exposed to temperatures of 4000°F for 30 minutes, this material developed an oxide surface coating to a depth of approximately .03 inches. The molybdenum volatilized from the surface leaving the oxide slag coating. This composite demonstrated excellent resistance to thermal shock and fair mechanical properties. Columbium and tantalum based systems which had been evaluated underwent catastrophic oxidation in less than 5 minutes at temperatures as low as 2000°F. Interest was expressed in attempting to modify the $HfO_2 \cdot 5\ CeO_2$ -Mo composites to enable formation of a protective slag type coating at temperatures of 2500°F and below. Initial compositional work was done in the ceramic phase to provide oxides which might be fluxed by oxides of molybdenum to form a surface coating. Additions of SiO_2 and alkaline earth metal oxides were found to improve oxidation resistance of the composite below 2500°F, but also reduced strength especially at elevated temperatures.

At the initiation of this contract, the 93.1 $HfO_2 \cdot 4.9\ CeO_2 \cdot 2$ MgO-Mo composition, which had the best compromise of oxidation resistance at 2500°F and strength, was selected for use in this study.

The properties of this composite containing 52 parts metal and 48 parts ceramic by weight made by a preliminary process are given in Table I. It was recognized that this was not an optimum material system and that additional compositional work would be needed. However, to aid in the ultimate development of the macrolaminate particle composite system, it was necessary to determine if the particle geometry is a significant factor, how macrolaminate composites can be fabricated, and what degree of improvement can be realized.

Table II lists the constituent materials used for this study.

III MACROLAMINATE PARTICLE GEOMETRY STUDY

The geometry study was to determine the mechanisms and effect of size, size distribution and shape of the laminate particles on the properties of the composite.

A. Evaluation of Layer Thickness

Prior to evaluating the effect of particle geometry, it was necessary to develop techniques for producing laminate sheets of alternate layers of metal and ceramic with controlled layer thicknesses. Three processes were evaluated; roll coating, silk screening and knife coating. Paints pigmented with the separate phases were developed to a degree adequate for producing laminate sheets by each technique. Paint formulations used for each type are shown in Table III.

The ceramic phase, 93.1 HfO_2 · 4.9 CeO_2 · 2 MgO was prepared as a painting pigment for this study as follows:

Hafnia and ceria are dry blended and heated in a zirconia crucible at 2700°F for 24 hours. This material is then crushed to pass a 65 mesh screen and ground to a powder in an air attrition mill (Trost Model Gem T-X). The material as ground is capable of producing paint films of uniform thicknesses below .0005 inch as indicated by a Hagman Gage. The magnesium oxide is added with the organic binder and solvents to the 95 Hafnia · 5 Ceria powder and mixed by ball milling to form the paint.

This method evolved from a previous compositional study in which additives were being investigated for use with a 95 HfO_2 · 5 CeO_2 ceramic phase. Other methods of preparation were investigated in the sintering study and are reported in that section.

The molybdenum was obtained from the Wah Chang Corporation purchased as screened through 325 mesh. It is described as 99.8 percent pure and is prepared by a hydrogen reduction process. Chemical analysis of the molybdenum and hafnia powders used are given in Table IV.

Roll coating was the least complicated of the three methods evaluated for preparing larger quantities of laminate sheets at a minimum cost, but it lacks mechanical control. Layer thickness was found to increase with successive layers, apparently due to the solvent being absorbed by the underlying material causing the paint to thicken, inhibiting its flow. This method was used at the start of the program to prepare a large quantity of laminate particles that were used for the forming and sintering studies conducted concurrently with the particle geometry study. In evaluating the microstructure of sintered specimens considerable mixing of phases was present. This was attributed to the rollers picking up pigment from the surface being painted and transferring it to the new layer as well as to the paint reservoir. Because of the lack of control and mixing of phases, this method of producing laminates was eliminated.

Swiss silk 200 x 200 mesh and stainless steel screens 200 x 200, 165 x 165 and 105 x 105 mesh were evaluated as screening materials through which pastes pigmented with molybdenum and the hafnia based ceramic could be passed alternately to provide uniform layers. Larger particles of the metal, as agglomerates, were retained on both the 200 x 200 and the 165 x 165 mesh screens; while small particles with excess organic material were pressed through the screen. This resulted in layers with average thicknesses of .0012 - .0015 inch, but with considerable variation in thickness within the layers due to lack of coverage by the pigment and excess binder in voids. The 105 x 105 mesh steel screen had openings large enough so that all the material passed through. Single layer thicknesses of .0018 to .0023 inch and

.0019 to .0025 inch, respectively, were obtained from the molybdenum and hafnia pastes. A laminate containing ten alternate layers varied in thickness from .015 to .020 inches.

Increasing the quantity of organic binder by 60 percent enabled reducing the layer thickness to .0012 and .0014 inches for molybdenum and hafnia, respectively. However, this produced an orange-peel-like surface and the continuity of the coating was lost. A laminate with ten alternate layers of molybdenum and hafnia had a thickness of .012 inch. Examination under a microscope showed that each layer penetrated the voids of the preceding layer.

Thinner starting layers were desired which could only be achieved with the finer screen sizes. Settling methods to eliminate coarse particles in the as-received metal were evaluated in attempting to obtain pigment which could be applied through the 165 x 165 mesh screen. A laboratory setup capable of separating out the minus 3 micron material is shown in Figure 2.

The separation is accomplished by blending 250 gms of as-purchased molybdenum powder with 1000 cc's of a liquid media consisting of 75 percent acetone and 25 percent ethyl cellosolve. The liquid media was selected on the basis of settling rate and chemical inertness to the metal powder for the time required to make the separation. (Molybdenum powder is oxidized by water, as shown by a blue coloration of the water upon short exposure to the metal powder). The liquid suspension is placed in a 2000 cc Squibb separatory funnel fitted with an air stirrer to keep the powder in suspension. The liquid is released slowly (approximately 50 cc per minute) into the trough which is inclined 20°. The powder fractions settle behind each insert and in the beaker.

Figure 3 shows electron micrographs of the molybdenum powder as-purchased and after separation. The oversize material is that settling out behind the first two inserts in the trough and the material being used is that collected behind the third and fourth inserts and in the beaker, amounting to 68-75 percent of the starting batch. Closer sizing is possible, but the yield of sized material decreases rapidly as the fraction spread is reduced.

Nonuniform silk screening characteristics were still present using the finer powder when the screen size was changed from 105 x 105 to 165 x 165 mesh. The liquid media passes through the screen more rapidly than the molybdenum powder leaving a dry paste at the end of the stroke. Agglomerates of the plate-like particles bridge openings in the screen, causing the nonuniform flow characteristics. The smaller particles did allow a slight reduction of the layer thickness using the 105 x 105 mesh screen and improved uniformity within the layers. Film thicknesses were .0017 to .0020 inches compared to the .0018 to .0023 inches produced from as-purchased powder.

A Gardner casting knife was used with a precision ground fixture for knife coating. The original fixture, made from aluminum plate, lacked dimensional stability. The final fixture (drawknife bed) used was machined and lapped from cast 355-T71 aluminum. Figure 4 shows a detailed drawing and photograph of the bed with the knife in position. The surface of the bed is covered with a .5 mil thick film of aluminized mylar which provides a mirror surface for applying the paint layers. The surface of the aluminum bed is coated with a thin film of grease to hold the mylar firmly in place. Any wrinkles in the film are removed using a rubber roller or squeege. The film is held in position by two teflon wedges placed in machined groves in the bed. The teflon wedges also act as a barrier to paint flow providing a definite edge to the panel preventing paint from running under the knife runners. After painting,a laminate has sufficient rigidity that it and the mylar film are readily parted from the greased surface of the bed. The very thin mylar film is then readily stripped from the back of the laminate sheet.

In the paint formulations used for knife coating (Table III) different acrylic binders and solvents were used with the different phases to prevent solvation and lifting between alternate layers as they are applied. The thickness of the painted film is a function of the flow and shrinkage characteristics of the paint, the height the knife blade is set above the bed, and the rate the knife is drawn across the bed. Viscosity of the paint and the rate the knife is drawn across the bed was held as constant as possible while varying the height of the blade above the bed to control thickness. The height of the blade is controlled by micrometer settings. For the initial layer the height of the knife is set .5 mils above that required to produce the required thickness. This compensates for the part of the layer which adheres to the mylar film when it is stripped and provides material to compensate for variations in the flatness of the bed and mylar film. The paint film is allowed to dry using warm air flowing across its surface until moisture is no longer visible, 7 to 8 minutes. The knife setting is then raised the desired height and a layer of the second material applied. This procedure is followed until a laminate sheet of the desired thickness has been built up. Layer thicknesses of less than .001 inches were produced in laminates.

The knife coating process was selected for producing laminates for the particle geometry study as it produced the thinnest layers with the least intermixing of the phases and appeared to be most versatile for varying layer thicknesses. The first variable to be evaluated was thickness of the alternate metal and ceramic layers in the laminate. It was desired to produce laminate sheets which had individual layer thickness of 3, 2, 1.5 and 1 mils.

In attempting to produce laminates with these layer thicknesses, it was found that variation in drying shrinkage of the paint as a function of film thickness was excessive.

Swelling of the layers occurred with a knife distance of .001 inches above the bed because of spring-back of particles pressed between the knife edge and the bed as the pressure was relieved. Using a .0015 inch setting, shrinkage of the film was slightly higher than swelling, resulting in layers less than .0015 inches. With a setting of .002 inches, drying shrinkage was in excess of 25 percent in both the metal and ceramic paints and increased further with increasing thickness.

Firing shrinkage was more uniform than drying shrinkage. Table V summarizes drying and firing shrinkages obtained from the molybdenum and the 93.1 HfO_2 · 4.9 CeO_2 · 2 MgO ceramic pigmented paints. Tabulated values were obtained by averaging the thickness of individual layers taken from a minimum of two laminate sheets.

To prevent layers from delaminating, it was necessary to apply a new layer before the previously applied layer had completely dried. This greatly complicated compensation for shrinkage in the top layers as the lower layers were continually changing dimension and the rate of change varied with each successive layer applied. Sorption of the solvent from the freshly painted layer into the underlying layer caused the drying rate of both layers to vary as the panel thickness increases.

A number of laminate sheets were made during this investigation in which layer thickness after sintering varied from .8 to 4.5 mils, some of which had relatively uniform layer thicknesses and others in which the layer thickness varied considerably. Although these sheets did not have the intended layer thicknesses, they were used in composite specimens to relate flexural, compressive and oxidation properties to the variations present.

These laminate sheets were cut to form laminate particles for the composite specimens using a Wiley Mill, shown in Figure 5 with the cutter cover removed. The laminate sheets were broken by hand to a size which could be fed into the mill. The cut particles were screened and any material which did not pass 24 mesh was returned to the hopper to again be passed through the cutting chamber. To avoid variables other than those introduced by knifing, the cut particles were further screened to size fractions of -24 + 48, -48 + 100, -100 +200, and -200 mesh. Each specimen from a given laminate sheet was then fabricated using the weight percent of each fraction shown in Table VI. This is necessary because of natural segregation of the different

particle sizes in a given container of material. Without this fractioning it is possible to have one specimen in a lot made with excessively fine laminate particles; while the next has a large percentage of coarser particles, depending on how they are removed from the storage container. The selection of the grain size fraction to be used was based on the average particle size distribution obtained from 8 screen analyses of particles cut in a Wiley mill from laminate sheets of the 93.1 HfO_2 · 4.9 CeO_2 · 2 MgO-Mo composite material, sized to pass a 24 mesh screen. The effect of particle size and size distribution was unknown at the time, thus this distribution resulted in a minimum loss of material from any given batch.

All specimens were fabricated by warm pressing using a temperature of 150°F and a pressure of 12.5 ksi. They were heated in argon, using the Number 1 time-temperature cycle shown in Figure 6, to remove the organic binder and to produce sufficient handling strength to enable transferring them from the inert gas furnace to a vacuum furnace. They were then sintered in a vacuum chamber at 3200°F, heating to temperature at a rate of 400°F/hr held at temperature 12 hours and cooled at a rate of 400°F/hr. The minimum pressure at temperature was 1.0×10^{-4} Torr. Table VII gives the dimensional and compositional variations in the laminate sheets and Table VIII gives the properties of composite specimens from the different laminate sheets.

Wide variations in properties of the composite specimens made from the various laminate sheets resulted; flexural strength varied from 27.5 to 80 ksi, compressive yield strength varied from 51.1 to 106.2 ksi and weight loss due to oxidation after 24 hours at 2500°F varied from 232 to 943 mg/cm^2. Information from these tests was inconclusive as to the effect of layer thickness, but indicated a rapid increase of flexural strength resulted when the layer thickness for both phases was kept below one mil and that no advantage appears likely using thicker layers.

Two relationships were established from this group of specimens: (1) All properties are directly related to the weight loss in specimens during sintering and (2) flexural strength is related to the differential shrinkage between the metal and ceramic phases during sintering. Flexural strength increased with increasing weight loss; while oxidation resistance, compressive strength and compressive deformation decreased with increasing weight loss. Figures 7, 8, 9 and 10 show these data. In each case there are points which are contrary to the trend, but in most instances they can be attributed to either layer thickness or metal-to-ceramic ratio effects. Figure 11 shows the variations of flexural strength with the difference in shrinkage between the metal and ceramic phase, and indicates an optimum situation occurs when the metal phase shrinks slightly more than the ceramic phase placing it in compression. When this variation becomes excessive, the stresses become too

high and weaken the structure. This appears to occur when the difference in shrinkage exceeds 2 to 4 percent. When the ceramic shrinks more than the metal, it is placed in tension. Figure 12 shows a polished section made from a flexural specimen prepared from laminate sheet B-7. The microcracks across the ceramic between layers is believed to be a result of the high shrinkage of the ceramic phase during sintering resulting in the low flexural strength which is a measure of tensile strength of the material. The compressive strength of specimens made from the B-7 laminate sheet is the highest, showing the microcracking is not detrimental to this property and that the tensile stresses in the ceramic increases the composites capacity for carrying compressive loads.

Weight loss is attributed to decomposition of the acrylic binder, volatilization of solvent remaining with the acrylic and to volatilization of magnesium oxide and impurities at high temperature during vacuum sintering. To determine to what degree the weight loss due to impurities (oxides of Mo) might be associated with the metal phase, specimens were prepared from the metal as-received, and from the -3 micron powder obtained from the separation process, as well as from as-received powder oxidized by placing it in water and air drying. The standard paint with 12.5 percent acrylic binder was made using each of the powders. The paint was spread out to form a sheet, dryed, cut to -20 mesh, pressed at 12.5 ksi and 150°F and sintered at 3200°F for 12 hours in vacuum. Weight change varied from 5.5 to 6 percent, being lowest in the as-received powder and highest in the -3 micron powder. Five percent of the weight loss can be attributed to decomposition of acrylic; the remaining .5 to 1 percent to volatilization of molybdenum oxide from the surface and/or remaining solvent. Thus losses in general are not associated with the molybdenum unless oxygen is being supplied from the ceramic phase to form volatile oxides.

In general the weight loss did increase with the percent ceramic, but direct correlation was not found between measured layer thickness and weight loss. Figure 13 shows photomicrographs of a specimen with the highest, intermediate and lowest amount of weight loss. The obvious variation is in the dark spots appearing in the ceramic. Approximately 50 percent of these are voids; while the majority of the others are glass phase inclusions. Figure 14 (1000X) shows the structure more clearly.

The size and distribution of the glass phase inclusion varied with each lot. Those most uniformly distributed throughout the ceramic phase produced the lowest strength, but produced better resistance to oxidation. Microprobe analysis showed the glass phase inclusions contained Si, Al and Mg in higher concentrations than the surrounding ceramic phase and that there was less Zr and Ce in the inclusion than in the surrounding ceramic phase. This shows the glass is a magnesium-aluminum-silicate with limited quantities of zirconium, hafnium and cerium. Si, Al and Zr are impurities associated with

Reactor Grade II hafnia, while Mg and Ce are introduced as oxides for the specific purpose of increasing the oxidation resistance of the composite. The concentrations of impurities in hafnia varies significantly from lot to lot of the as-purchased material and properties of composites made from different lots of hafnium oxide vary. This will be further discussed in Section C dealing with sintering.

Major sources of the wide variation in properties are believed to be due to the packing of particles in the various layers during the knife coating process and to segregation of constituents in the ceramic paint. Firing variables were not present as these specimens were sintered at the same time and duplicate specimens randomly separated in the vacuum furnace showed little variation in properties between specimens. The various laminates were prepared using the same lot of calcined hafnia·5 ceria so that the starting impurities were constant in all specimens.

To determine if segregation was occurring from one end of a laminate to the other or if inconsistancy is mainly between different laminates, specimens were cut from opposite ends of a laminate sheet and re-suspended by dissolving the organic binder. Samples from the suspensions were collected and examined using an electron microscope to compare particle sizes and shapes with those of the starting paint. No significant differences were observed. The magnesium oxide was observed as both a fine coating around single particles and in several agglomerates. Variations in the degree of coating of particles with magnesia and amount of agglomeration taking place is a likely cause of the wide variation in the oxidation resistance between samples from different laminate sheets.

Hardness measurements have been made on metal and ceramic laminae in flexural specimens having high, intermediate, and low strength. No correlation between hardness and strength was found. The molybdenum phase varied from 173 to 206 KHN and the ceramic from 650 to 694 KHN. The lowest hardness in the molybdenum phase existed at an intermediate strength level while low and high values were observed in specimens having equally high strengths.

B. Particle Size and Size Distribution Study

Laminate sheets .018 inch thick having nominal .001 inch alternate layers were prepared by knife coating, cut in a Wiley mill and screened to produce the following size (Tyler screen) fractions: -14 + 20, -20 + 48, -48 + 100, -100 + 200 and -200. Individual grain fractions were then used to produce flexural, oxidation and compression specimens. Specimens for these tests were also prepared from grain compositions containing the size fractions below any given screen size in the proportions reported in Table IX. All specimens were fabricated and sintered as previously described.

Table X summarizes the properties of these specimens. Figure 15 shows flexural strength of specimens as a function of original particle size. As can be seen, strength increases with decreasing particle size and higher strength is obtained in specimens made from a range of particle sizes rather than from those made from a single size fraction. Figure 16 is a plot of weight loss due to oxidation as a function of particle size, indicating a minimum weight loss in specimens made from -100 mesh particles. Specimens made from -200 mesh particles showed the highest oxidation rates. Specimens made using a single particle size fraction have better resistance to oxidation than specimens made from a large range of particle sizes.

Figure 17 is a plot of compressive deformation as a function of particle size. Deformation decreases slightly with decreasing particle size when a blend of particles are used. The -20 + 48 particle size fraction produced the highest deformation, while a minimum was obtained in the -100 + 200 size range. The increase in compressive deformation produced from specimens fabricated from -200 mesh material and the rapid increase in oxidation rate for -200 mesh material indicated possible preferential segregation of the metal and ceramic during the cutting. This was substantiated by X-ray fluorescence analyses which showed the -200 mesh material contained more molybdenum than the starting laminate sheet and that the -100 + 200 mesh particle size had a higher ceramic content. Specimens made from the smaller particle sizes produce higher strength and better oxidation resistance, but have less compressive ductility. Variations in the macrostructure of these specimens as a result of particle size are shown in Figure 18.

C Particle Shape Study

By varying the thickness of the laminate sheets from which the macroparticles are cut and screening them through various screen sizes, the shape of the particle can be varied. To evaluate the effect of particle shape, laminate sheets .006, .018 and .036 inches thick were prepared having nominal layer thicknesses of .001 inches and cut in the Wiley mill to pass a 20 mesh screen. Flexural, compressive and oxidation test specimens were fabricated from the resulting particles from each sheet after screening to provide the following grain size distribution:

Screen Size	Percent
-20 + 48	65.2
-48 + 100	18.8
-100 + 200	11.4
-200 + 325	2.1
-325	2.5

For the -20 + 48 mesh particles the .006 inch material produced thin plate-like particles, the .012 inch produced thicker plate-like particles;

while the .018 inch produced particles nearer to having the same dimension for all three axes. There are some larger plate-like particles from the .018 inch sheet resulting from splitting of the laminate during the cutting operation. The .036 sheet produced particles more rectangular in shape having one axis elongated. The above descriptions generally held true for the -48 + 100 mesh material as well. The -100 +200 mesh material for all laminate sheets produces particles more rectangular, having one elongated side. The number of layers in the particles is reduced due to shearing between layers. This holds true for the -200 + 325 mesh material, but the number of layers per particle is further reduced. The -325 mesh material consists of particles of either metal or ceramic with some of the other phase adhering to their surfaces.

Table XI lists the properties obtained. The only significant difference in flexural strength was observed in specimens produced from the particles cut from the .032 inch laminate sheet which have a rectangular cross section with one axis elongated. Oxidation resistance of specimens made using -20 mesh particles varied from .42 gm/cm^2 to .63 gm/cm^2. Specimens made from cubical particles had the highest resistance to oxidation while those made from plate-like particles had the lowest resistance. Compressive yield strength of specimens also followed this pattern with a high value of 138.6 ksi and a low value of 79.3 ksi. Specimens made from elongated rectangular particles produced oxidation and compressive properties nearly equal to those made from cubical particles and are therefore the preferred shape.

D. Metal-to-Ceramic Ratio-Study

Laminate sheets in which the metal content varies from approximately 30 to 70 percent were prepared by knife coating. Greatly improved control of layer thickness was obtained by using single layers of one phase and multiple layers of the second phase. Problems with lifting when painting multiple layers of the same coating were not encountered. Flexural, oxidation and compression specimens were fabricated from particles cut from the laminate sheets and screened to pass 20 mesh.

Flexural strength, compressive deformation and weight loss due to oxidation increased with increasing metal content. Specimens containing less than 50 percent metal failed in flexure prior to reaching a yield point, while specimens with the higher metal content reached a yield point and deformed plasticly prior to failure. The rate of weight loss due to oxidation increases as the metal content increases as shown by the curve in Figure 19. Figure 20 is a plot of the other properties of the composite as a function of metal content and Figure 21 shows the load deformation curves for flexural specimens with high and low metal contents.

IV FORMING STUDY

A. Warm Pressing

Warm pressing was evaluated at the start of the program to prepare specimens for the particle geometry study and the sintering study. Particles were cut to pass a 20 mesh screen from laminate sheets prepared by roll coating.

A tool steel die, heat treated and drawn to a Rockwell C hardness range of 58-60 was used for pressing the particles. It consisted of an upper and lower ram free to move in a retaining cavity producing a rectangular bar 2.75 x .38 inches. The thickness of the bars is determined by the quantity of material used, the pressure and temperature.

Maintaining pressure constant at 20 ksi, temperatures from 70°F to 400°F were evaluated to establish the practical temperature limits over which the laminate particles containing acrylic binder could be compacted into composite test shapes. Insufficient flow of the plastic below 100°F resulted in openings between particles and above 300°F sticking of the dies occurred.

Using the mean temperature, 200°F, the upper pressure limit was then determined as being 35,000 psi. Approximately 8 percent of the material extruded between the die wall and the ram at 40,000 psi and at 50,000 psi 38 percent of the material extruded. Three percent of the material extruded at 35,000 psi. Pressures below 10,000 psi were not sufficient to eliminate voids between particles.

A study was conducted to determine the interrelationship of these two variables with regard to the properties of the resulting composite parts. Bar specimens .15" x .38" x 2.75" for comparing density, fired shrinkage and flexural strength were fabricated using pressures of 10, 22.5 and 35 ksi with temperatures of 100°, 200° and 300°F for each pressure level. After fabrication all specimens were sintered simultaneously in argon using the time-temperature cycle shown in Figure 22.

Many of the specimens had bloated during sintering and all had small droplets of a vitreous material on their outer surfaces. The bloating was related to the pressing condition and was most pronounced in specimens pressed at the highest pressures and was not present in specimens pressed at the lowest pressure. This is attributed to the material being compacted to such a high degree at the higher pressures that gases absorbed on the powders and from the decomposition of the acrylic binder were trapped in the specimen, building up sufficient pressure to bloat the parts while they were in a plastic condition. The vitreous droplets were a glass produced by silica and other impurities in the hafnia combining with some of the magnesia and ceria in the ceramic phase. The glass did not wet the

molybdenum and was readily removed from the surface during grinding of the specimen for flexural testing.

Fired shrinkage decreases with increasing pressure and decreasing temperature. Apparent density reflects the number of closed pores in the system, but does not indicate the effect of the large open pores caused by bloating. No correlation between density and forming parameters or flexural strength was therefore evident. However, highest density was obtained from specimens pressed at 10,000 psi which did not bloat.

Flexural strength decreased with increasing forming pressure. It was essentially constant at all three temperature levels when a forming pressure of 10 ksi was used. Flexural strength was a complex function of temperature at the 22.5 ksi pressure level and increased with increasing temperature at the 35 ksi pressure level. Specimens prepared previously to determine the practical range of temperature to be evaluated using a constant pressure of 20 ksi showed the 150°F forming temperature to be optimum. Properties of specimens pressed using the various parameters discussed are given in Table XII.

Three general types of fracture surfaces and combinations of three types were observed. Figure 23 shows diagrams of the fractured surfaces. At the lowest pressure-temperature combinations, bars fractured in a single plane parallel to the direction of applied force and contained no evidence of internal flaws. Specimens pressed at the highest temperature and all pressures fractured on a diagonal plane 45° to the applied force. Specimens pressed at the intermediate and high pressure levels with low temperature fractured on a plane parallel to the applied force and showed laminar voids produced by the pressure of entrapped gases during sintering.

Comparison of flexural strength, density and fracture type of nonbloated specimens indicates that a pressure of 10 ksi at 150°F is near optimum for this material system. These were the conditions used for preparing specimens for the sintering study. Some scatter in properties in the specimens used in the sintering study indicated 10 ksi was probably borderline for obtaining complete compaction. The pressure was increased to 12.5 ksi for fabricating the majority of specimens in the geometry study.

As this study was conducted at the beginning of the program using particles cut from laminates made by roll coating, a second evaluation near the end of the program was made using particles cut from knife-coated laminates. For this evaluation temperature, the least critical variable, was held constant at 150°F and pressure was varied between 10 and 20 ksi. The

variation in properties with pressure was less than between specimens pressed at the same pressure. The highest average flexural strength was 51.2 ksi from specimens made using a pressure of 16 ksi and was the pressure used for preparing the final test parts.

B. Isostatic Pressing

The first method of isostatic pressing investigated used laminate particles containing organic binder as used for warm pressing in steel dies. These particles were placed in cylindrical rubber bags 1/2 inch in diameter, dealred by evacuating the bag through a hollow needle and sealed. The filled bags were then placed in a chamber filled with glycerine which could be heated to temperatures of 600°F at pressures to 15 ksi. Initial pressings were made between room temperature and 300°F using pressures from 10 to 15 ksi, and at room temperature at 40 ksi. Temperatures above 150°F were required to obtain adequate compaction. At 300°F the rubber bags were destroyed by the glycerine. A series of specimens were prepared using -20 mesh particles pressed at 150° and 250°F at pressures of 12.5 and 15 ksi for comparison with specimens made from the same lot of particles prepared by warm pressing at 150° and 12.5 ksi. Highest strength in the isostatically pressed and sintered specimens was 31.4 ksi obtained using a pressure of 12.5 ksi at 150°F; while a flexural strength of 42.8 ksi was achieved from the warm pressed specimens.

In a second method the laminate particles were heat-treated prior to pressing to eliminate the organic binder and then isostatically pressed at room temperature at pressures to 40 ksi. The removal of the organic binder was believed to be desirable especially when thicker parts are to be made, as it eliminates problems associated with the removal of binder from the center of specimens during sintering and reduces carbon contamination. Initially the particles were heated to 1000°F in hydrogen to decompose the organic. After this treatment, they maintain their laminate form, but can not stand abrasion without powdering. These particles pressed well and sintered to a high density, but they had poor handling strength in comparison to those made by warm pressing with binder. Polished sections showed the resulting structure to be mixed between that of a laminate particle composite and a cermet.

Particles were heat treated to 1500° and 2000°F in hydrogen in attempting to provide some strength so they could be packed in the rubber bags without powdering. A similar microstructure was obtained from the particles treated at 1500°F, but those treated at 2000°F produced a very different structure. First a large number of particles were oriented with planes running parallel to the cross section instead of at some oblique angle

and thus appeared as large areas of metal or ceramic. Also, the ceramic penetrated through the metal layers producing a discontinuous metal network. This structure was weak in comparison to that of the mixed laminate particle and cermet structure (26 ksi as compared to 59.3 ksi).

Figure 24 shows the structures of specimens made from the same lot of laminate particles fabricated by warm pressing and by isostatic pressing with and without organic binder. More orientation of particles is evident in the specimens pressed directionally in the steel die than in the isostatically pressed specimens which was expected. The orientation of particles in the warm pressed specimens places the majority of laminae parallel to the direction of tensile stress in the flexural test specimen. A larger percentage of laminae are perpendicular or nearer to being perpendicular to the direction of tensile stress in the isostatically pressed specimens. Their lower strength indicates a weakness in the metal-ceramic bond or a lower strength in one or both phases. For this material system the ceramic is the weaker phase.

C. Hot Pressing

To establish hot pressing parameters, a blend of particles remaining from laminate sheets B-1 through L-11 described in Table VII were used. They were prepared for pressing by heating in vacuum at 1100°F for 3 hours to remove the organic binder. The liners of the graphite dies used for pressing were coated with an alumina pigmented paint to prevent sticking of the composite material to the die and to avoid reduction of the ceramic phase. The particles were loaded in the graphite dies, inductively heated under an argon cover atmosphere to the desired temperature and pressure was applied. Specimens were pressed at temperatures from 2400° to 2800°F in 100° intervals using a pressure of 4 ksi. The dies were brought to the respective temperatures in a period of 30 minutes, pressure was applied, and the temperature and pressure held for one hour. The parts pressed at temperatures from 2400° to 2700°F released from the coated dies with no difficulties. At 2800°F the part adhered to the die and was broken in the center as a result of the tensile force caused by differential expansion between it and the graphite.

The alumina adhered to the surface of the specimens and was removed by diamond grinding prior to testing for flexural strength, density and

apparent porosity. Flexural strength varied from 21.8 to 43.3 ksi. The low value was obtained from the specimen pressed at 2400°F and the high value was produced at 2500°F. Densities varied from 8.87 to 9.37, progressively increasing with increasing temperatures. Properties are listed in Table XIII.

Additional pressings were made at 2500°F, using times at temperature of 30 minutes and 2 hours. The shorter time produced the higher flexural strength, 41.1 ksi compared to 37.4 ksi; but neither were as strong as the original specimen pressed for one hour.

For the previous pressings the laminate particles were brought to temperature in the die prior to applying pressure. An additional pressing was made in which pressure was applied after reaching a temperature of 1950°F rather than after reaching the maximum hold temperature. The 1950°F temperature was selected as being about the threshold of sintering and was sufficiently high to enable outgassing from the particles. For this material applying the pressure sooner at a lower temperature provided no advantage. Lower total compaction in the specimen was obtained and the flexural strength was reduced to 34 ksi.

Post-heat-treatement to allow gases to escape which are entrapped during hot pressing and to promote further sintering has been found to improve properties of hot pressed materials. Halves of specimens made during the initial evaluation of hot pressing were used for this evaluation. The time-temperature cycle shown in Figure 25 was used. Argon was used in this treatment to allow CO_2 to diffuse out of the specimens prior to introducing hydrogen to promote sintering. Early introduction of hydrogen reduces entrapped CO_2 leaving a carbon residue. Table XIII also lists the flexural strengths and densities of these specimens after post-heat-treatment. The as-pressed specimens were broken on a two inch span using four point loading and the post-heat-treated half-specimens were broken on a one inch span using center point loading. These values are not directly comparable. In work accomplished to date in testing macrolaminate composites, higher strengths have generally been obtained from the two inch span using four point loading which is opposite of what is observed with ceramics. This is attributed to some stress distribution due to the metal phase which is more operative when the stress is applied to a larger area. Post-heat-treatment did produce significant improvement in all specimens except BGH-2 which had the highest strength (43.3 ksi) in the as-pressed condition. Specimen BGH-3 pressed at 2600°F had the highest strength (55.2 ksi) after post-heat-treatment.

Figure 26 shows polished sections of specimens made using increasing temperatures, holding time and pressure constant. Figure 27 shows specimens pressed at 2500°F and 4000 psi with varying times. The molybdenum phase was dense in all specimens, but considerable porosity was observed in the ceramic phase. Grain size increased with increasing temperature and time at temperature. Variations observed in the microstructure within a single specimen were similar to variations observed in specimens made from particles cut from the individual laminate sheets B-1 through B-11.

To compare hot pressing with warm pressing and sintering, a new lot of laminate particles was prepared. A higher purity grade of HfO_2 was used in the ceramic phase; Reactor Grade S, instead of Reactor Grade II. Chemical analyses for these two types of hafnia are given in Table IV. Hot pressings were made at 2600°F using a pressure of 4 ksi. Heating to temperature was accomplished in 30 minutes, pressure was applied and held for one hour at 2600°F.

Warm pressed parts were made in a tool steel die heated to 150°F using a pressure of 16,000 psi. Specimens were sintered at 3400°F for 12 hours in a wet hydrogen atmosphere.

The as-hot-pressed specimens had an average flexural strength of 50 ksi while the warm pressed and sintered parts had an average flexural strength of 38 ksi. The average density of the hot-pressed specimens was 9.56 compared to 9.29 gm/cc for the sintered specimens. Post heat treating the hot-pressed specimens at 2400°F in a hydrogen atmosphere reduced their strength to an average value of 35 ksi. This heat treatment had previously been used and found to increase the strength of hot-pressed specimens. Sufficient work has not been accomplished to explain this difference. Grain growth took place in the metal phase during post-heat-treatment in both cases which would normally produce lower strength. The sintered specimens had a very different ceramic structure and a large grain size in the metal phase in comparison to that in hot pressed and post-heat-treated specimens. Photomicrographs are shown in Figure 28. Hot pressing produced much greater orientation of the laminate particles than warm pressing (see Figure 28). The flatening and elongation of particles also reduced thickness of the individual layers in particles oriented with the laminae perpendicular to the pressing direction.

D. Warm Extrusion

To determine the feasibility of warm extruding the macrolaminate composite from laminate particles containing organic binder the fixture shown in Figure 30 was designed and fabricated. A Tinius Olsen Universal Test machine with a 6 ton capacity (equipped with a circulating air oven) was used to provide the ram driving force. Head travel can be controlled while measuring the force required for extrusion.

Macrolaminate particles were warm pressed at 150°F at a pressure of 12.5 ksi to form billets for extrusion. Initial attempts to extrude the billets were made at temperatures from 200 to 400°F with extrusion rates varying from .2 to 2 inches per minute. Feather-edging occurred in all specimens, but decreased in severity with increasing temperature and extrusion rate. Heating the extrusion fixture in the oven and extruding the part in the hot oven was not feasible as the extruded stock had insufficient strength to maintain its shape and be handled. Extruding from a hot fixture to room temperature allowed the plastic to set and produced good handling strength.

Polished sections parallel and transverse to the direction of extrusion were made from parts extruded at 300°F into a 300°F oven and from the fixture preheated to 400°F and extruded to room temperature. They show the macrolaminate structure to be quite different than that obtained by warm pressing, hot pressing or isostatic pressing. Figure 30 shows a section near an exterior edge made parallel to the direction of extrusion. At the surface the laminae are oriented with extrusion direction. Back from the edge a large particle has been sheared on a plane approximately 45° to the extrusion direction.

Figure 31 is a photomicrograph of a cross section of a corner showing cracks caused by drag of the material on the exterior of the die wall.

To eliminate feather edging and cracking, greater plasticity in the starting material and improvements in die design are required. Higher extrusion temperatures would increase plasticity and die lubrication would reduce drag; increased amounts of organic binder in the particles would also increase plasticity. It is quite certain that this process can be developed, but due to difficulties encountered in sintering and problems involved in the particle geometry study, time was not available to pursue this forming method to the point where sound parts could be fabricated.

V SINTERING STUDY

Composite bar specimens .15 x .38 x 2.75 were fabricated using minus 20 mesh particles cut from roll coated laminate sheets. These particles were from the same lot used in the initial warm pressing study and were pressed in the previously-described steel die using a pressure of 10 ksi at a temperature of 150°F. Specimens of molybdenum and of 93.1 HfO_2 · 4.9 CeO_2 · 2 MgO were also prepared by the same process for comparison.

Using the time-temperature cycle diagrammed in Figure 22, specimens were sintered in atmospheres of argon, wet hydrogen, dry hydrogen and a vacuum of 1×10^{-4} Torr to evaluate the effects of atmosphere on the properties of the composite and its individual constituents. Table XIV lists the flexural strength, density, apparent porosity and linear fired shrinkage for the composite specimens and Tables XV and XVI list the properties for the metal and ceramic phases.

The average flexural strength for specimens fired in the various atmospheres varied from 35.8 ksi to 57 ksi, indicating the significance of this variable. The highest strength in the composite was obtained from those specimens fired in wet hydrogen and the lowest strength was produced from an atmosphere of hydrogen which had been dried by passing it through a liquid nitrogen freeze trap. The dry hydrogen reduced part of the ceramic phase lowering the strength of the composite. Vitreous droplets did not form on specimens fired in any atmosphere other than argon.

Molybdenum sintered in argon had the highest strength but failed without plastic deformation. This is attributed to interstitial contamination which increases the strength of molybdenum, but embrittles it. The next highest strength, accompanied by some ductility, was measured on specimens fired in dry hydrogen. The specimens sintered in vacuum had the lowest yield strength, but were quite ductile. Ground specimens 0.1 inches thick bent to an angle of 43° prior to formation of the first crack on the 2 inch test span.

The strength of the bulk ceramic specimens was consistently low regardless of the sintering atmosphere. The low strength caused by porosity and flaws masked any effect of sintering atmosphere. The thin layers of ceramics in the macro-particles are not as subject to flaws and are considerably stronger than is indicated by the bulk body, but considerable improvement in strength of the ceramic phase is still required.

Achieving ductility in the system was considered more important than maximizing composite strength. Results from sintering the metal in various atmospheres indicated the use of vacuum was most likely to produce ductility. The composite specimens sintered in vacuum were nearly as strong as those sintered in wet hydrogen although they were considerably more porous. This indicated that improvements in the vacuum firing cycle would further improve the strength of the composite and

vacuum was selected for use in the statistically planned sintering study to establish the optimum combination of temperature, time at temperature and heating and cooling rates.

A Greco 3 x 3 Latin design experiment was selected for evaluating the above parameters. Temperature and time at temperature were considered to be the most critical variables and were both evaluated at all three levels while heating and cooling rates were considered less critical and were used to meet the design requirements as shown in Table XVII. Previous experience had indicated temperatures around 3300°F were required to adequately sinter the system. Temperatures of 3200°, 3300° and 3400°F were evaluated. Twelve hours as the maximum time at temperature was considered ample for establishing the effect of this variable; thus 0, 6 and 12 hour time periods were used.

Heating and cooling rates were based on as wide a base as possible within the capabilities of the available vacuum furnace. The degree of vacuum achieved ranged from 5×10^{-5} to 1×10^{-4} Torr, depending on outgassing as a function of heating rate, temperature and the seal obtained.

Prior to vacuum sintering all specimens were heated in argon per Cycle 1 shown in Figure 6 to remove the organic binder, thus avoiding loading the high vacuum system with excessive quantities of organic material. The rapid heating and cooling portion of this cycle between 1000°F and 2000°F produced sufficient sintering in the specimens to enable transferring them from the inert gas furnace to the vacuum furnace. Because of this preheating, heating and cooling rates above and below 2000°F were not considered critical and were not held constant due to timing involved in starting and stopping cycles during normal working periods.

The nine cycles to meet the requirements of the Latin design were conducted and a tenth firing to determine reproducibility was made and found satisfactory. Three flexural test specimens of the composite material, a molybdenum, and a ceramic specimen were included in each firing. Table XVIII gives the sintering parameters used for the nine cycles and lists the fired shrinkage, density, apparent porosity and flexural strengths of the composite specimens. Table XIX lists the properties of the molybdenum specimens. The bulk ceramic specimens were highly stressed and fractured in the majority of cases either during sintering or while grinding and flexural strength data was not obtained.

Composite specimens sintered using cycles L-1, -6 and -8 failed prior to reaching a yield stress, while specimens sintered using the other 6 cycles produced load deformation curves which changed slope prior to failure. The amount of deformation

after exceeding the proportional limit is small (.001" to .005") and the change in slope is more gradual than that produced by molybdenum metal. As the yield strength is below those obtained from the bulk metal specimens, either progressive ceramic failure which locally loads the metal to a sufficient degree to allow plastic deformation, or slippage at the interface between metal and ceramic layers is occurring. Figure 33 shows a load deformation curve from a composite specimen exhibiting each type of failure and from a molybdenum specimen exhibiting plastic deformation.

The properties of the molybdenum specimens varied to a greater degree than those of the composite material. Some contamination of the molybdenum from the roller used to make the composite specimens was found in photomicrographs of specimens made for evaluating the effects of sintering atmosphere. Transfer of ceramic from the composite to the paint batch introduced the ceramic into the metal paint. The same batch of paint was used for both sets of specimens to keep them as similar as possible. This mechanism also produced contamination of the layers within the composite and is one of the reasons roll coating was abandoned as a method for producing macrolaminate composites. The ceramic acts as a dispersion hardner and accounts for the high yield strength obtained in some of the specimens.

The mathematical analysis of the experiment shows that ultimate strength is significantly affected by time at maximum temperature and by the heating rate. The highest level of time (12 hours) and the medium heating rate (400°F/hr) produced the better properties. The data does not indicate that maximum temperature within the range of values used (3200°-3400°F) significantly affects strength nor does it indicate cooling rates between 100° and 700°F/hr are significant. A variance in excess of 5 percent is considered significant.

The analysis also indicates that density is significantly affected by the maximum temperature and by time at maximum temperature. There was insufficient evidence that either the heating or cooling rate significantly affect density - the highest temperature, 3400°F, and the longest time, 12 hours, produced the highest density.

Polished sections of composite specimens and molybdenum fired for each of the nine conditions of the Latin design experiment are shown in Figures 34 and 35 respectively. The composite specimens were polished using 600 grit silicon carbide followed by 6 micron diamond, followed by Linde A.3 micron alumina and finished using Linde B.05 micron alumina. Etching was initially done on the ceramic phase using concentrated HF. This passivates the surface of the molybdenum which requires a second light polish followed by etching in dilute (1:10) Murakami's reagent to show the structure of molybdenum. The molybdenum specimens were polished in a similar manner and etched in the dilute Murakami's reagent.

The molybdenum samples show variations in grain size with firing condition as would be expected. Longer time and higher temperatures produced the largest grain size with the exceptions of samples sintered using cycles L-2 and L-5 at the 3300°F temperature level. Their grain size was very large, comparable to that of the specimen sintered for the longest time at the highest temperature, cycle L-1. Some voids are present, but the majority of dark spots are due to the hafnia contaminate which was introduced into the molybdenum during painting. Flexural yield strength increases with decreasing grain size while the relative order of ductility had no direct relationship to grain size. Specimens, having the intermediate grain size, sintered using cycles L-3, L-6 and L-7 were the least ductile. The impurities and their distribution undoubtedly play a major role, but a direct correlation from the microstructure is not evident.

Variations in grain size in the composite specimen are less evident because of the thin alternate layers, but the grain size of the metal phase follows that of molybdenum by itself. The ceramic phase has a columnar growth between the metal layers with the strength of the composite apparently dependent upon the continuity of the ceramic phase. The dark spots distributed in the ceramic phase are in some instances glassy inclusions formed from impurities in the hafnia or are voids as indicated previously in the section on macrolaminate particle geometry.

Plots of the least squares estimates for flexural strength and density as a function of the three levels of each variable from which all but the effects of the parameter being investigated have been averaged are shown in Figures 36 and 37 respectively. The data indicate that sintering cycles in excess of 12 hours should be evaluated to both increase the strength and reduce porosity in specimens. The heating rate significantly affects strength, and assuming symetry in the plot of the least squares estimated value, a maximum should occur around a heating rate of 475°F/hr.

Highest density was achieved at 3400°F and, although there was no indication that strength improved with the higher temperature, complete densification is needed for improved oxidation resistance. The cycle predicted to improve properties was: heating to 3400°F at a rate of 475°F per hour, holding at 3400°F for 12 hours and cooling at some rate lower than 700°F per hour. The cooling rate used was 275°F per hour and indicated the maximum for strength from the plots of the least squares estimate.

Flexural specimens were fabricated from the original lot of particles used in the Latin design experiment. Specimens were also fabricated from particles made from laminate sheets prepared by knife coating using hafnia from two other lots of material of higher purity than that used in the initial sintering study. Chemical compositions of the separate grades of Hafnia are given in Table IV.

Prior to vacuum sintering, duplicate specimens from each of the three types of specimens were preheated using the cycle shown in Curves 1 and 2 of Figure 6. The first cycle, using an argon atmosphere, was that used for preparing specimens in the Latin design experiment. The second cycle, using soft vacuum, was used to determine if improved properties could be obtained by preventing premature sintering in either phase and to possibly provide more efficient removal of the organic binder.

The specimens made from the macrolaminate particles used in the original sintering study made by roll coating had higher strengths than specimens made from particles prepared by knife coating using higher purity hafnium oxide. Removing the organic binder in argon produced higher strength parts than removing it in soft vacuum. Properties of these specimens are listed in Table XX.

The strengths of all of these specimens were lower than anticipated, but density increased as predicted. Assuming that the predicted cycle should produce properties comparable to those obtained by the best cycle in the Latin Design experiment (58 ksi instead of 45 ksi), some other factor was present. As previously mentioned, firings of specimens for the Particle Geometry Study had also produced lower than anticipated flexural strengths using the best firing cycle from the Latin Design experiment. In attempting to duplicate 80 ksi values previously obtained from specimens prepared by knife coating, flexural strengths of only 40 ksi were achieved. As these specimens were also made from the macrolaminate particles from the same laminate sheet and were fabricated by identical procedures, they indicated that sintering conditions were not being reproduced.

The difficulty in vacuum sintering was attributed to variations in pressure and atmosphere. While conducting the Latin Design experiment, ultimate pressures of 1×10^{-4} Torr were being obtained at maximum temperature with a minimum pressure during cool down of 5×10^{-5} Torr. A leaking seal was introducing oxygen, causing deterioration of the heating elements. After completion of the Latin Design experiment, the vacuum chamber was reconditioned and new elements installed. Strengths of all specimens fired since the reconditioning of the furnace have been lower. Currently a pressure of 1×10^{-5} Torr is obtained while at maximum temperature and is further reduced to 5×10^{-6} Torr during cool down. It was assumed that volatilization due to the reduced pressure inhibited sintering, or that oxygen introduced through leakage was necessary for sintering and/or bonding of phases.

To determine if pressure was the major factor causing the reduced strength, specimens were sintered at 3400°F for 12 hours. Heating to temperature was at a rate of 475°F/hr and cooling from temperature was at a rate of 275°F/hr, while maintaining the pressure above 1×10^{-4} Torr. Specimens made from the original

lot of laminate particles made by roll coating as well as specimens made from particles prepared by knife coating were included in the firing. Laminate particles made by knife coating were prepared using both Reactor Grade II and Reactor Grade S hafnia in the ceramic phase. Little improvement in strength was noted in specimens prepared using particles made by roll coating, 47.3 ksi compared to 45 ksi; while the strength of the specimens made from particles prepared by knife coating using Reactor Grade S hafnia increased from 35 to 45 ksi.

Using the same firing cycle, specimens were also sintered in wet hydrogen for re-evaluation. Similar strengths were obtained, but specimens deformed plastically prior to ultimate failure which was not obtained in the later vacuum firings.

The impurities in the hafnia and the additives to it, CeO_2 and MgO, critically affect the properties of the composite. Diffusion of impurities from the ceramic to the molybdenum account for much of the embrittlement; thus the manner in which they are combined in the ceramic structure is important as well as the atmosphere and pressure at which sintering takes place. In all previous work the ceramic phase has been prepared by prereacting hafnia and ceria at 2700°F and adding the MgO as a mill addition. The distribution of the magnesia appeared to be a critical factor affecting properties as it can react with silica impurities forming glass phase inclusions, go into solid solution with hafnia forming a cubic phase, or volatilize from the system. Also, ceric oxide can be reduced to a lower melting cerous oxide or react with hafnia depending on atmospheric conditions and impurities present.

An experiment was conducted to compare the above method with heating all three ingredients together and heating hafnia with magnesia, adding the ceria as a mill addition. When used with molybdenum in the composite and sintered in wet hydrogen, highest flexural strength and greatest compressive deformation were obtained in specimens having the ceramic made by prereacting hafnia with magnesia and adding ceria as a mill addition. Little reaction had occurred between the magnesia and the hafnia at 2700°F thus a second lot of the 98 HfO_2 · 2 MgO was prereacted at 3750°F. X-ray diffraction patterns showed the magnesia had reacted with hafnia at this temperature producing mixed cubic and monoclinic phases, while at the lower temperature it is still present as magnesia. The composite using this material sintered in wet hydrogen at 3400°F for 12 hours had a flexural strength of 49 ksi and exhibited increased ductility in comparison to composites in which the MgO was added as a mill addition to HfO_2 · $5CeO_2$ or by prereaction at 2700°F with HfO_2, and appears to be a preferred method.

This system has proven to be very complicated and, because of the variety of microstructures which can be achieved due to interactions between constituent materials and impurities, all reaction mechanisms have not been completely identified.

VI PREPARATION OF FINAL TEST SPECIMENS

Results of the concurrent studies evaluating particle geometry, forming methods, sintering and the metal-to-ceramic ratio have shown the major properties of interest, strength, ductility and oxidation resistance, are at approximately opposite points of a triangle for this system. This is expected to be the case for any system in which the metal matrix is not inherently resistant to oxidation. For any practical application the laminate particle size, the metal to ceramic ratio and the forming method would be selected on the basis of the shape and size of the part to be fabricated and its end use. Thus these variables of the final test parts to be fabricated were selected to obtain a compromise of these properties.

The ceramic phase was prepared by prereacting HfO_2 with magnesia at 3750°F and adding ceria as a mill addition. The high purity Reactor Grade S hafnia was used to eliminate impurities affecting the ductility of molybdenum. During the sintering study this method for preparing the ceramic phase had produced the highest degree of ductility in the composite.

Laminate sheets were prepared by knife coating. They had a nominal metal thickness of .001 inches and a ceramic thickness of .0077 inches measured on the laminate sheet by optical techniques after sintering. They were cut to pass a 48 mesh screen and the -200 mesh material was discarded. The fines were eliminated to aid oxidation resistance and the size range selected to compromise strength and ductility.

Test parts were fabricated from the particles by warm pressing in steel dies at a temperature of 150°F using a pressure of 16 ksi. Warm pressing was selected over the other techniques as it produces an intermediate degree of orientation of the particles which again compromises strength and ductility.

The specimens were heated in argon using Cycle 1 shown in Figure 6 with the exception that heating was continued at a rate of 475°F per hour to a temperature of 3400°F and held for 12 hours. Wet hydrogen was introduced after a temperature of 2000°F was reached.

The various shapes of specimens (flexural, compression, oxidation and tensile test blanks) sintered to different densities all of which were lower than any obtained throughout the course of the program (7.88 to 8.27). Although each of the steps incorporated had provided improvements in a specific test, the combination was not satisfactory. The major difficulties were the following: (1) The high prereaction temperature of the ceramic and the higher purity reduced its activity making it more difficult to sinter to high density. (2) Cutting all the particle to pass a 48 mesh screen rather than screening fractions cut to -20 mesh increased

the quantity of fine material (-200 mesh) and metal powder. Quantitative analysis showed the specimen to contain 34.2 percent metal instead of the intended 56 percent metal of the starting laminate sheet. (3) The particular size fraction packed better than previous combinations of sizes containing finer and closer single size fractions. The 16 ksi pressure bordered on being too high and decomposition of the binder produced lamilar voids in 40 percent of the specimens; being most prevalent in the oxidation and tensile test blanks which had thicker cross sections. The variation in specimen size was responsible for the differences in densities between specimen types and is related to removal of the organic biner.

Even with low density, high porosity and lower metal content, some improvement in the average flexural strength over that obtained from the original process was realized, 40.5 ksi compared to 35.4 ksi. Also, the material exceeded the proportional limit prior to failing, deforming more than specimens containing 72 percent metal in the previous metal-to-ceramic ratio study. The porosity of the specimens could be a factor allowing the metal to yield to a greater extent while the porous ceramic progressively fails. The load deformation curve is shown in Figure 38.

The average room temperature tensile strength was 15.6 ksi with a total deformation on a one inch gage length of .001". Only one of three specimens tested broke within the gage section indicating lack of alignment. Maximum strength was 16.9 ksi obtained from a specimen that broke out of the gage section.

The average compressive yield strength was 73.1 ksi with 4 percent compressive deformation prior to failure. The material has a linear coefficient of thermal expansion of 4.92×10^{-6} in/in °C from 20 to 1000°C.

Weight loss due to oxidation as a function of time was determined at temperatures of 1800°, 2200° and 2500°F. At 1800°F it was a linear function for the first 5 hours and then decreased in rate. At 2200°F very rapid weight loss occurred during the first 30 minutes and then oxidation was linear at a slower rate than at 1800°F. Total weight loss was slightly lower at 2200°F after the 24 hour test period with the cross over point occurring after 22 hours. At 2500°F the rate was much greater and changes slope several times indicating possible reactions taking place between the ceramic and the metal oxides being formed. Also, the actual surface area of exposed metal changes rapidly, producing the appearance of decreasing rate. The very open structure of these specimens greatly reduces the oxidation resistance and is responsible for the relatively large weight loss at 2500°F for the low volume of metal present.

Several trials for combining the various factors learned during this study would be required to provide significant improvements in the strength of the material for a given metal-to-ceramic ratio and could not be accomplished within the limits of this program.

VII CONCLUSIONS

Laminate layer thicknesses below 20 microns are desirable, but could not be achieved by the coating processes evaluated using available sizes of molybdenum and hafnia powders.

Strength of the 93.1 HfO_2 · 4.9 CeO_2 · 2 MgO-Mo macrolaminate composites increases with decreasing particle size and is higher when a range of sizes are used compared to use of single size fractions.

Oxidation resistance of the 93.1 HfO_2 · 4.9 CeO_2 · 2 MgO-Mo increases with decreasing particle size until the laminate structure is destroyed (-200 mesh).

During cutting of laminate particles, the metal phase tends to powder to a greater extent than the ceramic phase, thus variations between size fractions of particles are masked by variations in the metal to ceramic ratio.

A trend toward increased ductility with increased laminate particle size was noted. The sensitivity of molybdenum to impurities and the weakness of the ceramic phase limited ductility to such an extent that a definite conclusion in this area cannot be drawn.

The particle shape study indicated elongated particles oriented parallel to the direction of applied tensile force produce higher tensile strength than cubic or plate-like shapes.

Isostatic pressing produces very random laminate orientation. Warm pressing produces some orientation of laminae perpendicular to the direction of applied force, but to a much lesser degree than hot pressing. Warm extrusion of the particles tends to reduce the size of the laminate particles by shear and orients laminae at the exterior parallel to the direction of extrusion. Particles near the center of the extrusion are more nearly the same starting size and are more randomly oriented.

Lower flexural strength in the randomly oriented isostatically pressed specimens in comparison to the more directionly oriented warm pressed specimens is due to fracture in one phase preferentially over the second phase or to a weak bond between phases. In the 93.1 HfO_2 · 4.9 CeO_2 · 2 MgO-Mo composite the ceramic is the weaker phase.

In the 93.1 HfO_2 • 4.9 CeO_2 • 2 MgO-Mo composite, strength increases at a decreasing rate with metal content; while compressive deformation increases at an increasing rate. Weight loss due to oxidation increases at an increasing rate with metal content.

Fabrication by warm pressing of laminate particles using acrylic binders must be done within a relatively broad, but sharply defined range of pressure and temperature. Complete contact of the macrolaminate particles is needed, but individual particles should not be pressed to the degree that the binder is forced out of them. This seals the body, preventing gases produced during decomposition of the binder from escaping and results in bloating of the part and laminar voids.

Differential shrinkage between the metal and ceramic phases during sintering is critical. It is desirable for the metal phase to shrink more than the ceramic phase, placing the ceramic in compression. Higher shrinkage in the ceramic phase, placing it in tension, produces microcracks reducing the flexural strength. The surface activity of the starting powders, packing density of the powder and heating rate during sintering must be controlled to achieve the desired shrinkage. This has not been completely achieved for the 93.1 HfO_2 • 4.9 CeO_2 • 2 MgO-Mo composite. Control of impurities and sintering atmosphere is also essential, but has not been adequately achieved.

HfO_2 - Mo based systems do not show promise for use in applications requiring extended time periods in oxidizing environments at elevated temperature because of their high oxidation rate. However, work outside of this contract indicates they have potential for use at very high temperatures for short periods of time under highly erosive and oxidizing environments. In this type of application, the molybdenum provides excellent thermal shock resistance to the composite.

VII RECOMMENDATION

Due to the complexity of the 93.1 HfO_2 • 4.9 CeO_2 • 2 MgO-Mo and the susceptibility of molybdenum to embrittlement by impurities, it is not a good model system for evaluating the macrolaminate particle concept. It has no foreseeable potential for long time exposures at elevated temperatures in oxidizing environment which is a major objective for this program. Therefore, it is recommended that this material system not be used for further study of the macrolaminate particle concept.

This program has shown indications of effects of particle size, shape and orientation on the properties of the composite. It would be desirable to use a model system where the metal phase is known to be ductile and has a lower yield

strength than the ultimate strength of the ceramic phase. Impact strength, thermal shock resistance, oxidation rates and tensile properties for the following systems should be compared: (1) Powder blend of the metal and ceramic, (2) near cubical laminate particles, (3) laminates cut to produce needle-like particles with length to thickness dimensions in the range of 100 to 1. With currently known techniques the three types of particles can be prepared which have identical metal-to-ceramic ratio, powder, reactivity, and binder content. Prior to selecting a model system, basic information on variations in diffusion rates between the metal and the ceramic should be evaluated to avoid difficulties with void formation at the interface between the phases (Kirkendall effect).

Demonstration of advantages of the laminate system should then lead to a detailed investigation of compositional improvements to achieve a reliable structural material for use at temperatures above 2000°F in oxidizing environments for extended periods of time.

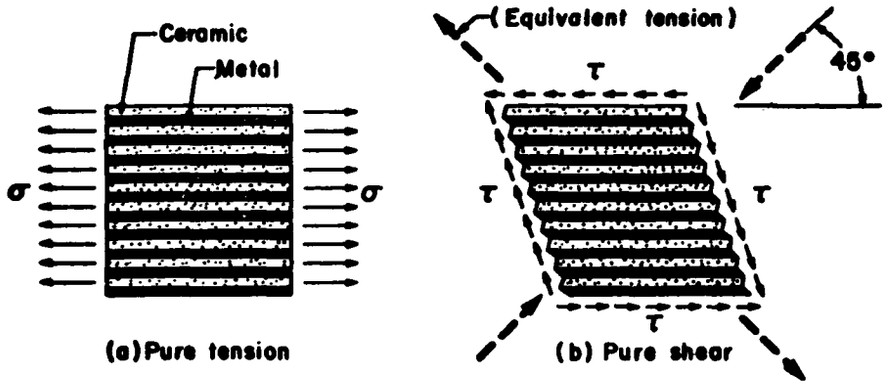

Slip of a laminated element (schematic)

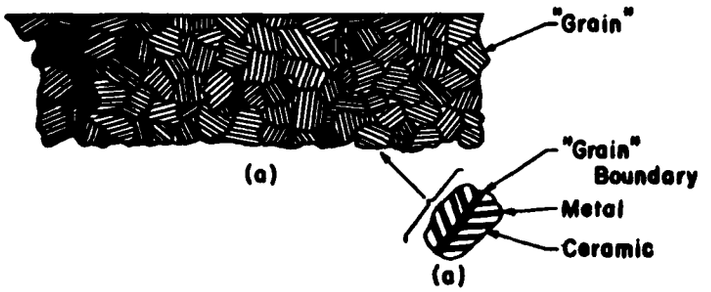

Schematic drawing of cross-section (magnified) through randomly laminated material

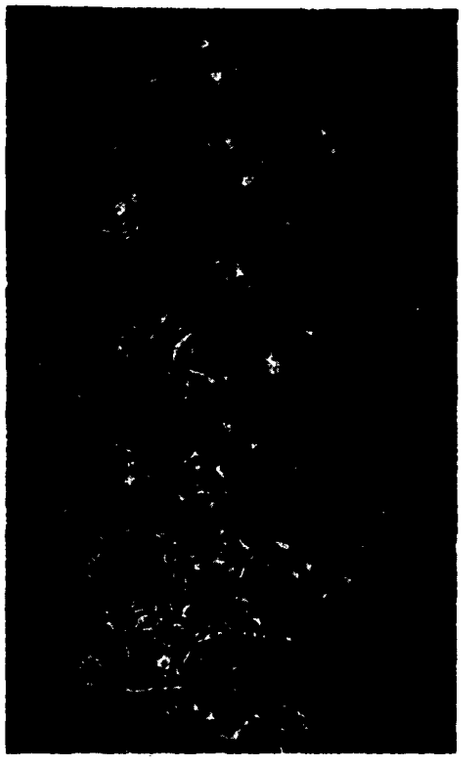

POLISHED SECTION

FIGURE 1 - MACROLAMINATE PARTICLE COMPOSITE SYSTEM

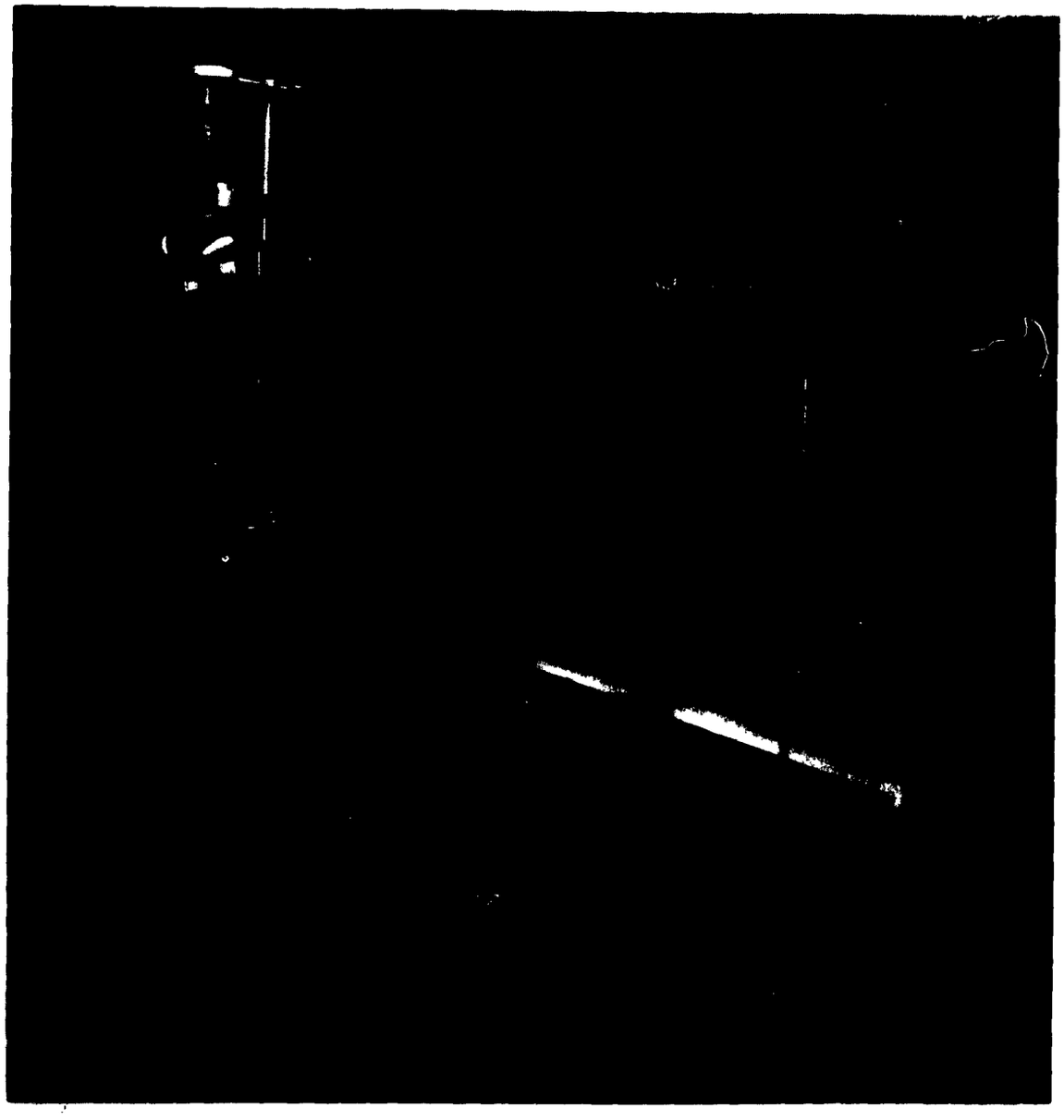

FIGURE 2 APPARATUS FOR PARTICLE SIZE SEPARATION

MOLYBDENUM POWDER
AS PURCHASED

MOLYBDENUM POWDER
OVERSI ZE

MOLYBDENUM POWDER
BEING USED

FI GURE 3 MOLYBDENUM POWDER BEFORE AND AFTER SI ZI NG

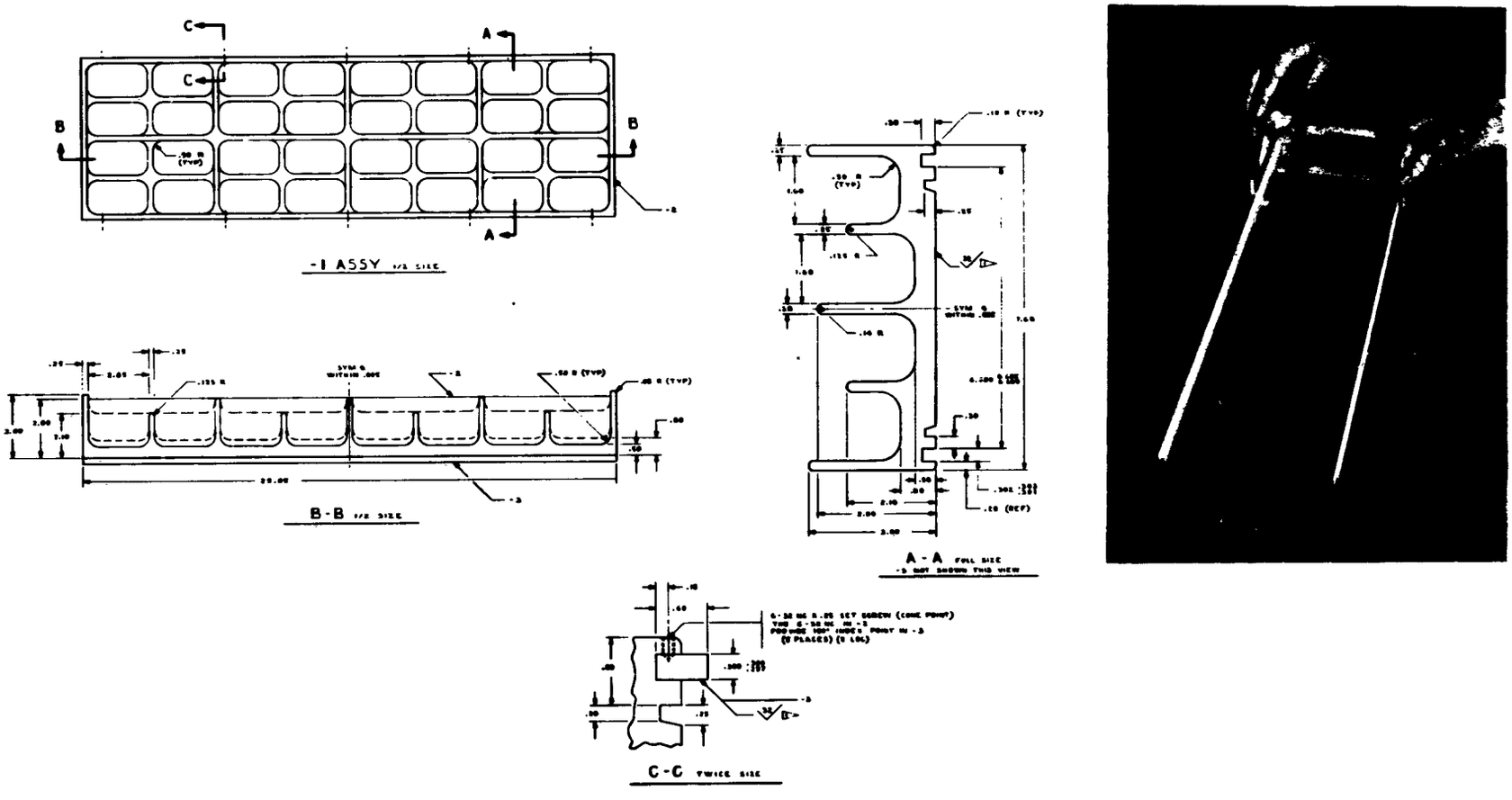

FIGURE 4 - DRAWKNIFE COATING FIXTURE

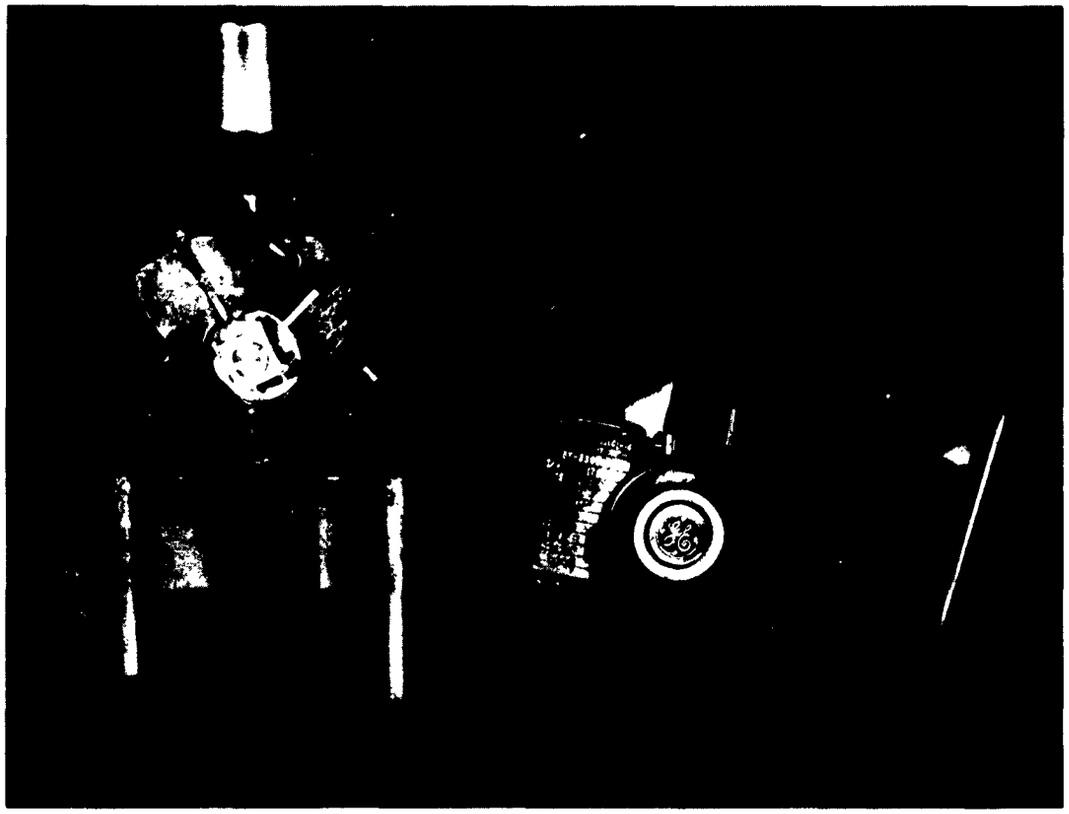

FIGURE 5 - WILEY MILL USED FOR CUTTING LAMINATE SHEET TO FORM LAMINATE PARTICLES

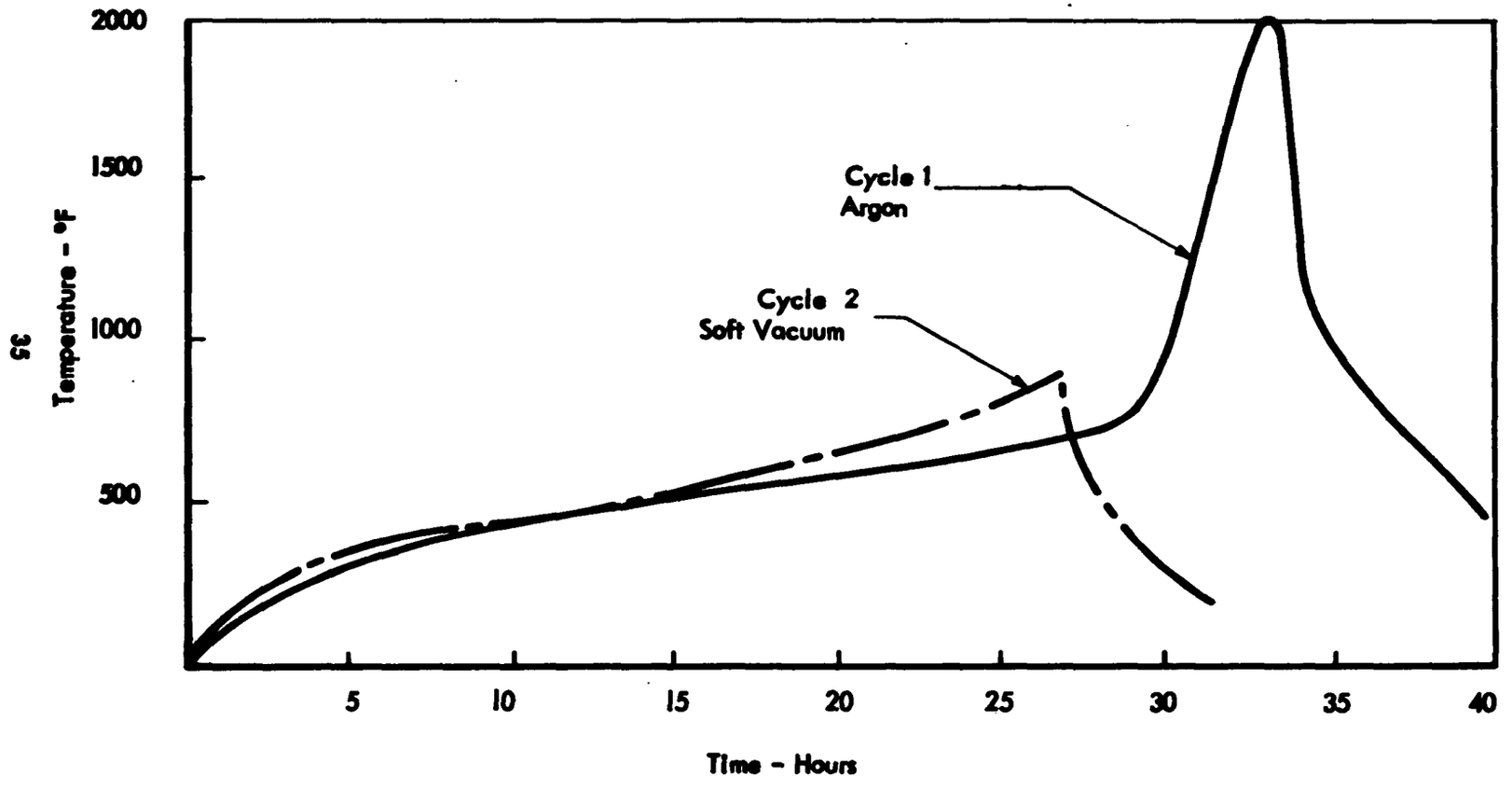

FIGURE 6 - TIME-TEMPERATURE CYCLES USED FOR REMOVING ORGANIC BINDER FROM SPECIMENS AND/OR PARTICLES

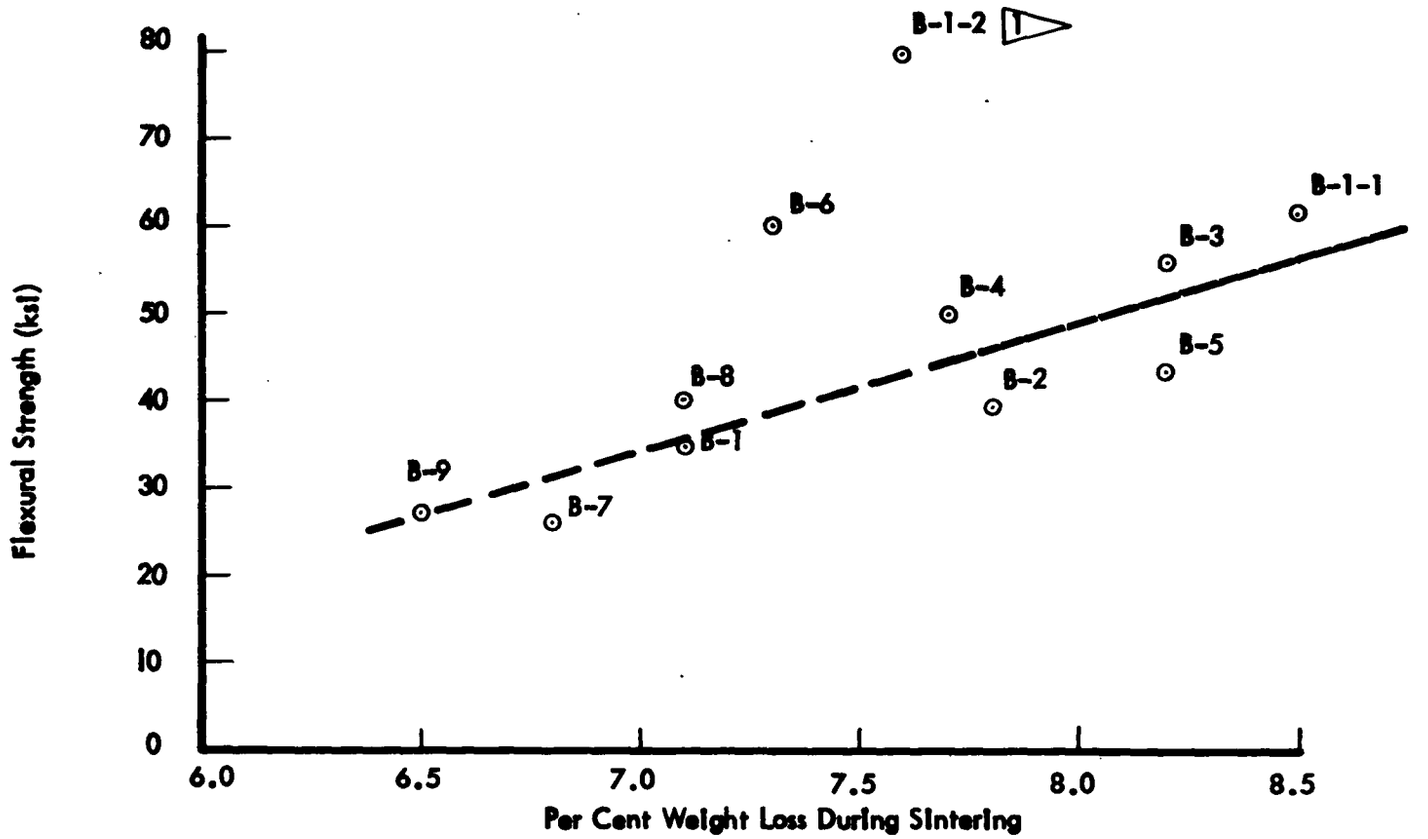

Only specimen with layer thickness below .001

FIGURE 7 FLEXURAL STRENGTH vs. WEIGHT LOSS FOR SPECIMENS PREPARED FROM LAMINATE SHEETS MADE BY KNIFE COATING HAVING VARIATIONS IN LAYER THICKNESS AND METAL-TO-CERAMIC RATIO

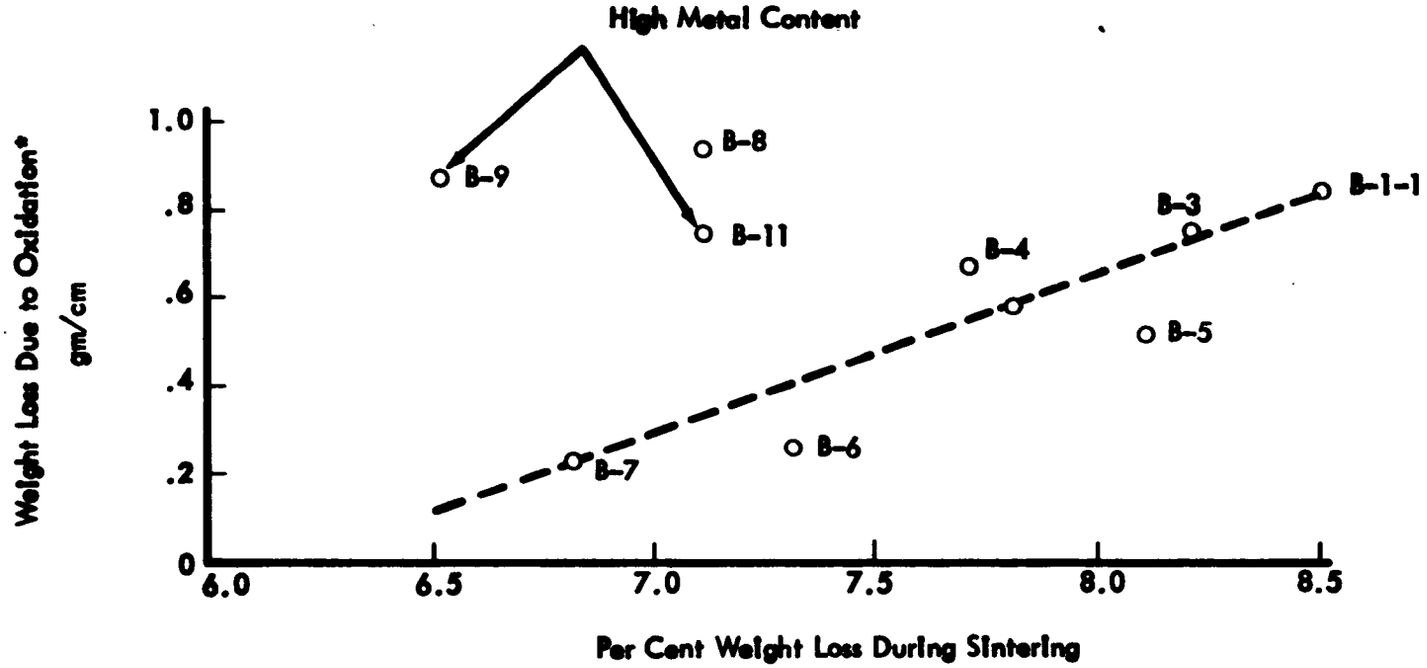

* Weight loss after 24 hours at 2500°F in air

FIGURE 8 WEIGHT LOSS DUE TO OXIDATION VS WEIGHT LOSS DURING SINTERING FOR SPECIMENS PREPARED FROM LAMINATE SHEETS MADE BY KNIFE COATING HAVING VARIATIONS IN LAYER THICKNESS AND METAL-TO-CERAMIC RATIO.

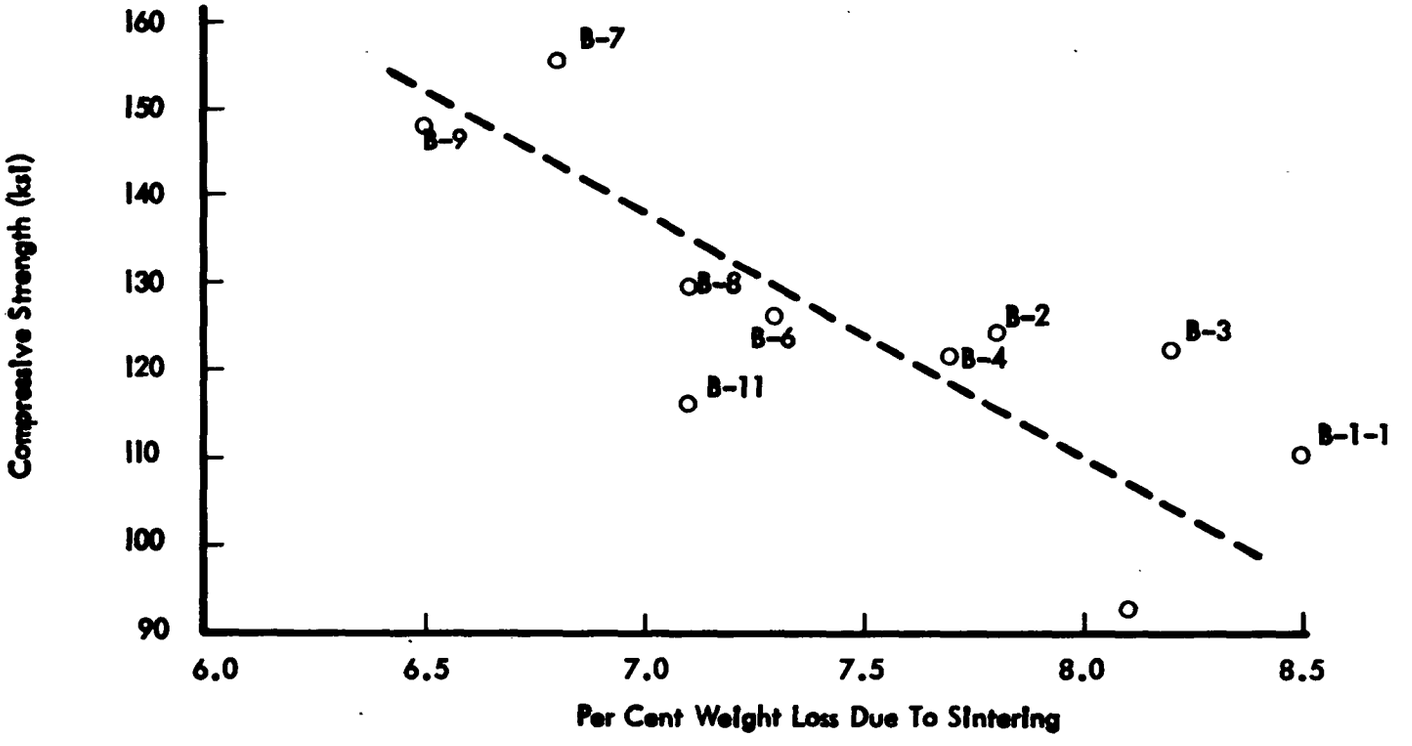

FIGURE 9 COMPRESSIVE STRENGTH VS WEIGHT LOSS DURING SINTERING FOR SPECIMENS PREPARED FROM LAMINATE SHEETS MADE BY KNIFE COATING HAVING VARIATIONS IN LAYER THICKNESS AND METAL-TO-CERAMIC RATIO

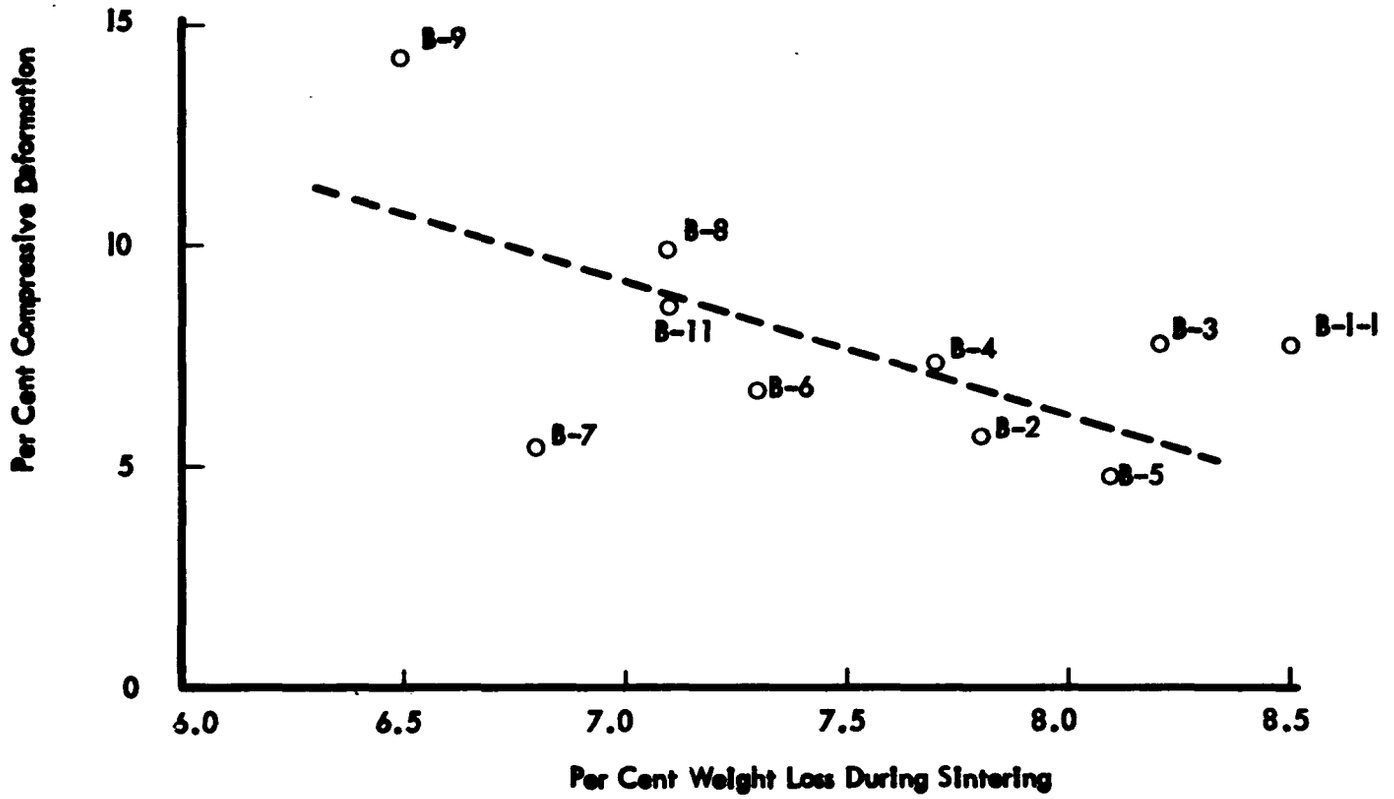

FIGURE 10 PER CENT COMPRESSIVE DEFORMATION VS PER CENT WEIGHT LOSS DURING SINTERING FOR SPECIMENS PREPARED FROM LAMINATE SHEETS MADE BY KNIFE COATING HAVING VARIATIONS IN LAYER THICKNESS AND METAL-TO-CERAMIC RATIO

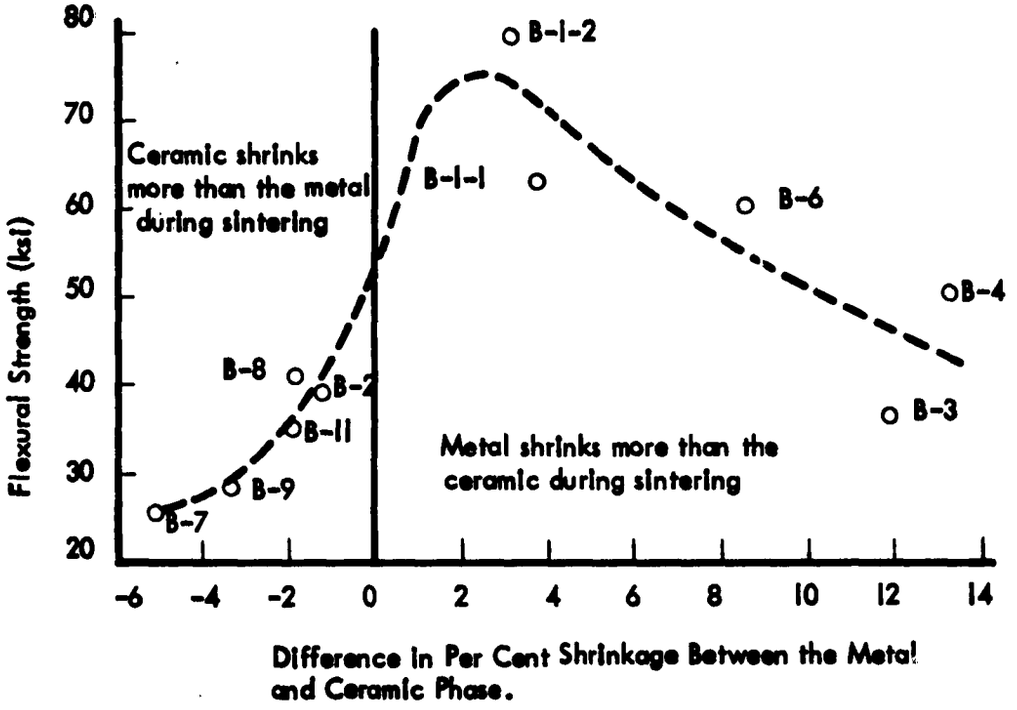

FIGURE 11 - FLEXURAL STRENGTH VS DIFFERENCE IN PERCENT SHRINKAGE BETWEEN THE METAL AND CERAMIC PHASE

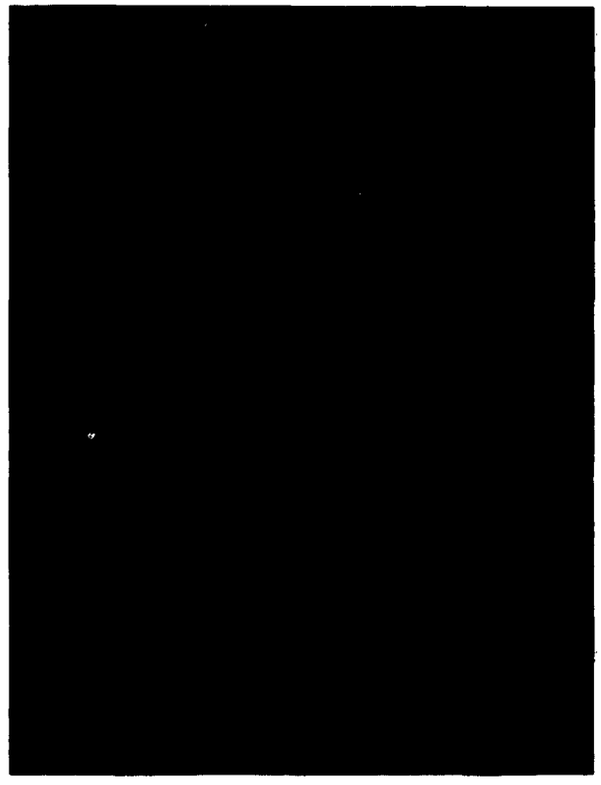

FIGURE 12 · PHOTOMICROGRAPH OF MICROCRACKS IN THE CERAMIC PHASE OF A 93.1 HfO_2·4.9 CeO_2· 2 MgO–Mo MACROLAMINATE PARTICLE COMPOSITE RESULTING FROM THE CERAMIC PHASE SHRINKING MORE THAN THE METAL PHASE DURING SINTERING

Specimen from laminate
Sheet No. B-14 (160X)
Wgt. Loss During Sintering 8.5%
Flexural Strength 63 ksi

Specimen from laminate
Sheet No. B-4 (160X)
Wgt. Loss During Sintering 7.7%
Flexural Strength 50.3 ksi

Specimen from laminate
Sheet No. B-9 (160X)
Wgt. Loss During Sintering 6.5%
Flexural Strength 27.5 ksi

FIGURE 13- PHOTOMICROGRAPHS OF SPECIMEN FROM LAMINATE SHEET WHICH PRODUCED THE HIGHEST, INTERMEDIATE AND LOWEST PERCENT WEIGHT LOSS DURING SINTERING

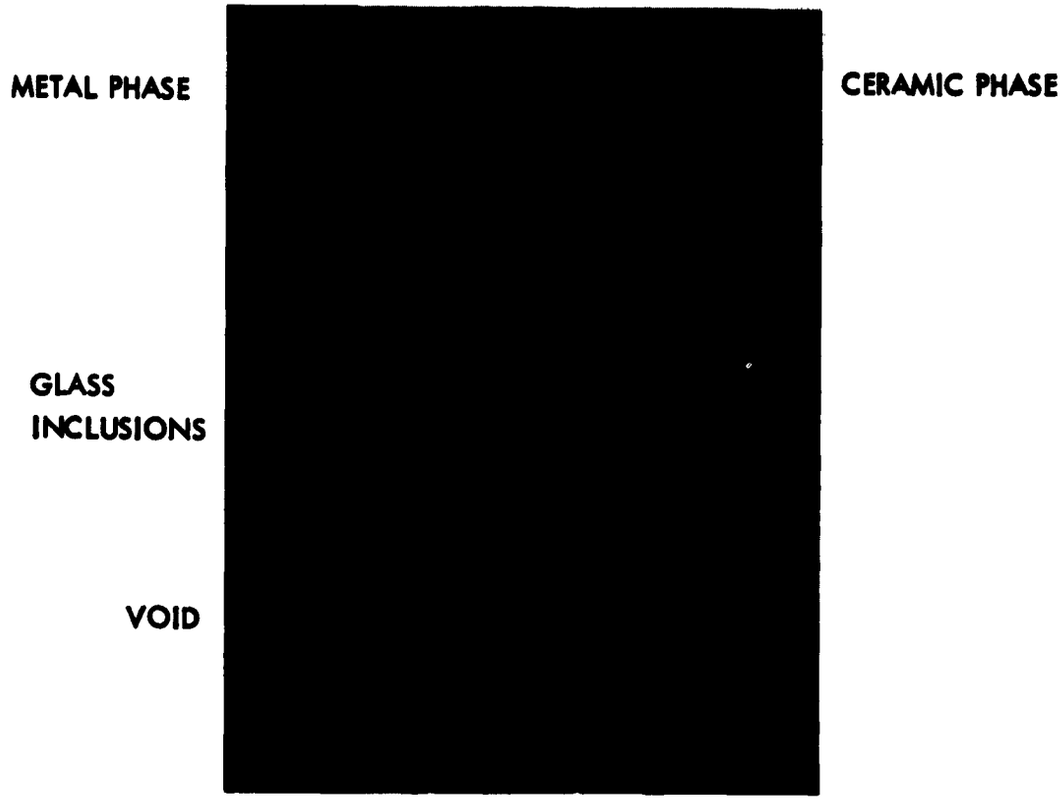

FIGURE 14 - PHOTOMICROGRAPH SHOWING GLASS INCLUSION IN THE CERAMIC PHASE OF THE 93.1 HfO_2·4.9 CeO_2· 2 MgO-Mo MACROLAMINATE PARTICLE COMPOSITE

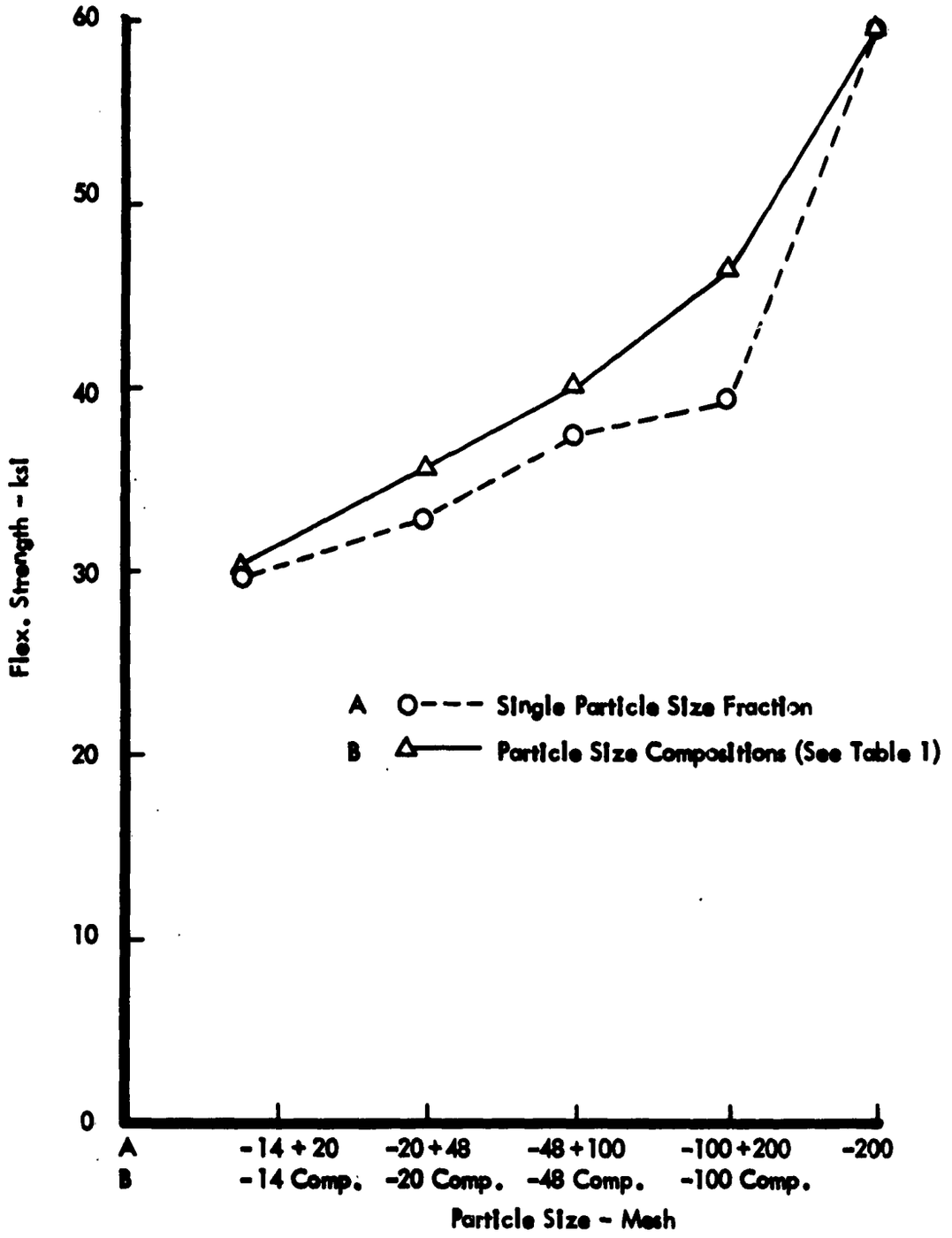

FIGURE 15 - FLEXURAL STRENGTH PLOTTED AS A FUNCTION OF PARTICLE SIZE.

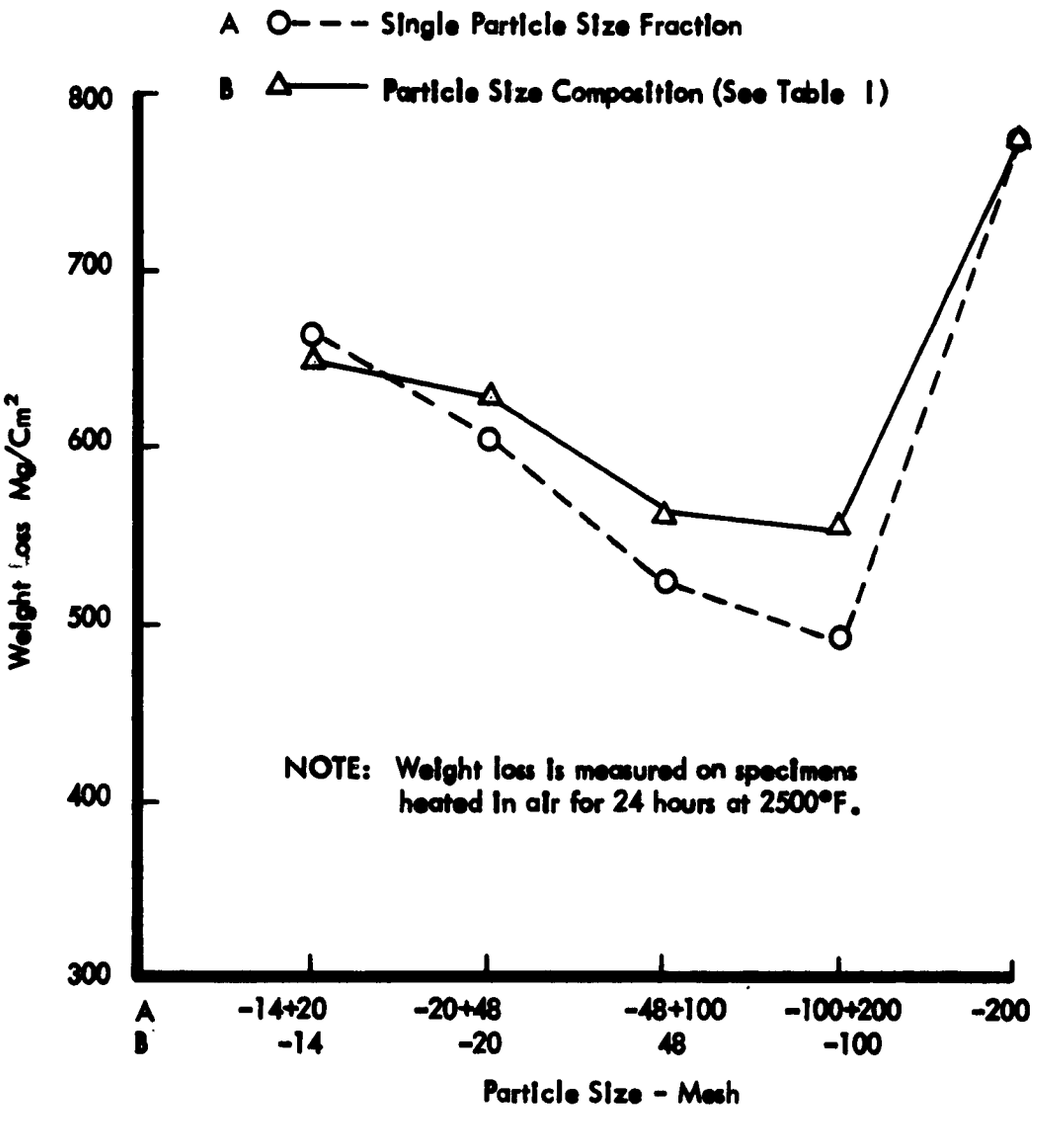

FIGURE 16 - WEIGHT LOSS DUE TO OXIDATION AS A FUNCTION OF PARTICLE SIZE

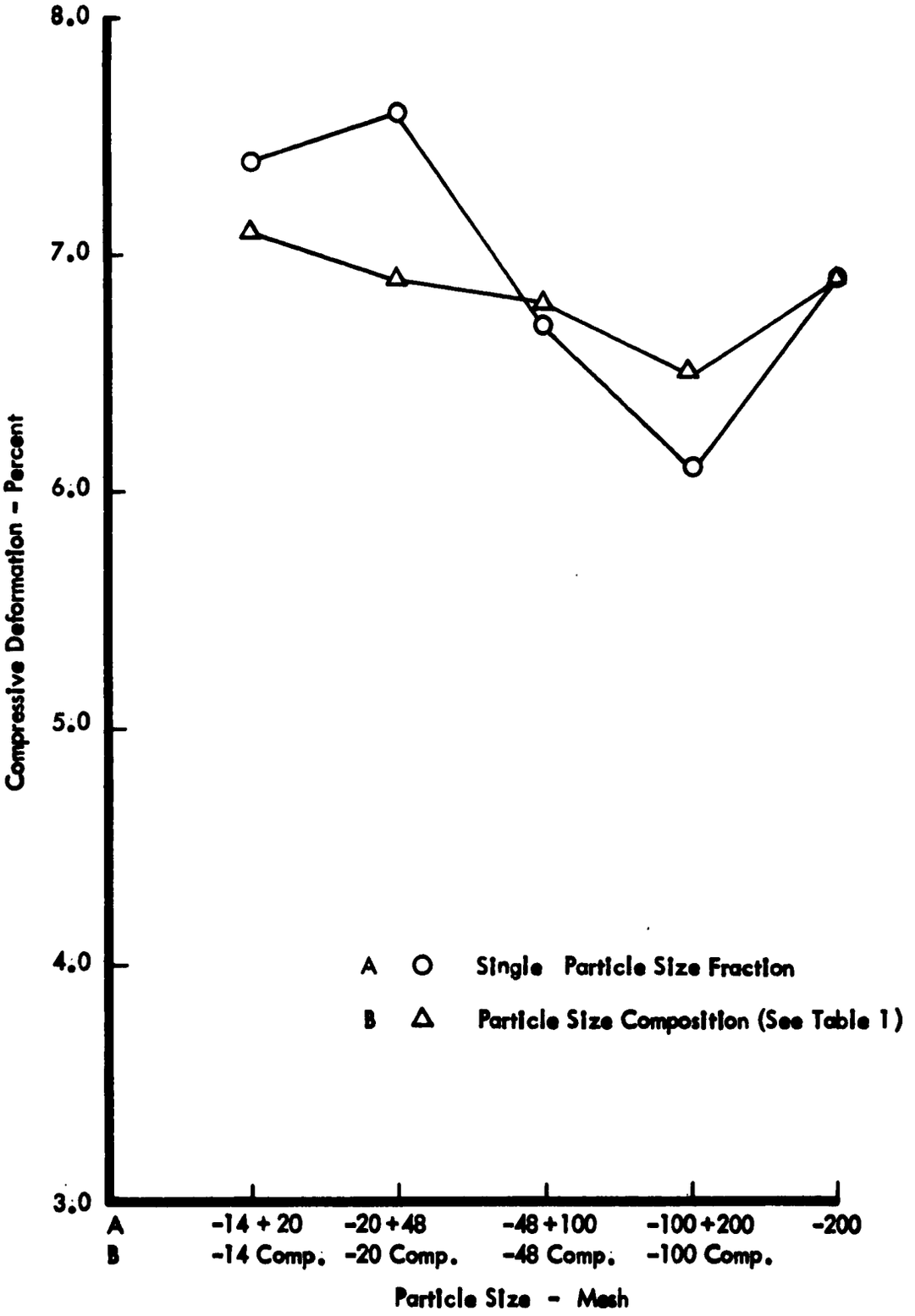

FIGURE 17 - COMPRESSIVE DEFORMATION PLOTTED AS A FUNCTION OF PARTICLE SIZE

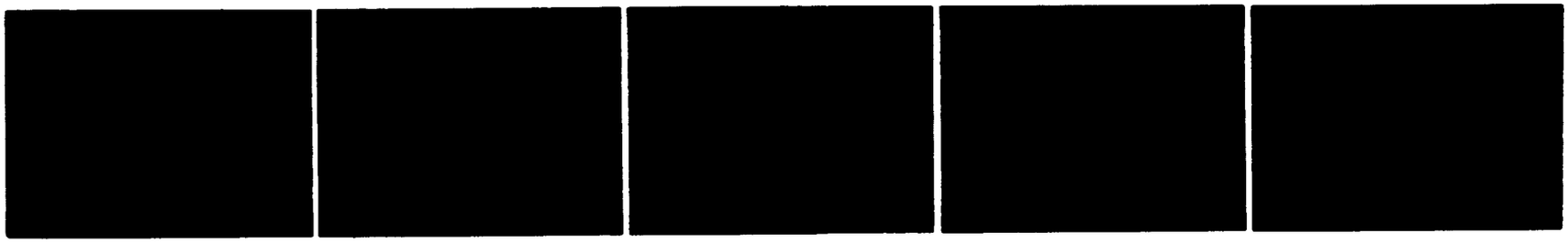

-14 + 20 -20 + 48 -48 + 100 -100 + 200 -200

Single Particle Size Fraction

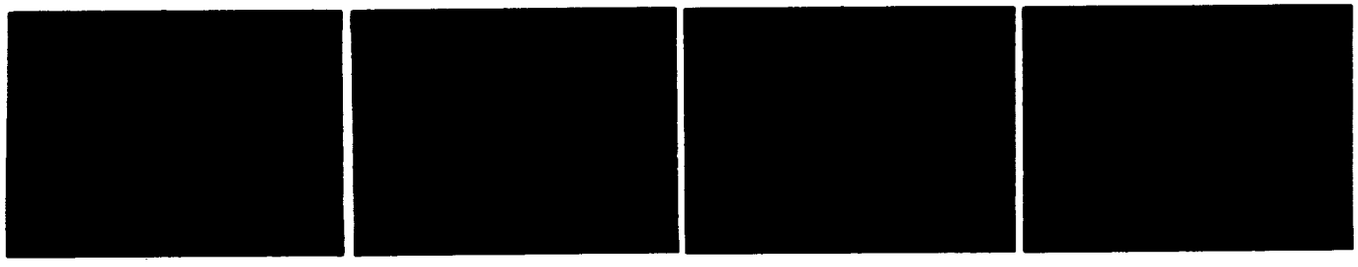

-14 -20 -48 -100

Particle Size Composition (See Table IX)

NOTE: Polished surface parallel to pressing.
Original microphotograph taken at 10X

FIGURE 18 - EFFECT OF PARTICLE SIZE ON THE MACROSTRUCTURE OF THE 93.1 HfO_2 • 4.9 CeO_2 • 2 MgO MACROLAMINATE PARTICLE COMPOSITE

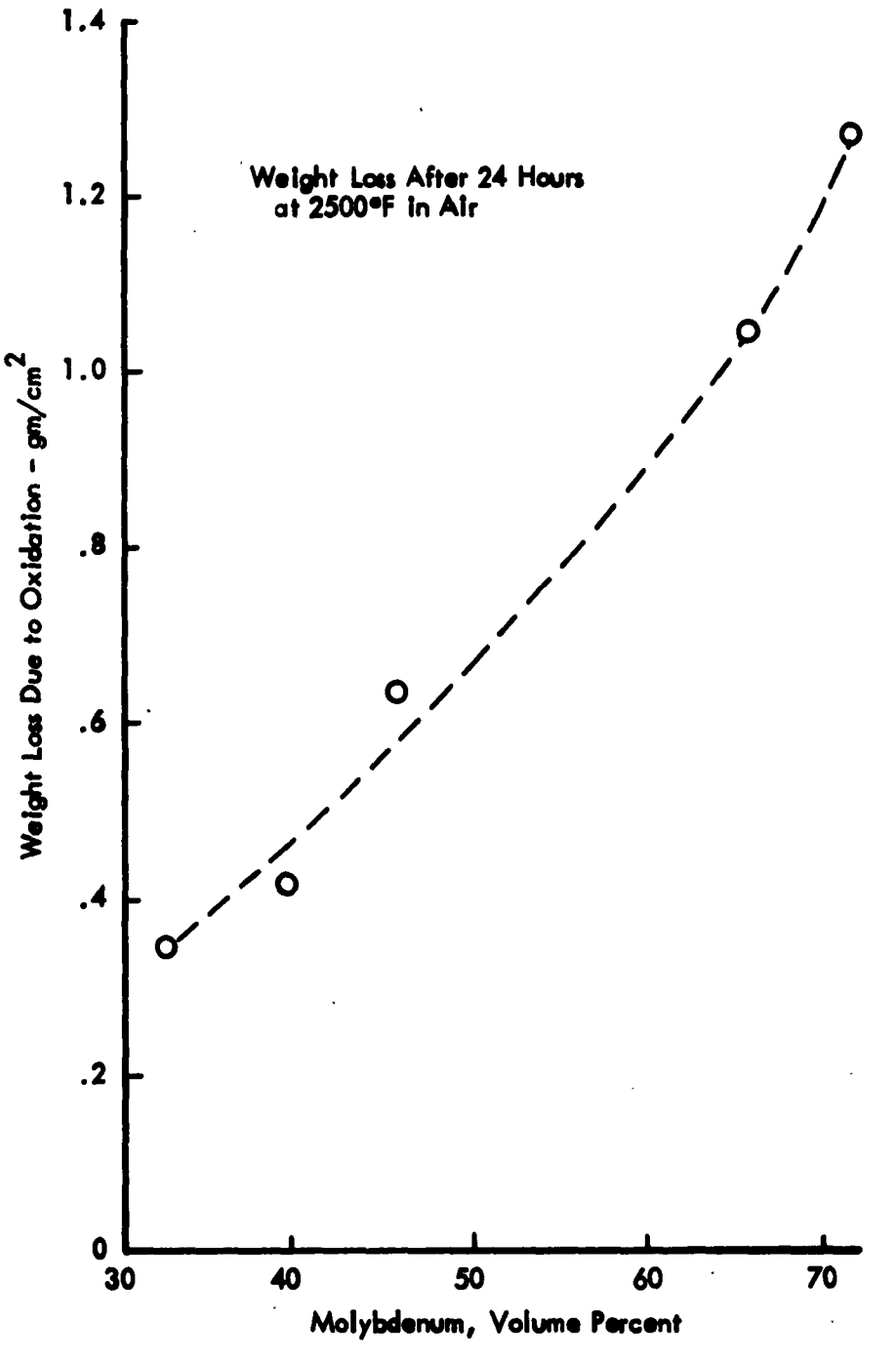

FIGURE 19- WEIGHT LOSS DUE TO OXIDATION OF 93.1 HfO_2·4.9 CeO_2·2 MgO-Mo MACROLAMINATE PARTICLE COMPOSITES AS A FUNCTION OF METAL CONTENT

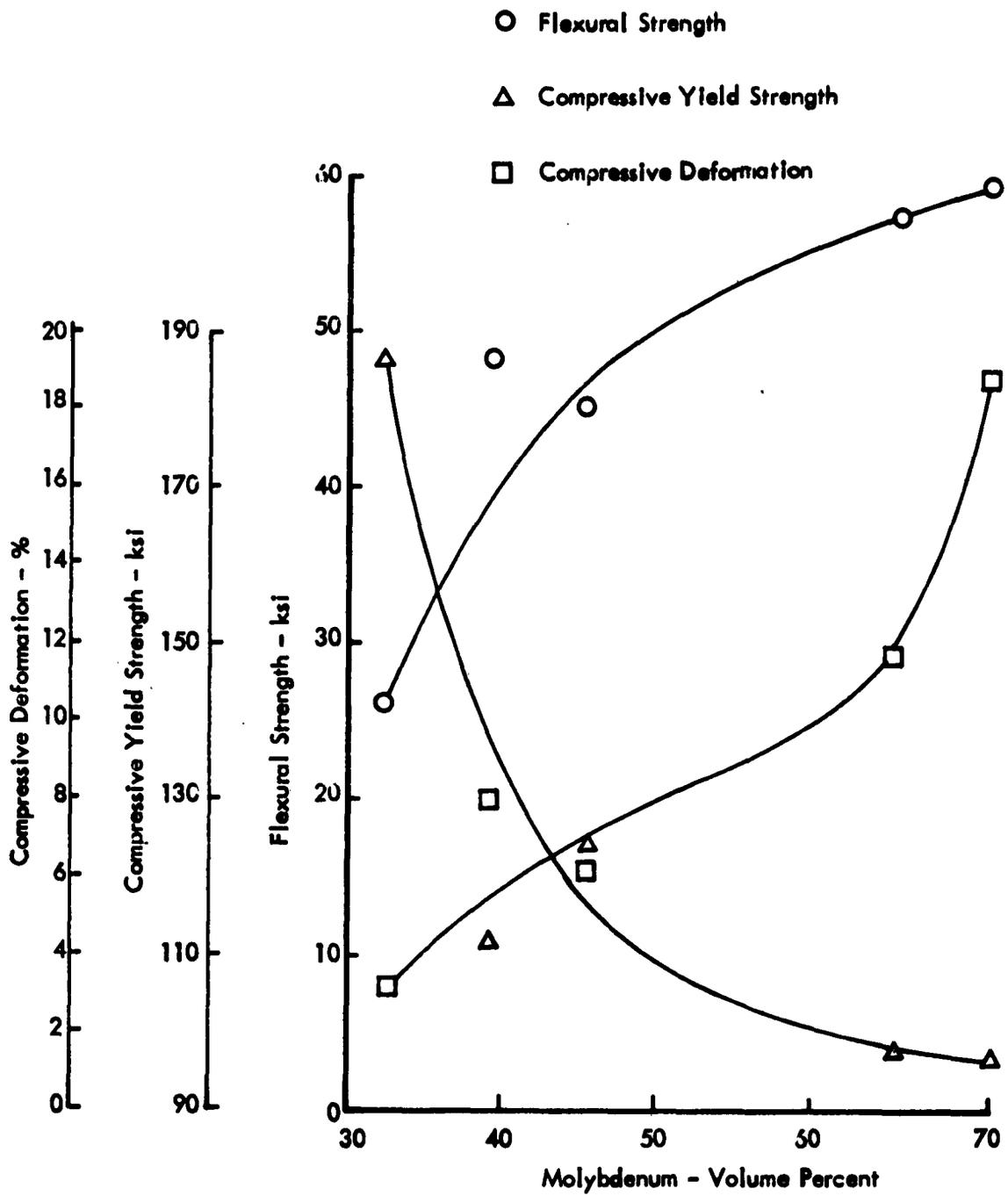

FIGURE 20- PROPERTIES OF 93.1 HfO_2·4.9 CeO_2·2 MgO–Mo MACROLAMINATE PARTICLE COMPOSITES AS A FUNCTION OF METAL CONTENT

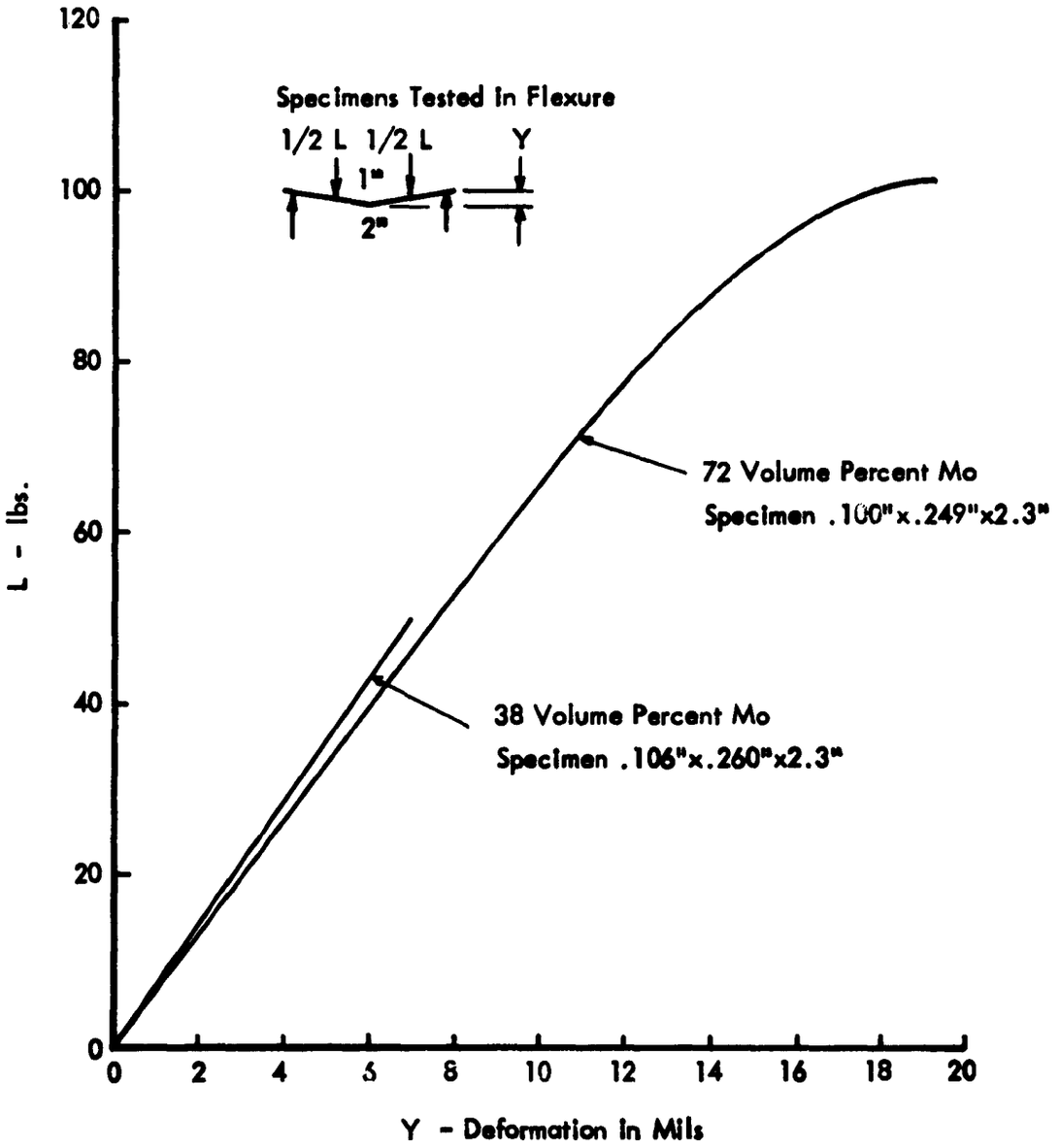

FIGURE 21- FLEXURAL LOAD DEFORMATION CURVES FOR 93.1 HfO_2· 4.9 CeO_2·2 MgO-Mo MACROLAMINATE COMPOSITES

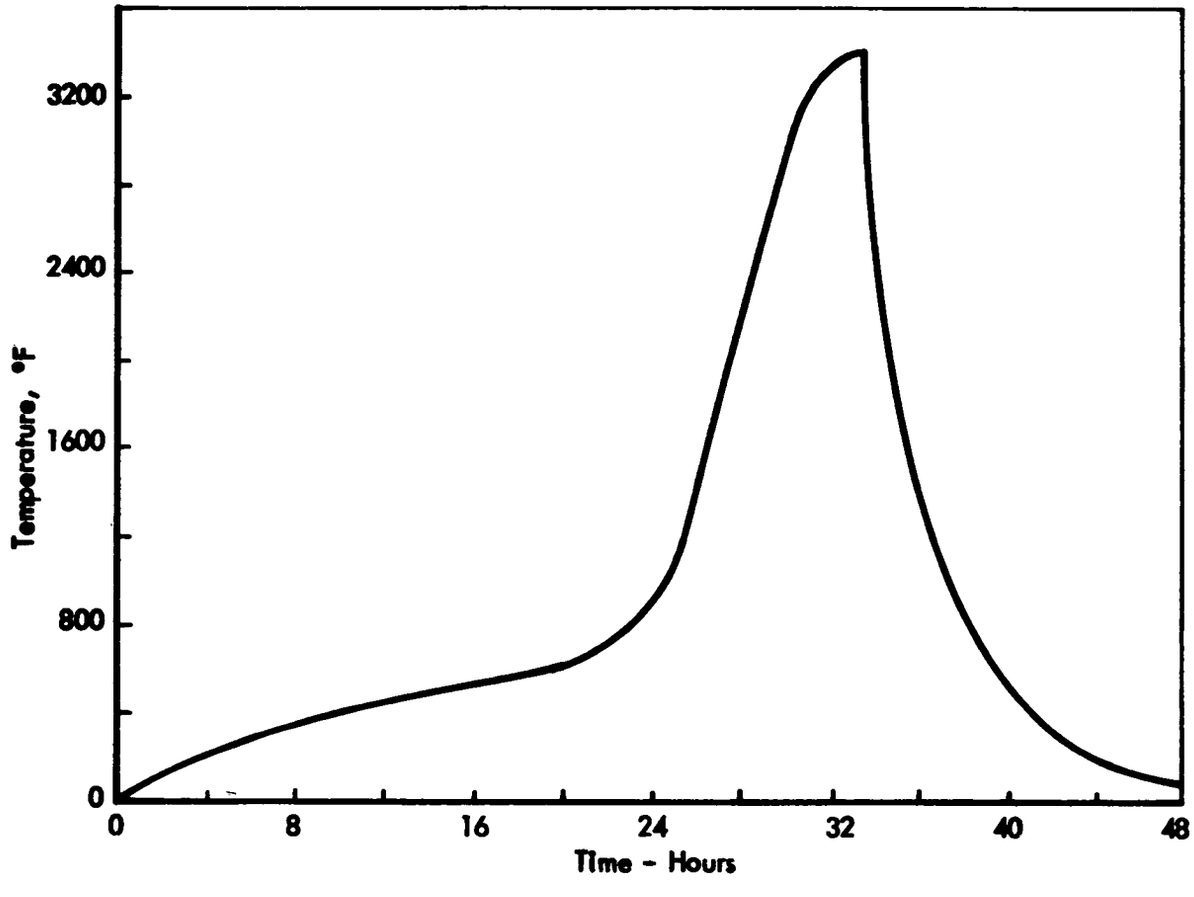

FIGURE 22 TIME-TEMPERATURE CYCLE USED TO SINTER TEST PARTS FOR EVALUATING WARM PRESSING PARAMETERS

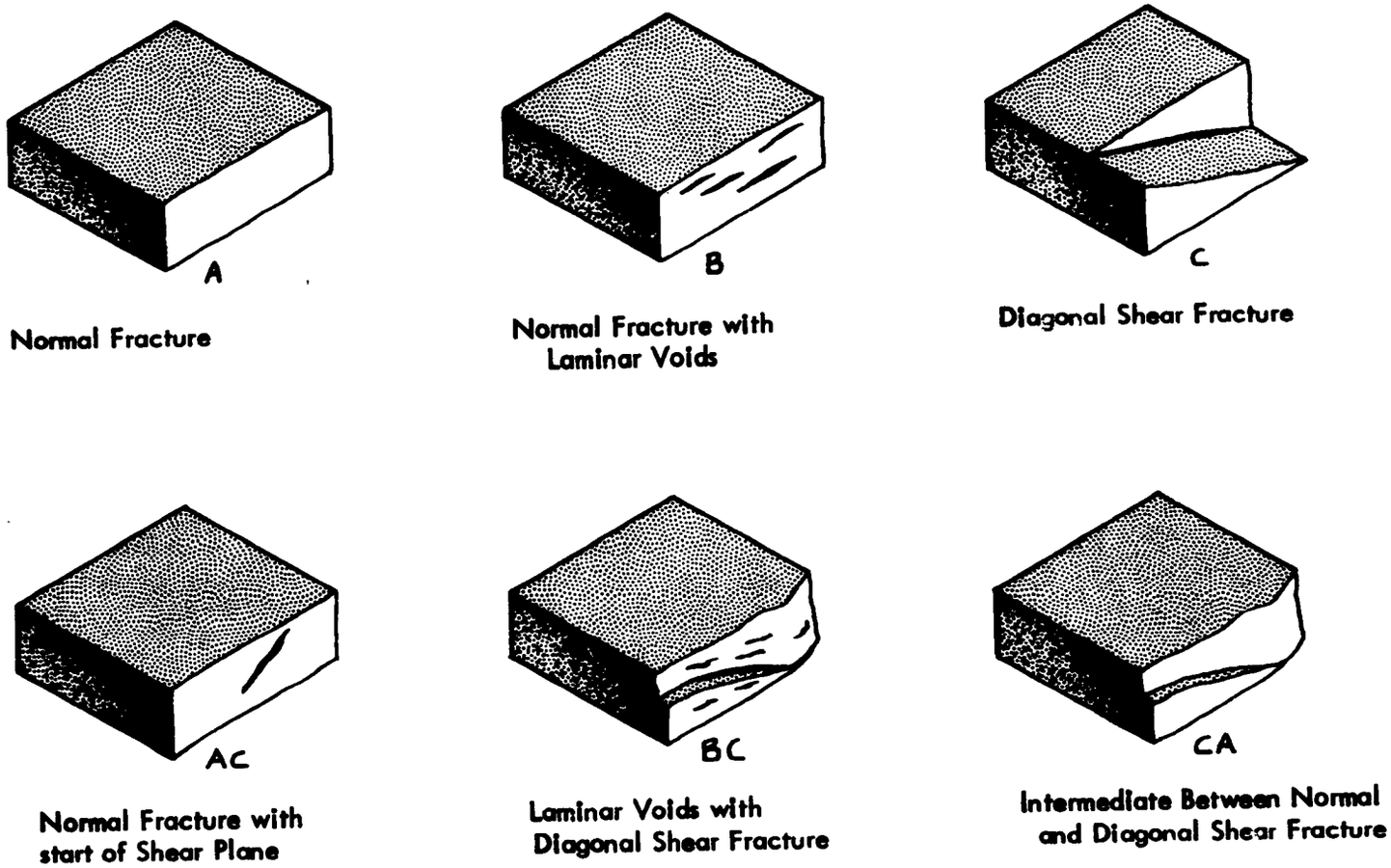

See Table XII for Pressing Parameter producing the various types of fracture surfaces
Specimens were broken in flexure using 4 point loading

FIGURE 23 - TYPES OF FRACTURE OBTAINED IN SPECIMENS WARM PRESSED AT DIFFERENT LEVELS OF TEMPERATURE AND PRESSURE

Pressed in Steel Die
12.5 ksi 150°F

Isostatically Pressed
15 ksi at 250°F
Particles with Binder

Isostatically Pressed
40 ksi R.T. Particles
H.T. at 1500°F to
eliminate binder

Isostatically Pressed 40.0 ksi
Particles H.T. at 2000°F to
eliminate binder

Original photos taken at 100X

FIGURE 24 - STRUCTURE OF WARM PRESSED AND ISOSTATICALLY PRESSED MACROLAMINATE PARTICLE COMPOSITES

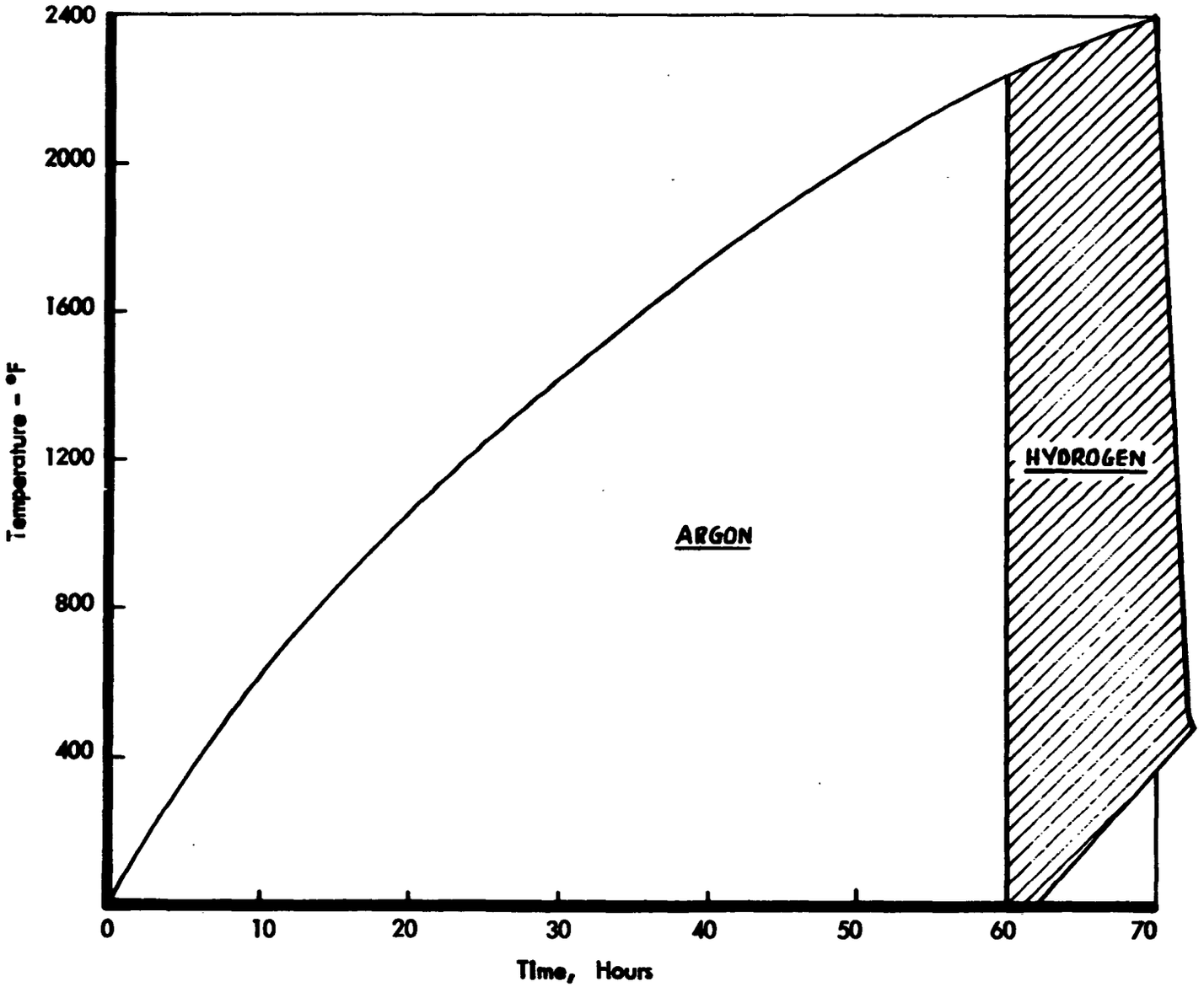

FIGURE 25- TIME-TEMPERATURE CYCLE USED FOR POST-HEAT- TREATING HOT PRESSED SPECIMENS

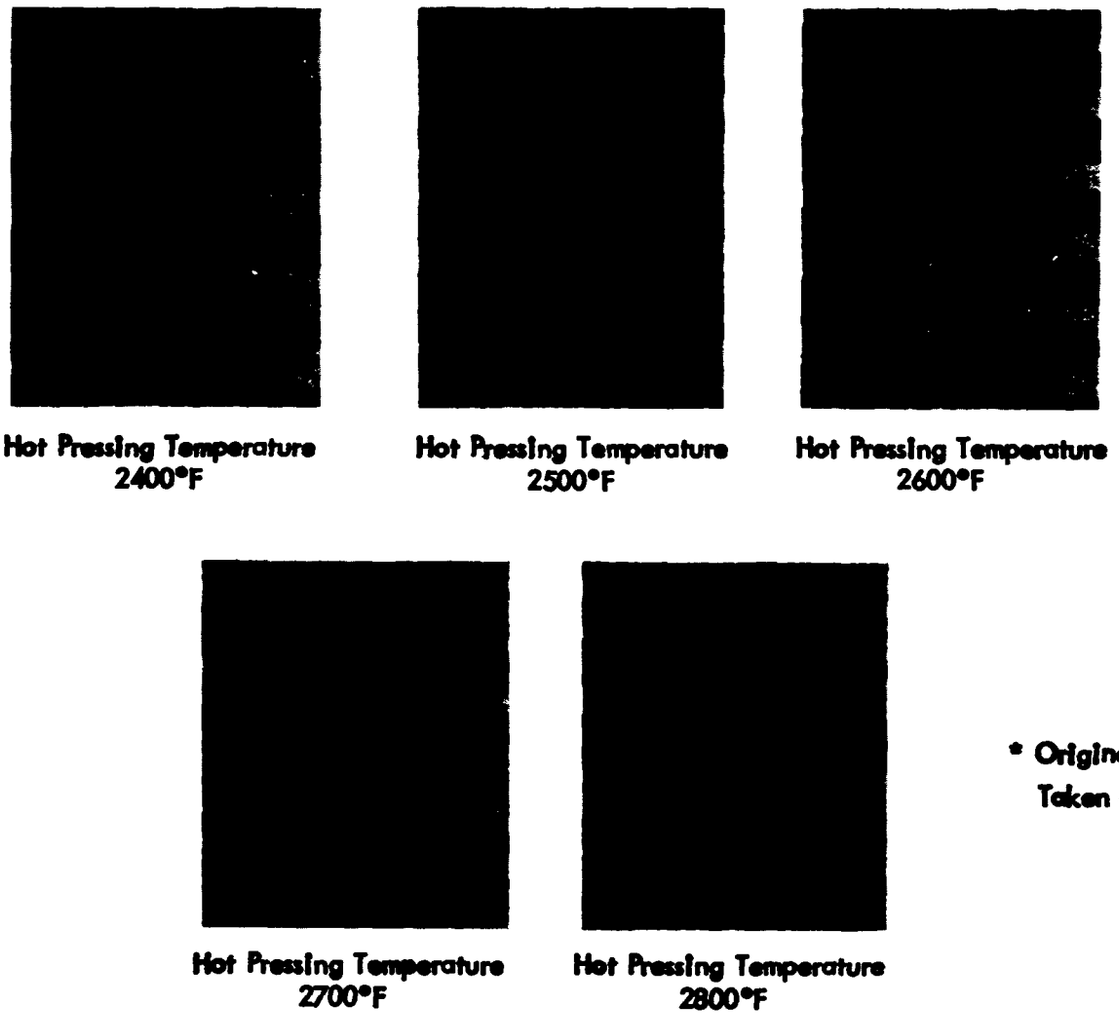

* Original Microphotographs Taken at 500x

FIGURE 26- MICROSTRUCTURE OF 93.1 HfO_2 • 4.9 CeO_2 • 2 MgO–Mo MACROLAMINATE PARTICLE COMPOSITE SPECIMENS HOT PRESSED AT DIFFERENT TEMPERATURES

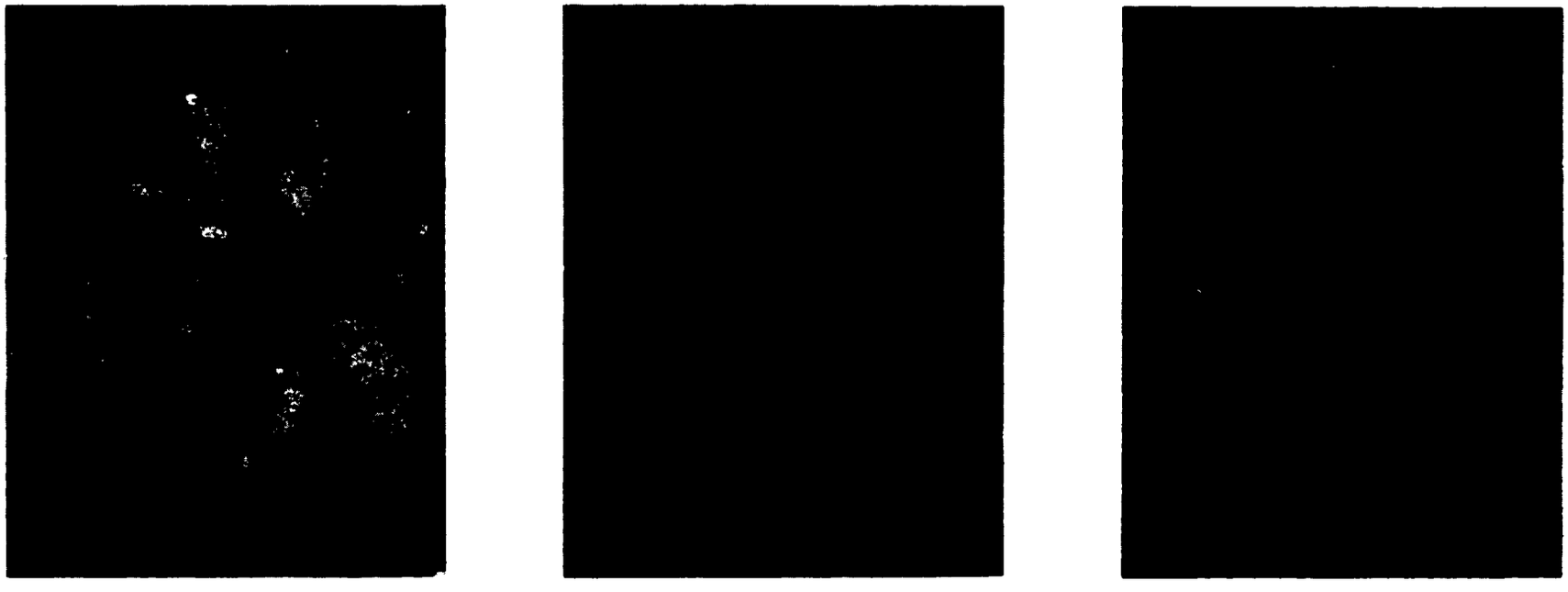

Warm Pressed and
Sintered 3400°F
12 Hours

Hot Pressed
2600°F, 4ksi, 1 hr.

Hot Pressed
2600°F, 4ksi, 1 hr.
PHT 2400°F, H_2

Original Pictures Taken at 500X

FIGURE 28 - COMPARISON OF MICROSTRUCTURES PRODUCED BY HOT PRESSING AND WARM PRESSING

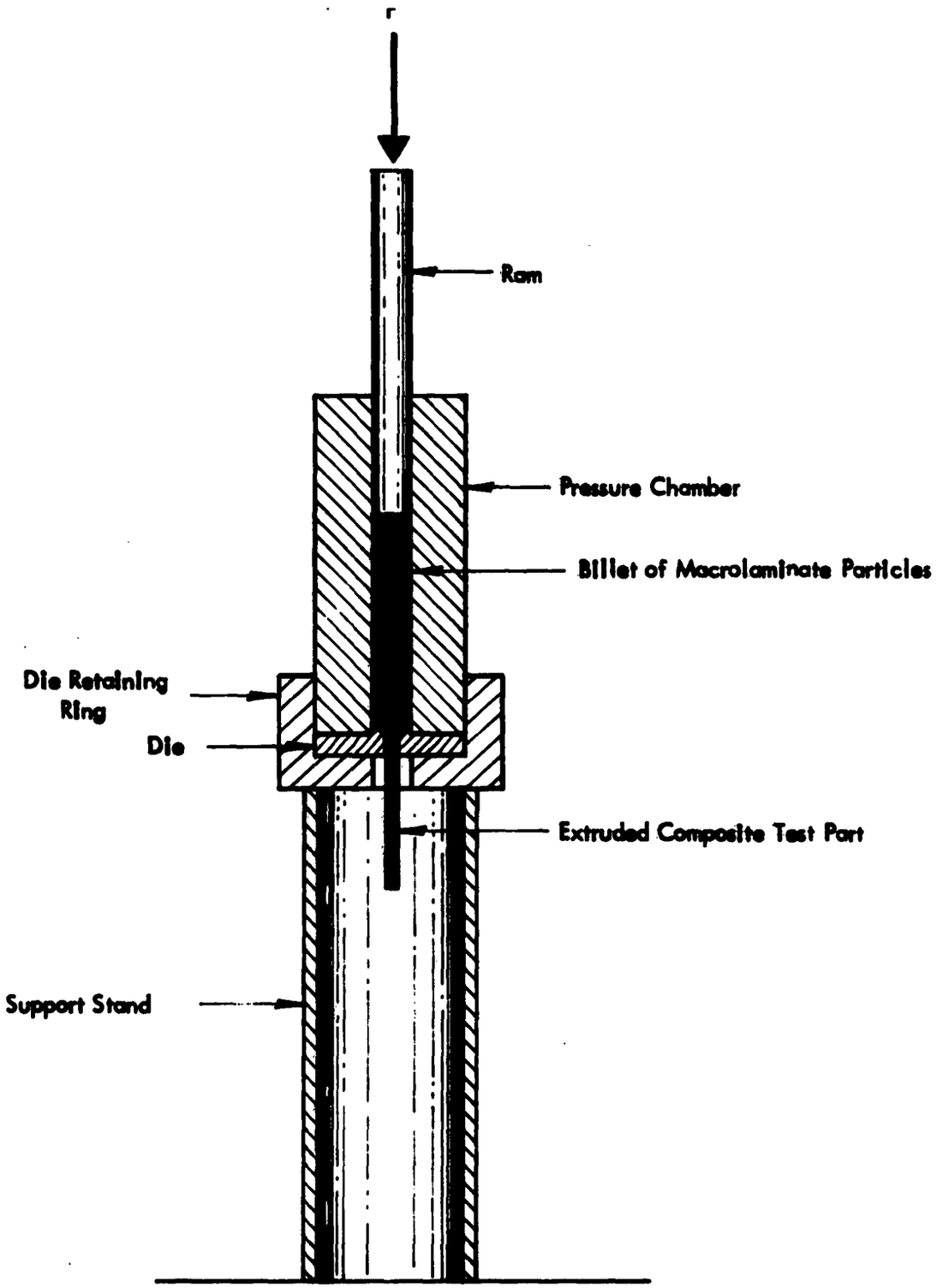

FIGURE 30 - SCHEMATIC OF EXTRUSION FIXTURES

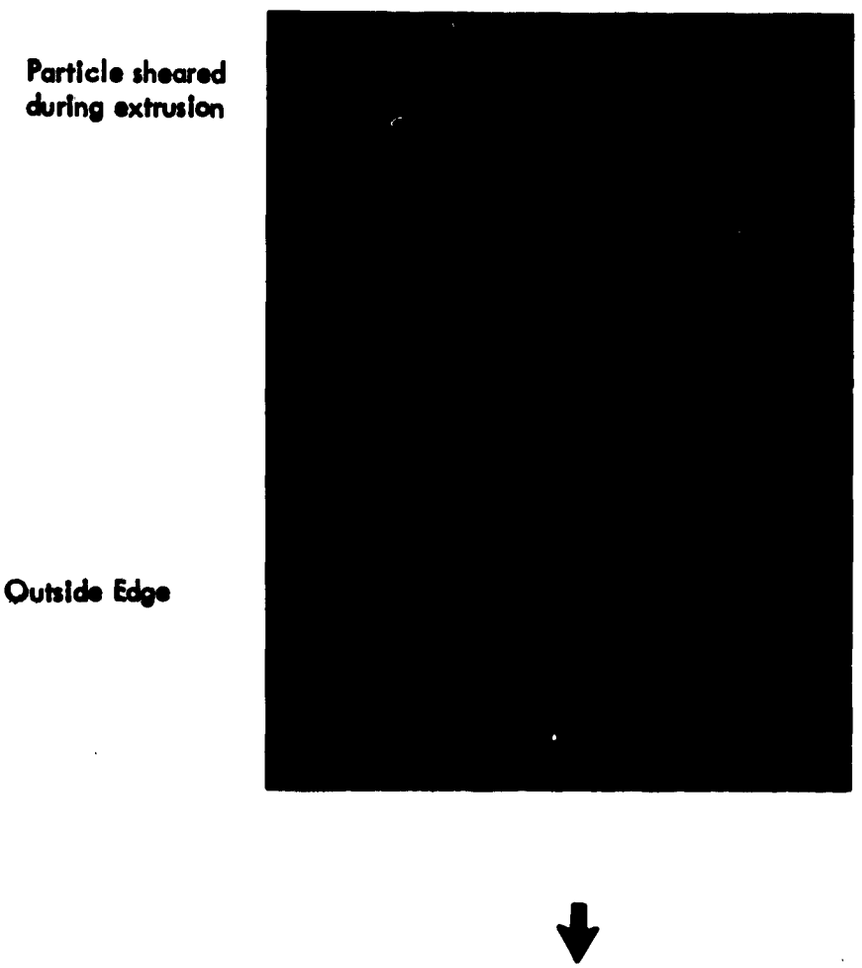

FIGURE 31 - STRUCTURE OF A WARM EXTRUDED MACROLAMINATE COMPOSITE MATERIAL

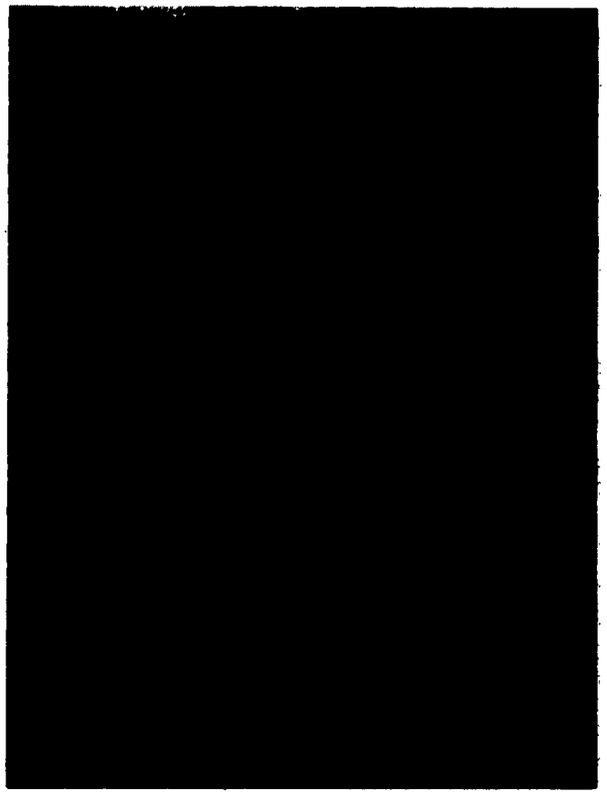

FIGURE 32 - CROSS SECTION OF AN EXTRUDED MACROLAMINATE COMPOSITE SHOWING CRACKS CAUSED BY DRAG

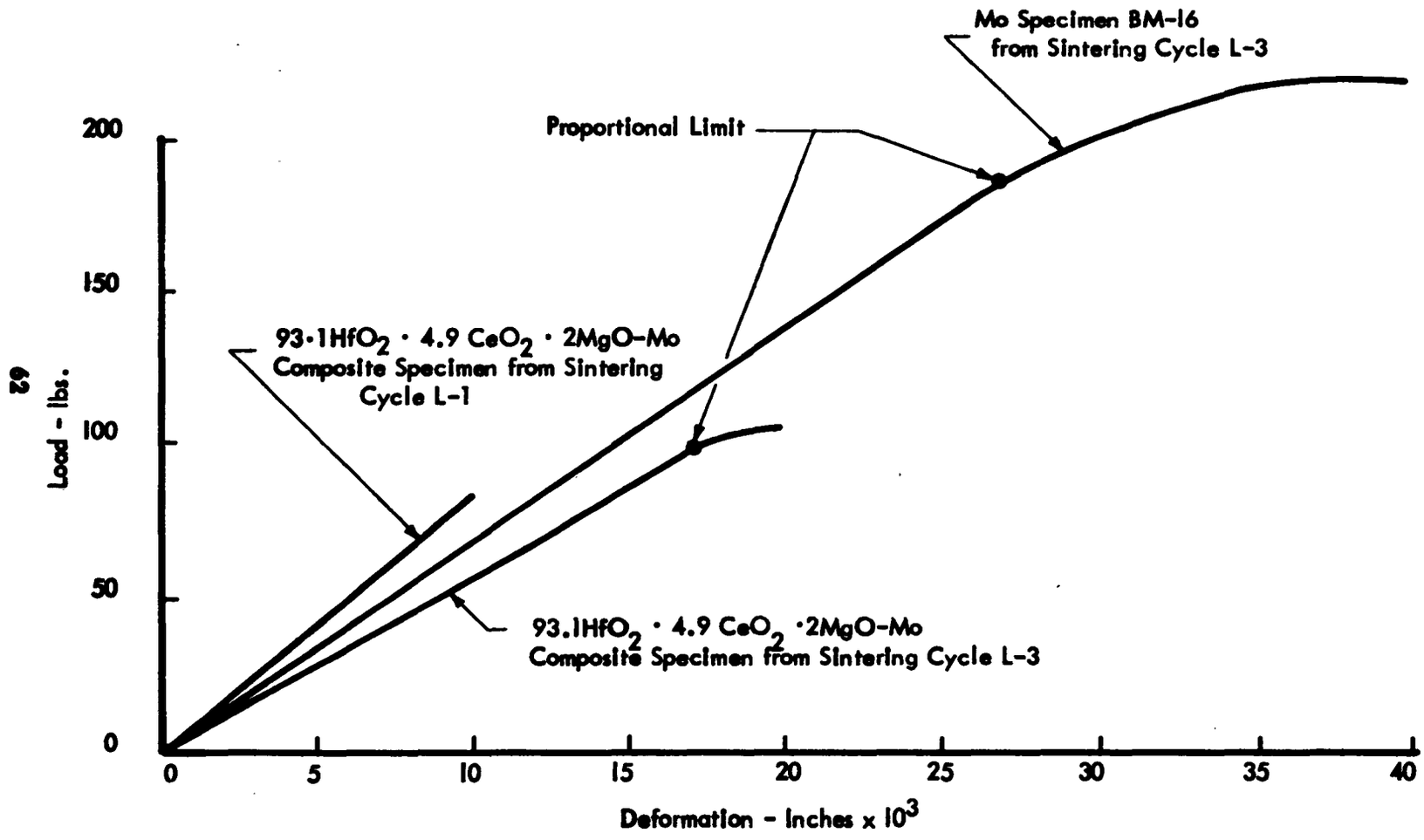

FIGURE 33 - LOAD DEFORMATION CURVES FOR MACROLAMINATE COMPOSITES AND MOLYBDENUM SHOWING DIFFERENCES IN TYPES OF FAILURE FROM THE SINTERING STUDY

Sintering Cycle L-1

Sintering Cycle L-2

Sintering Cycle L-3

Sintering Cycle L-4

Sintering Cycle L-5

Sintering Cycle L-6

Sintering Cycle L-7

Sintering Cycle L-8

Sintering Cycle L-9

FIGURE 34 - MICROSTRUCTURE OF 93.1 HfO_2· 4.9 CeO_2· 2 MgO-Mo MACROLAMINATE COMPOSITES SINTERED USING CYCLES L-1 THROUGH L-9 FOR A GRECO LATIN DESIGN EXPERIMENT

Sintering Cycle L-1

Sintering Cycle L-2

Sintering Cycle L-3

Sintering Cycle L-4

Sintering Cycle L-5

Sintering Cycle L-6

Sintering Cycle L-7

Sintering Cycle L-8

Sintering Cycle L-9

FIGURE 35 - MICROSTRUCTURE OF MOLYBDENUM SINTERED USING CYCLES L-1 THROUGH L-9 FOR A GRECO LATIN DESIGN EXPERIMENT

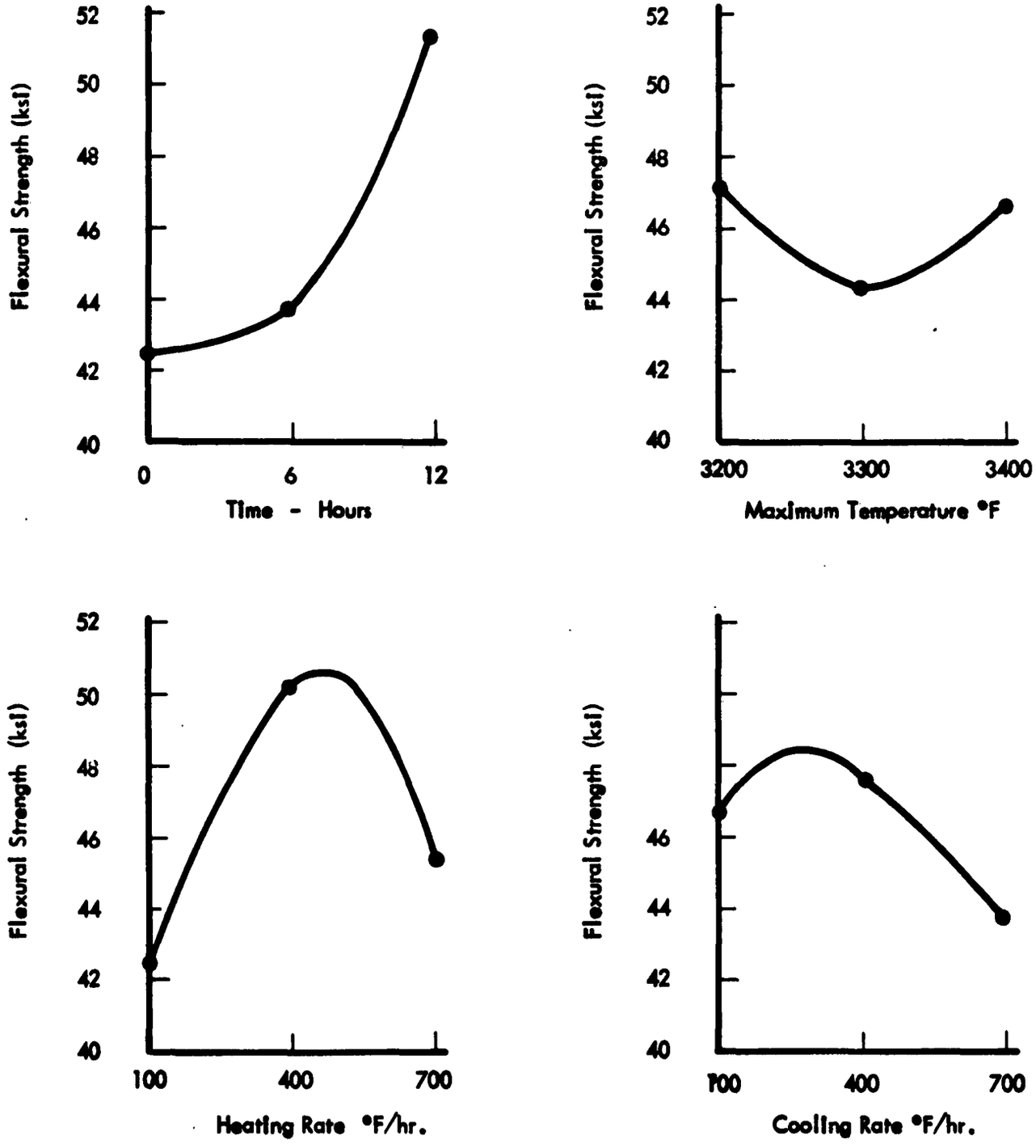

FIGURE 36 PLOTS OF THE LEAST SQUARES ESTIMATES FOR FLEXURAL STRENGTH AS FUNCTIONS OF SINTERING PARAMETERS IN WHICH THE EFFECT OF ALL PARAMETERS OTHER THAN THE ONE PLOTTED HAVE BEEN AVERAGED

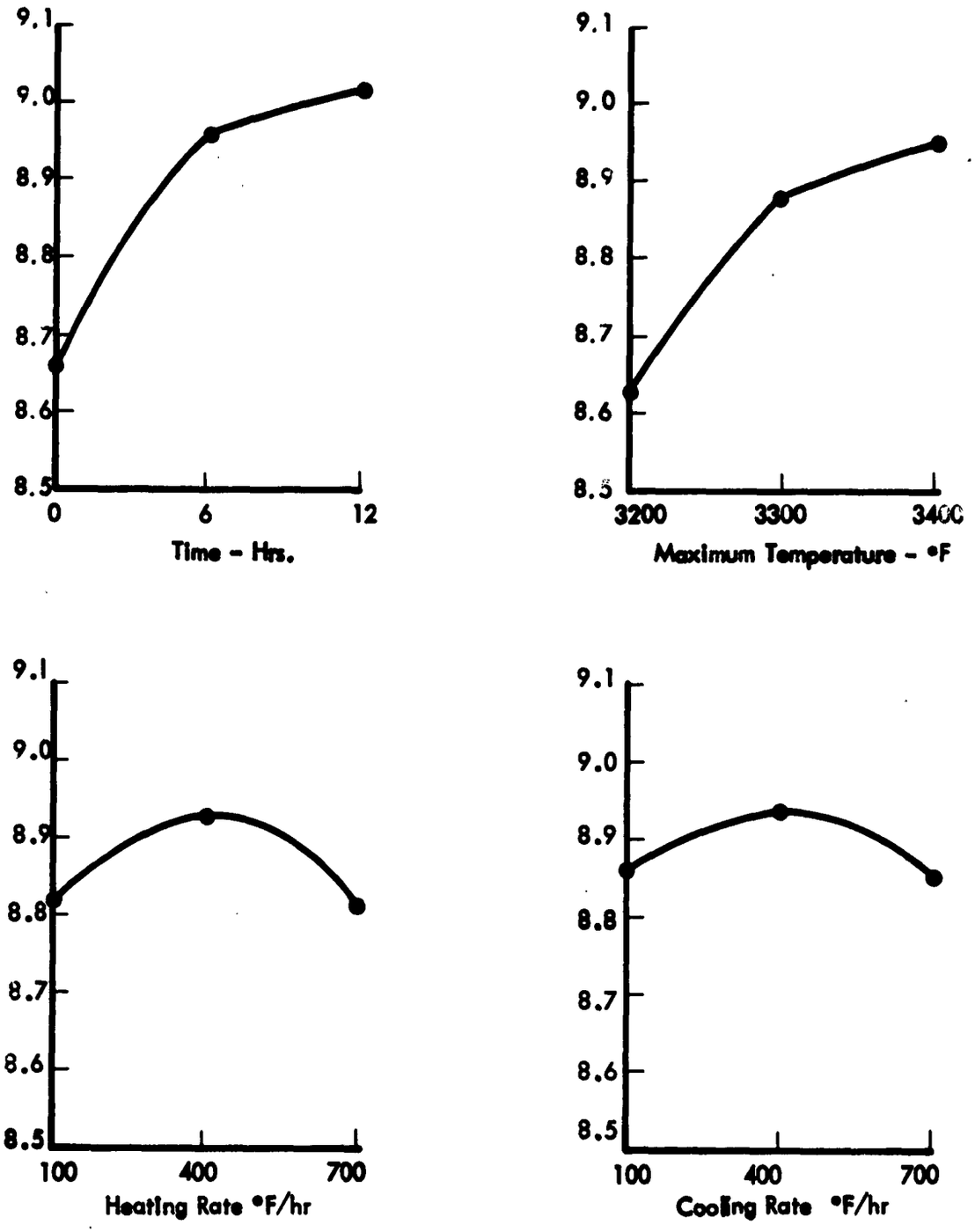

FIGURE 37- PLOTS OF THE LEAST SQUARES ESTIMATES OF DENSITY AS A FUNCTION OF SINTERING PARAMETERS IN WHICH THE EFFECTS OF ALL PARAMETERS OTHER THAN THE ONE PLOTTED HAVE BEEN AVERAGED.

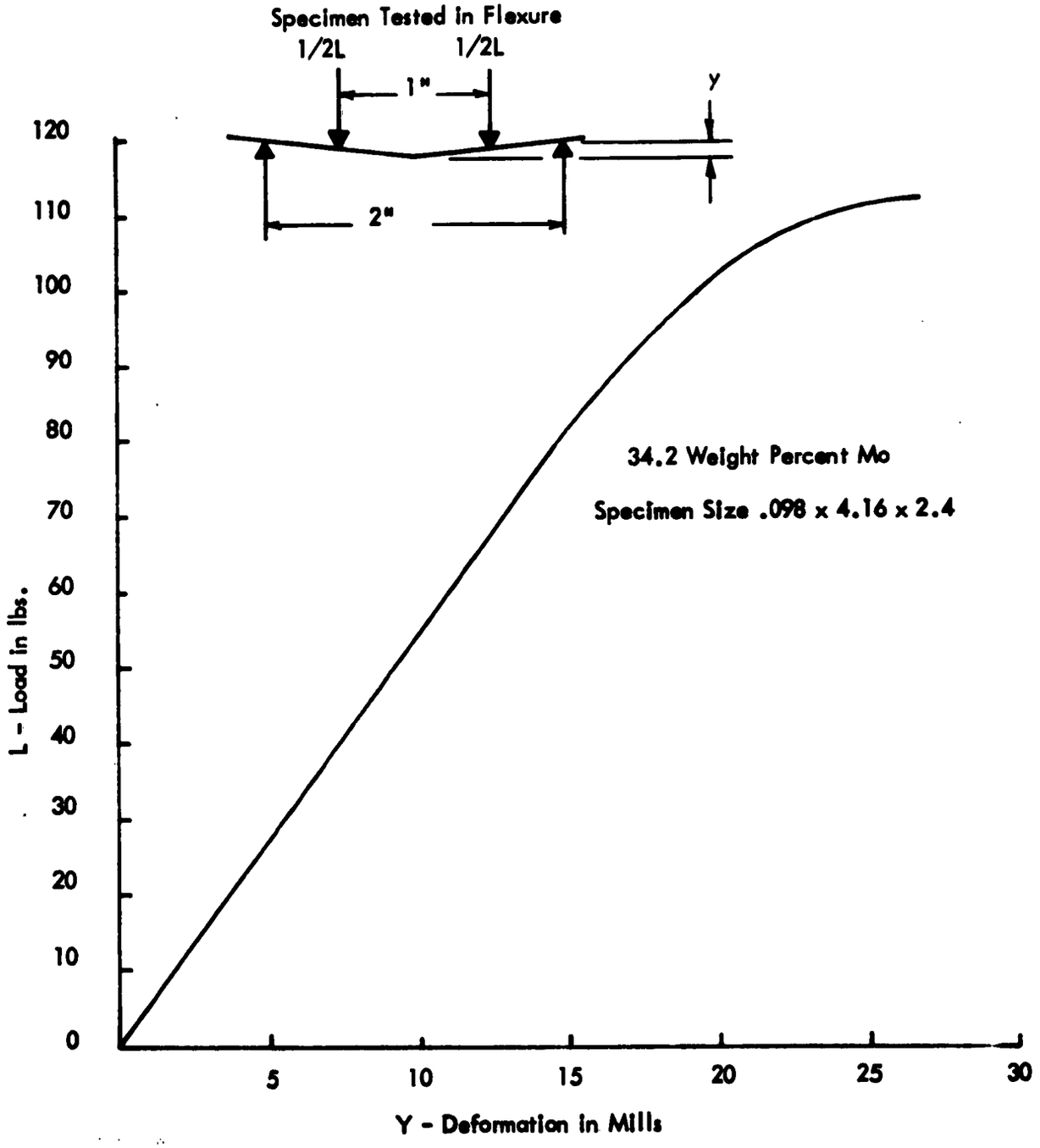

FIGURE 38 - LOAD DEFORMATION CURVE FOR FINAL FLEXURAL TEST SPECIMENS

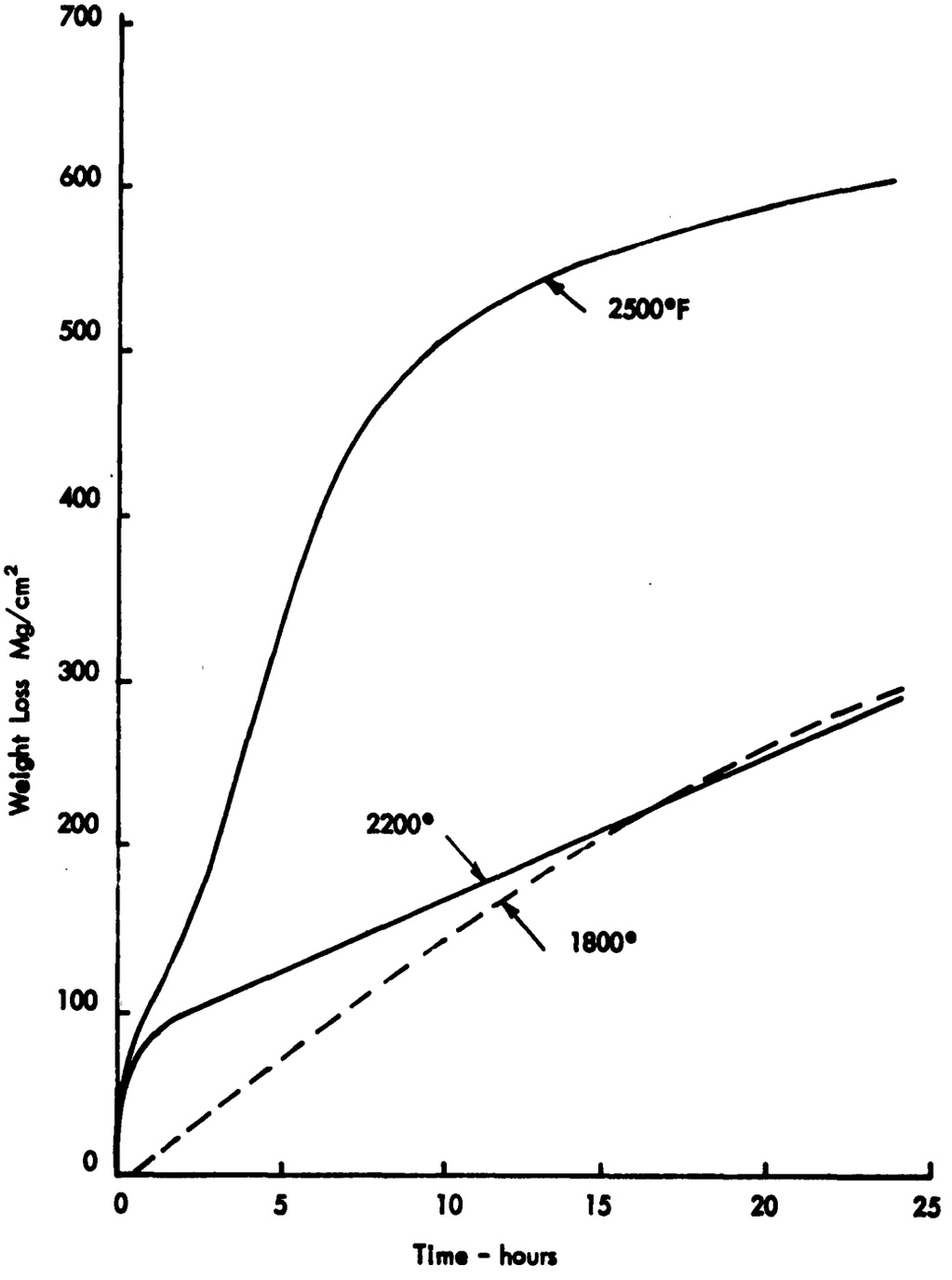

FIGURE 39 - WEIGHT LOSS DUE TO OXIDATION FOR VARIOUS TEMPERATURES AS A FUNCTION OF TIME

TABLE I

PROPERTIES OF 93.1 HfO_2 · 4.9 CeO_2 · 2MgO-Mo MACROLAMINATE COMPOSITE CONTAINING 48 WEIGHT PERCENT CERAMIC, 52 WEIGHT PERCENT METAL

Density	9.2 gm/cm^2
Weight Loss Due to Oxidation	
1 hr. at 2500°F	.07 gm/cm^2
28 hrs. at 2500°F	.25 gm/cm^2
Flexural Strength	
Room Temperature	35,400 psi
2500°F	23,500 psi

TABLE II

LIST OF MATERIALS

Material	Type	Vendor
Hafnia	Reactor Grade II	Wah Chang Corp.
Hafnia	Reactor Grade S	Wah Chang Corp.
Ceria	Reagent Grade	GF Fredericks & Co.
Magnesia	Reagent Grade	Mallenkrodt Chemical Co.
Molybdenum	99.8 Pure Powder	Wah Chang Corp.
Acryloid F10	Commercial Grade	Rohm and Hass Co.
Acryloid B66	Commercial Grade	Rohm and Hass Co.
Acryloid B72	Commercial Grade	Rohm and Hass Co.
Butyl Cellosolve	Commercial Grade	Scientific Supply Co.
Ethyl Cellosolve	Commercial Grade	Scientific Supply Co.
Solvent No. 350	Commercial Grade	Standard Oil Co.
Nuosperse 657	Commercial Grade	Neodex Products Co.
Solvent No. 325	Commercial Grade	Standard Oil Co.
Stoddard Solvent	Commercial Grade	Standard Oil Co.

TABLE III
PAINT FORMULATIONS USED FOR ROLL COATING, SILK SCREENING AND KNIFE COATING

Materials	Roll Coat Paint parts by weight	Silk Screen Paste part by weight	Knife Coat Paint part by weight
METAL PAINT FORMULATIONS			
Molybdenum Powder	88.0	87	87.5
Acryloid B66 40% by weight solids	5.3	--	--
Acryloid F10 40% by weight solids	6.7	12.5	12.5
Butyl Cellosolve	7.5	--	--
Ethyl Cellosolve	38.6	--	--
Nuosperse 657	--	.5	--
Solvent No. 350	--	14.0	11.0
Solvent No. 325	--	--	8.5
Ethyl Alcohol	--	--	2.4
Stoddard Solvent	--	--	.5
CERAMIC PAINT FORMULATIONS			
(HfO_2 - $5CeO_2$)	86.34	85.47	85.75
MgO	1.76	1.53	1.75
Acryloid B66 40% by weight solids	--	--	12.5
Acryloid F10 40% by weight solids	12.0	12.5	--
Solvent No. 350	31.7	6.5	--
Ethyl Cellosolve	--	--	8.0
Butyl Cellosolve	--	--	.8
Nuosperse 657	--	.5	--

TABLE IV
CHEMICAL COMPOSITIONS OF MOLYBDENUM AND HAFNIA POWDERS

		Impurities PPM							
Molybdenum	Lot No.	Al	C	Fe	O	Si	Sn	W	NVM
99.8%	Mo 221	30	41	80	860	150	60	400	200
99.8%	Mo 229		50	30	1200	80	50	100	

		Impurities PPM										
Hafnia *	Lot No.	Al	Cb	Cu	Fe	Mg	Ni	Pb	Si	Ta	Ti	Zr
RG11	90	240	100	40	4200	100	--	50	2500	200	2700	5500
RG11	I-11-A	70	--	40	2400	--	75	--	150	--	250	12,500
RG-S	RX364168	--	100	40	50	--	--	--	40	200	--	8400

* 96% minimum hafnia content

TABLE V

AVERAGE DRY AND FIRED SHRINKAGE FOR DIFFERENT THICKNESSES OF KNIFE COATED LAYERS IN METAL-CERAMIC LAMINATE SHEETS

Paint Type	Knife Distance Above the Bed Mils	Dry Shrinkage %	Fired Shrinkage %	Total Shrinkage %
Metal	1.0	+8.0	27.1	21.0
Mo	1.5	3.3	26.7	29.1
	2.0	28.5	30.3	48.5
	3.0	32.5	29.3	51.3
Ceramic	1.0	+11.0	25.5	14.0
$93.1HfO_2$ ·	1.5	3.3	21.3	25.0
4.9CeO ·	2.0	29.5	22.2	37.5
2MgO	3.0	46.0	27.1	63.7

Note: Dry shrinkage is the difference in dimensions between the knife setting and the film produced after drying divided by knife setting.

Fired shrinkage is the difference in dimensions between the thickness of dryed and fired layers divided by the thickness of dryed layer.

Total shrinkage is the difference in dimensions between the knife setting above the bed and the final sintered dimensions of the layers divided by the knife setting

TABLE VI

PARTICLE SIZE FRACTIONS USED TO FABRICATE COMPOSITE SPECIMENS FOR EVALUATING EFFECTS OF VARYING LAYER THICKNESS IN LAMINATE SHEETS

Mesh Size	Weight Per Cent
-24 + 48	57.5
-48 + 100	22.5
-100 + 200	10.5
-200	9.5

TABLE VII - DIMENSIONAL AND COMPOSITIONAL VARIATIONS IN LAMINATE SHEETS PREPARED BY THE KNIFE COATING PROCESS

Laminate Sheet No.	Average Fired Layer Thickness Mils		Variation in Fired Layer Thickness - Mils				Volume % Metal *	Avg. Fired Shrinkage of Layers in Laminate Sheets - %		Difference In Fired Shrinkage Between the Metal and Ceramic
			Metal		Ceramic					
	Metal	Ceramic	Max.	Min.	Max.	Min.		Metal	Ceramic	
B-1-1	1.6	1.3	1.9	1.2	1.4	.95	55.2	27.3	23.5	3.8
B-1-2	.8	.8	1.0	.5	1.0	.4	53.7	28.2	25.0	3.2
B-2	1.0	1.2	1.3	.9	1.5	1.0	45.5	28.2	29.4	-1.2
B-3	1.0	1.2	1.4	.8	1.4	.8	45.5	37.5	25.0	12.5
B-4	1.6	2.0	2.1	1.2	2.9	1.0	44.4	33.3	20.0	13.3
B-5	4.5	3.6	6.4	2.8	5.7	.7	55.5	29.7	20.0	9.7
B-6	1.1	1.1	1.5	.9	1.4	1.0	50.0	35.3	26.7	8.6
B-7	1.3	1.5	1.6	1.2	1.9	1.2	46.4	23.5	28.6	-5.1
B-8	1.1	1.0	1.5	.9	1.3	.9	52.4	31.3	33.1	-1.8
B-9	1.8	.8	2.5	1.3	1.1	.7	69.0	28.0	31.2	-3.2
B-11	2.0	1.5	2.5	1.9	2.0	1.2	58.3	23.1	25.0	-2.1

* The volume percent metal was determined from optical measurements of the layer thicknesses in the laminates and does not compensate for variations in porosity.

TABLE VIII - PROPERTIES OF SPECIMENS PREPARED FROM LAMINATE SHEETS MADE BY KNIFE COATING HAVING DIMENSIONAL AND COMPOSITIONAL VARIATIONS

Laminate Sheet No.	Fired Shrinkage %	Weight Loss %	Apparent Porosity %	Closed Pores %	Apparent Density gm/cc	% of Theoretical Density	Flexural Strength ksi	Compressive Strength-ksi Yld.	Compressive Strength-ksi Ult.	Compressive Deformation %	Weight Loss Due to Oxidation mg/cm^2
B-1-1	17.2	8.5	1.5	2.8	9.40	95.7	63.0	51.1	111.1	7.9	820
B-1-2	17.5	7.6	4.3	2.2	9.14	93.5	80.0	77.6	128.3	5.8	734
B-2	16.7	7.8	5.2	4.1	8.91	90.7	39.8	79.1	124.6	5.7	580
B-3	17.6	8.2	1.5	4.8	9.20	93.7	55.9	65.3	123.5	7.9	753
B-4	16.9	7.7	1.8	4.4	9.21	93.8	50.3	71.6	122.7	7.5	661
B-5	16.5	8.1	2.2	6.6	8.85	90.2	44.3	62.6	93.4	4.8	508
B-6	16.8	7.3	3.3	4.4	9.17	92.3	60.4	74.5	126.2	6.9	262
B-7	15.3	6.8	1.9	12.2	8.44	85.9	25.6	106.2	156.2	5.4	232
B-8	17.5	7.1	.8	4.8	9.42	96.4	40.2	69.6	129.7	10.0	943
B-9	16.2	6.5	.8	8.6	8.98	90.6	27.5	74.4	147.6	14.3	874
B-11	17.0	7.1	.8	2.1	9.55	97.1	35.0	55.8	115.2	8.8	735

* Specimens exposed to 2500°F in Air for 24 Hours

TABLE IX

PARTICLE COMPOSITIONS OF SPECIMENS FABRICATED FOR PARTICLE SIZE AND SHAPE STUDIES

	Mesh Size - % by Weight				
Composition	-14 +20	-20 +48	-48 +100	-100 +200	-200
-14	52	--	21.4	13.3	13.3
-20	--	52.0	21.4	13.3	13.3
-48	--	--	44.0	28.0	28.0
-100	--	--	--	50.0	50.0

TABLE X - PROPERTIES OF 93.1 HfO_2 · 4.9 CeO_2 · 2 MgO-Mo MACROLAMINATE COMPOSITES FABRICATED USING DIFFERENT PARTICLE SIZES

Particle[1] Size Mesh	Fired Shrinkage %	Density gm/cc	Apparent Porosity %	Flexural Strength ksi	Compressive Yld. Str. ksi	Compressive Deformation %	Weight[2] Loss Due To Oxidation mg/cm^2
-14+20	15.2	8.97	1.9	29.6	96.8	7.4	664
-20+48	15.2	8.91	1.4	32.9	97.6	7.6	605
-48+100	14.8	8.87	1.7	37.4	103.4	6.7	523
-100+200	14.6	8.82	1.9	39.3	121.8	6.1	391
-200	16.4	8.91	1.3	59.8	111.1	6.9	779
-14 Comp.[3]	15.3	9.20	2.9	30.3	115.5	7.1	648
-20 Comp.[3]	15.1	8.90	2.8	33.7	108.6	6.9	623
-48 Comp.[3]	15.1	8.97	1.5	40.0	107.5	6.8	566
-100 Comp.[3]	15.4	9.05	1.3	46.3	130.9	6.5	553

1 All particles were cut from .018 inch thick laminate sheet.

2 Weight loss due to oxidation was measured from specimens exposed to 2500°F in air for 24 hours.

3 Table IX lists the grain composition used.

TABLE XI

PROPERTIES OF 93.1 HfO_2 · 4.9 CeO_2 · 2 MgO-Mo MACROLAMINATE PARTICLE COMPOSITE SPECIMENS MADE FROM DIFFERENT PARTICLE SHAPES

Particle Shape	Laminate Sheet Thickness (mils)	Particle Size Mesh	Final Shrinkage (%)	App. Porosity (%)	App. Density (gm/cc^2)	Flexural Strength (ksi)	Comp. Yld. Str. (ksi)	Weight Loss Due to Oxidation After 24 hrs at 2500°F (mg/cm^2)
Plate-like	6	-20	15.9	4.2	8.81	25.5	79.3	632
Rectangular Cross Section One Axis Shortened	12	-20	15.5	5.1	8.70	24.8	133.6	518
Cubical	18	-20	15.7	3.1	8.85	25.2	138.6	424
Rectangular Cross Section One Axis Elongated	36	-20	15.7	1.1	9.10	32.8	131.1	541
Plate-like	6	-20 +48	15.3	5.4	8.83	27.0	72.3	650
Rectangular Cross Section One Axis Shortened	12	-20 +48	15.3	3.1	8.80	25.1	143.7	491
Cubical	18	-20 +48	15.5	4.2	8.81	24.7	124.2	501
Rectangular Cross Section One Axis Elongated	36	-20 +48	15.2	.6	9.07	30.4	129.8	539

TABLE XII

SINTERED PROPERTIES OF MACROLAMINATE COMPOSITE SPECIMENS FABRICATED TO EVALUATE WARM PRESSING PARAMETERS

Forming Pressure ksi	Forming Temp. °F	Appr. Density gm/cc	Flexural Strength ksi	Linear Fired Shrinkage %	Fracture Type*
20	100	9.25	50.3	15.37	B
20	150	8.97	54.0	14.97	B
20	300	9.34	51.4	14.38	C
20	350	9.23	50.3	13.79	A
20	400	9.31	42.6	14.21	B
50	200	9.31	-	12.80	B
40	200	9.06	45.9	13.10	B
10	100	9.26	49.8	14.95	A
10	100	9.31	48.9	15.07	A
10	200	9.47	48.7	14.97	A
10	200	9.46	53.1	15.18	AC
10	300	9.36	49.3	14.82	CA
10	300	9.32	51.4	15.04	CA
22.5	100	9.22	47.3	13.79	B
22.5	100	9.23	45.6	13.56	B
22.5	200	9.21	44.9	13.75	C
22.5	200	9.38	40.4	14.03	C
22.5	300	9.32	46.6	14.15	C
22.5	300	9.34	45.3	13.77	C
35	100	9.03	33.7	13.18	B
35	100	8.92	38.8	13.21	B
35	200	9.16	38.7	13.32	BC
35	200	9.06	36.9	13.14	BC
35	300	8.65	42.1	13.45	BC
35	300	9.26	38.9	13.50	C

*Letters relate to fracture types shown in Figure 23

TABLE XIII
PROPERTIES OF 93.1 HfO_2 · 4.9 CeO_2 · 2 MgO-Mo MACROLAMINATE PARTICLE COMPOSITES PREPARED BY HOT PRESSING

Specimen Code No.	Hot Pressing Temperature °F	Time at Temp. min.	Flexural Strength		Density	
			As Pressed [1] ksi	Post-Heat-Treated [2,3] ksi	As Pressed gm/cc	Post-Heat-Treated [3] gm/cc
BGH 1	2400	60	21.8	44.7	8.87	8.85
BGH 2	2500	60	43.3	41.3	9.29	9.33
BGH 3	2600	60	42.4	55.2	9.30	9.26
BGH 4	2700	60	32.6	47.4	9.37	9.40
BGH 5	2800	60	Specimen broken due to adherence to the graphite die			
BGH 6	2500	30	41.0	49.3	9.21	9.40
BGH 7	2500	120	34.0	34.6	9.32	9.33

1 Specimens tested on a 2 inch span using 4 point loading.
2 Specimens tested on a 1 inch span using center point loading.
3 See Figure 25 for the time-temperature cycle used for post-heat-treating specimens.

TABLE XIV
PROPERTIES OF MACROLAMINATE COMPOSITE SPECIMENS SINTERED USING VARIOUS ATMOSPHERES

Atmosphere	Flexural Strength ksi	App. Density gm/cc	App. Porosity %	Linear Fired Shrinkage %
Argon	49.1	9.33	.0	15.0
Argon	53.5	9.50	.0	14.9
Argon	50.7	9.45	.0	15.2
Hydrogen [1]	50.8	9.28	.0	15.2
Hydrogen [1]	65.0	9.59	.0	14.7
Hydrogen [1]	55.2	9.46	.0	15.2
Hydrogen [2]	33.7	9.42	.0	15.0
Hydrogen [2]	39.5	9.25	.0	15.0
Hydrogen [2]	33.7	9.02	1.9	15.1
Vacuum [3]	55.7	8.81	5.1	13.7
Vacuum [3]	48.8	8.75	5.2	13.5
Vacuum [3]	48.6	9.18	.0	13.4

1 Hydrogen as-purchased.
2 Hydrogen dryed and purified by passing it through a liquid nitrogen freeze trap.
3 Vacuum 1×10^{-4} Torr.

TABLE XV
PROPERTIES OF MOLYBDENUM SINTERED USING VARIOUS ATMOSPHERES

Atmosphere	Flexural Yield Strength ksi	Deformation inches	App. Density gm/cc	App. Porosity %	Linear Fired Shrinkage %
Argon	114.0	.00	9.24	5.4	18.4
Hydrogen [1]	66.6	.020	9.73	0.0	20.4
Hydrogen [2]	75.0	.063	9.61	0.0	20.5
Vacuum [3]	65.5	.313	9.66	0.0	20.4

1 Hydrogen as-purchased.
2 Hydrogen dryed and purified by passing it through a liquid nitrogen freeze trap.
3 Vacuum 1×10^{-4} Torr.

TABLE XVI
PROPERTIES OF 93.1 HfO_2 · 4.9 CeO_2 · 2 MgO CERAMIC SINTERED USING VARIOUS ATMOSPHERES

Atmosphere	Flexural Strength ksi	App. Density gm/cc	App. Porosity %	Linear Fired Shrinkage %
Argon	12.7	8.28	0.0	13.9
Hydrogen [1]	11.8	7.90	1.4	12.4
Hydrogen [2]	+	8.23	6.8	-
Vacuum [3]	+	-	-	-

1 Hydrogen as-purchased
2 Hydrogen dryed and purified by passing it through a liquid nitrogen freeze trap.
3 Vacuum 1×10^{-4} Torr
+ Specimens broke in several pieces during grinding.

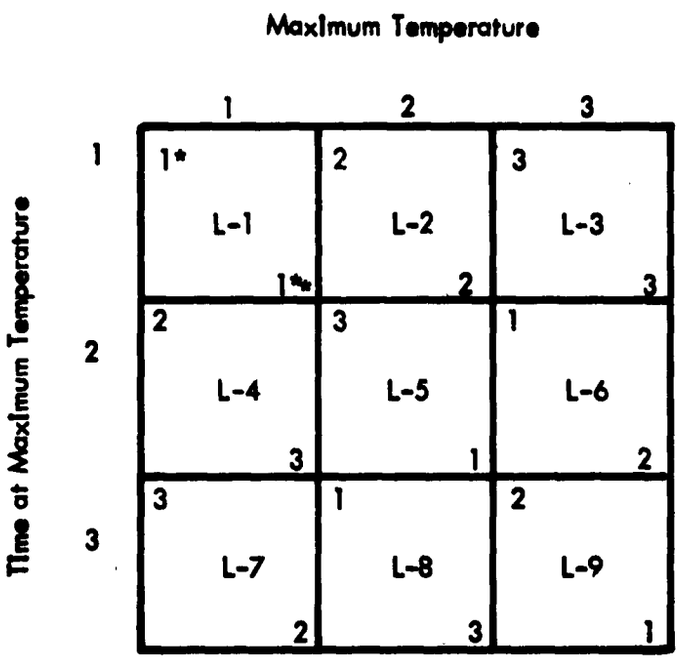

* Heating rate
** Cooling rate

	Variables			
Level	Temp.	Time	Heating Rate	Cooling Rate
High	1 - 3400°F	1 - 12 hrs.	2 - 700 °F/hr.	1 - 700 °F/hr.
Medium	2 - 3300°F	2 - 6 hrs.	3 - 400 °F/hr.	3 - 400 °F/hr.
Low	3 - 3200°F	3 - 0 hrs.	1 - 100° F/hr.	2 - 100 °F/hr.

Numbers chosen from a 10 digit random number table used to establish experimental conditions. For Square A, use the highest temperature level, longest time at maximum temperature, slowest heating rate and fastest cooling rate. For Square B, use medium temperature level, longest time at maximum temperature, fastest heating rate and slowest cooling rate.....etc.

TABLE XVII GRECO LATIN SQUARE DESIGN FOR SINTERING STUDY

TABLE XVIII

PROPERTIES OF 93.1 HfO_2 · 4.9 CeO_2 · 2 MgO–Mo MACROLAMINATE PARTICLE COMPOSITE SPECIMENS PREPARED FOR EVALUATION OF SINTERING PARAMETERS

Cycle No.	Heating Rate °F/Hr.	Temp. °F	Time at Temp hrs.	Cooling Rate °F/hr.	Specimen Number	Density gm/cc	App. Porosity %	Fired Shrink. % Linear	Flexural Properties Yld. Str. ksi	Flexural Properties Ult. Str. ksi
L-1	100	3400	12	700	B77	9.10	1.0	14.4	--	47.8
					B78	8.96	4.1	14.9	--	44.0
					B79	9.44	1.6	14.5	--	47.0
L-2	700	3300	12	100	B80	9.28	1.5	13.9	41.6	49.6
					B81	9.18	2.8	13.8	46.2	50.9
					B82	8.78	6.4	14.2	42.0	49.9
L-3	400	3200	12	400	B74	8.64	8.2	13.5	52.9	61.9
					B75	8.92	4.9	13.6	53.5	59.5
					B76	8.77	5.8	13.5	46.5	52.9
L-4	700	3400	6	400	B65	9.18	2.8	13.7	38.2	45.5
					B66	8.95	4.2	14.0	33.6	41.5
					B67	8.97	5.2	13.7	38.2	48.2
L-5	400	3300	6	700	B62	8.98	2.1	14.0	47.7	49.2
					B63	9.14	3.5	13.8	44.4	46.5
					B64	9.04	5.2	13.7	--	37.5
L-6	100	3200	6	100	B71	8.78	6.5	14.0	--	40.1
					B72	8.68	7.3	13.9	--	41.5
					B73	8.92	5.8	13.9	--	45.5

TABLE XVIII (CONTINUED)

Cycle No.	Heating Rate °F/Hr.	Temp. °F	Time at Temp hrs.	Cooling Rate °F/hr.	Specimen Number	Density gm/cc	App. Porosity %	Fired Shrink. % Linear	Flexural Properties Yld. Str. ksi	Flexural Properties Ult. Str. ksi
					B59	9.19	4.5	13.4	47.3	49.5
L-7	400	3400	0	100	B60 [2]	8.84	5.4	13.4	42.4	46.3
					B61 [2]	8.86	3.9	13.5	--	--
					B68	8.51	10.8	14.2	--	39.5
L-8	100	3300	0	400	B69	8.57	7.9	14.2	--	37.2
					B70	8.57	8.4	14.0	--	40.6
					B56	8.52	10.8	12.0	39.0	43.2
L-9	700	3200	0	700	B57	8.30	10.5	12.3	40.0	44.4
					B58	8.23	14.1	12.5	--	34.5
					B84	9.08	1.4	14.0	43.9	45.9
L-5	400	3300	6	700	B85	8.98	3.4	13.7	41.0	44.1
					B86	9.20	0.0	14.1	39.1	43.4

[1] Yield strength is determined from load deformation curves based on the proportional limit of the material. The dash line indicates the specimen broke prior to reaching a nonlinear point in the deformation curve.

[2] Specimen broke during grinding.

TABLE XIX
PROPERTIES OF MOLYBDENUM[1] SPECIMENS PREPARED FOR EVALUATION OF SINTERING PARAMETERS

Cycle No.[2]	Specimen No.	Density	App. Porosity	Fired Shrink.	Flexural Yld. Str. ksi	Relative Ductility Ranking 1-9[3]
L-1	BM-17	9.77	0	18.7	61.3	5
L-2	BM-18	9.80	0	19.6	52.4	6
L-3	BM-16	9.57	0	19.6	101.0	7
L-4	BM-13	9.52	0	19.8	62.0	1
L-5	BM-12	9.63	0	19.5	64.0	2
L-6	BM-15	9.42	5.4	18.9	102.0	9
L-7	BM-11	9.45	.8	18.3	90.3	8
L-8	BM-14	8.96	8.1	18.2	104.0	3
L-9	BM-10	8.38	18.5	15.6	109.0	4

1 Molybdenum contaminated during fabrication with 93.1 HfO_2 · 4.9 CeO_2 · 2 MgO
2 See Table XVIII for sintering parameters which correspond to the cycle number.
3 Deformation in specimens varied from less than .005 to greater than .200 inches. Due to range changes total deflection was not accurately measured for a number of specimens thus they were ranked from 1-9 with 1 being the most ductile specimen and 9 the least ductile.

TABLE XX

PROPERTIES OF VACUUM SINTERED 93.1 HfO_2 · 4.9 CeO_2 · 2 MgO–Mo MACROLAMINATE PARTICLE COMPOSITES MADE FROM DIFFERENT LOTS OF HAFNIA

Specimen Code No.	Hafnia Grade and Lot No.	Organic Burn Out Cycle [1]	Flexural Strength ksi [2]	Density gm/cc	Apparent Porosity %	Linear Fired Shrinkage %	Weight Loss During Firing
B 83 [3]	RG11 Lot 90	3	44.3	9.52	.3	14.5	7.2
B 84 [3]	RG11 Lot 90	3	43.8	9.46	.3	15.0	7.2
B 85 [3]	RG11 Lot 90	2	38.3	9.40	.3	14.2	6.6
B 86 [3]	RG11 Lot 90	2	45.3	9.36	.9	14.7	6.8
BG 195	RGS LotRX364168	2	33.3	0.12	.5	15.2	6.2
BG 196	RGS LotRX364168	2	38.6	9.20	.8	14.5	6.2
BG 197	RGS LotRX364168	3	31.7	9.24	.5	14.0	6.1
BG 198	RGS LotRX364168	3	36.8	9.33	.4	14.1	6.1
BG 205	RG11 Lot 1-11-A	2	40.8	9.11	0	14.6	6.7
BG 206	RG11 Lot 1-11-A	2	40.8	9.24	.3	14.9	6.5
BG 213	RG11 Lot 1-11-A	3	32.1	9.11	0	14.7	6.5
BG 214	RG11 Lot 1-11-A	3	37.2	9.06	0	14.6	6.6

1 Cycles shown in Figure 6.

2 All specimens broken using four point loading except No. B 85 which was broken using center point loading.

3 Specimens made from the original lot of macrolaminate particles prepared by roll coating used in the warm pressing and sintering studies.

APPENDIX

Test Procedures

Bulk Density - Density measurements were made using emersion techniques. Specimens were saturated by boiling in a liquid media for 2 hours. Calculations were based on the formula:

$$Db = \frac{W}{Wx - Wy} K$$

Where: Db = Bulk density

W = Weight of specimen

Wx = Weight of specimen saturated with liquid

Wy = Weight of saturated specimen suspended in liquid

K = Specific gravity of liquid (both water and kerosene were used at different times as the liquid).

Apparent Porosity - Apparent porosity was determined using measurements of liquid absorbed and bulk volume of specimens obtained while determining bulk density. Calculations were based on the following formula:

$$\% \text{ Apparent porosity} = \frac{Wx - W}{Wx - Wy} \cdot 100$$

Flexural Strength - Flexural strength was measured on bar specimens with a rectangular cross section prepared by diamond surface grinding and hand polishing on 600 grit silicon carbide paper. Four point loading using the fixture shown in Figure 40 was used for all specimens except when noted differently in the text. The fixture used is self contained so that upper load points are centered with the bottom points. The distance between the upper and bottom load points are fixed at 1 and 2 inches, respectively, producing a gage section of 1 inch in the test bar which is nominally 2.3 inches long. Width and thickness measurements varied due to differences in fired shrinkage and the amount of material that had to be removed to achieve parallel sides. The fixture is designed so that load points can rotate in any direction to compensate for any lack of parallelism in the ground specimens. The fixture is used in a Tinius Olsen test machine with ranges from 120 to 12,000 lbs of load. Head travel was constant at .05 inches per minute. Load deformation curves were obtained by measuring head travel using a Tinius

Olsen Model D-2 deflectometer. Values were calculated using the formula

$$F = \frac{3La}{bd^2}$$

Where: F = Flexural strength, psi

L = Load, lbs

a = Distance from point of load to point of reaction, inches

b = Specimen width, inches

d = Specimen depth, inches

Compression Testing - Compression tests were conducted on right circular cylindrical specimens approximately .3 inch diameter by .6 inch height prepared by a centerless grinding and trueing the ends to be flat and parallel to .0005 inches. Aluminum oxide cylinders 1 inch in diameter were used as hard facing material with a spherically seated head. The same test equipment was used as described for flexural testing.

Tensile Testing - Tensile tests were conducted on specimens of the configuration shown in Figure 41 using a Baldwin Lima Hamilton PTE Universal Test Machine. Strain was measured using Baldwin Model No. TSM-D1 microformer type extensometer and the strain rate was held constant at .005 in/in/min, using a strain rate pacer.

Oxidation Testing - Oxidation testing for comparing series of specimens was conducted using right circular cylinders approximately .5 inches in diameter by .4 inches in height. The whole series would be placed in the hot furnace and held for 24 hours. Specimens were supported on zirconium oxide rods, laying to provide horizontal rails, allowing air to pass completely around the specimens except at the tangent intersection. Some discoloration of the zirconia indicated diffusion from the specimen to zirconia. Weight loss was reported as the change in weight divided by the original surface area. Weight loss as a function of time was measured directly from specimens hung from a balance in a platinum basket in a vertical tube furnace.

Thermal Expansion - Thermal expansion was measured in a resistance heated tube furnace under an argon atmosphere, heating the specimen at a rate of 7°F per minute. The expansion of the specimen was transmitted to a linear variable differential transformer through a fused silica extension rod. The output from the transformer is fed into the Y axis of a function plotter while the specimen temperature is simultaneously recorded on the X axis.

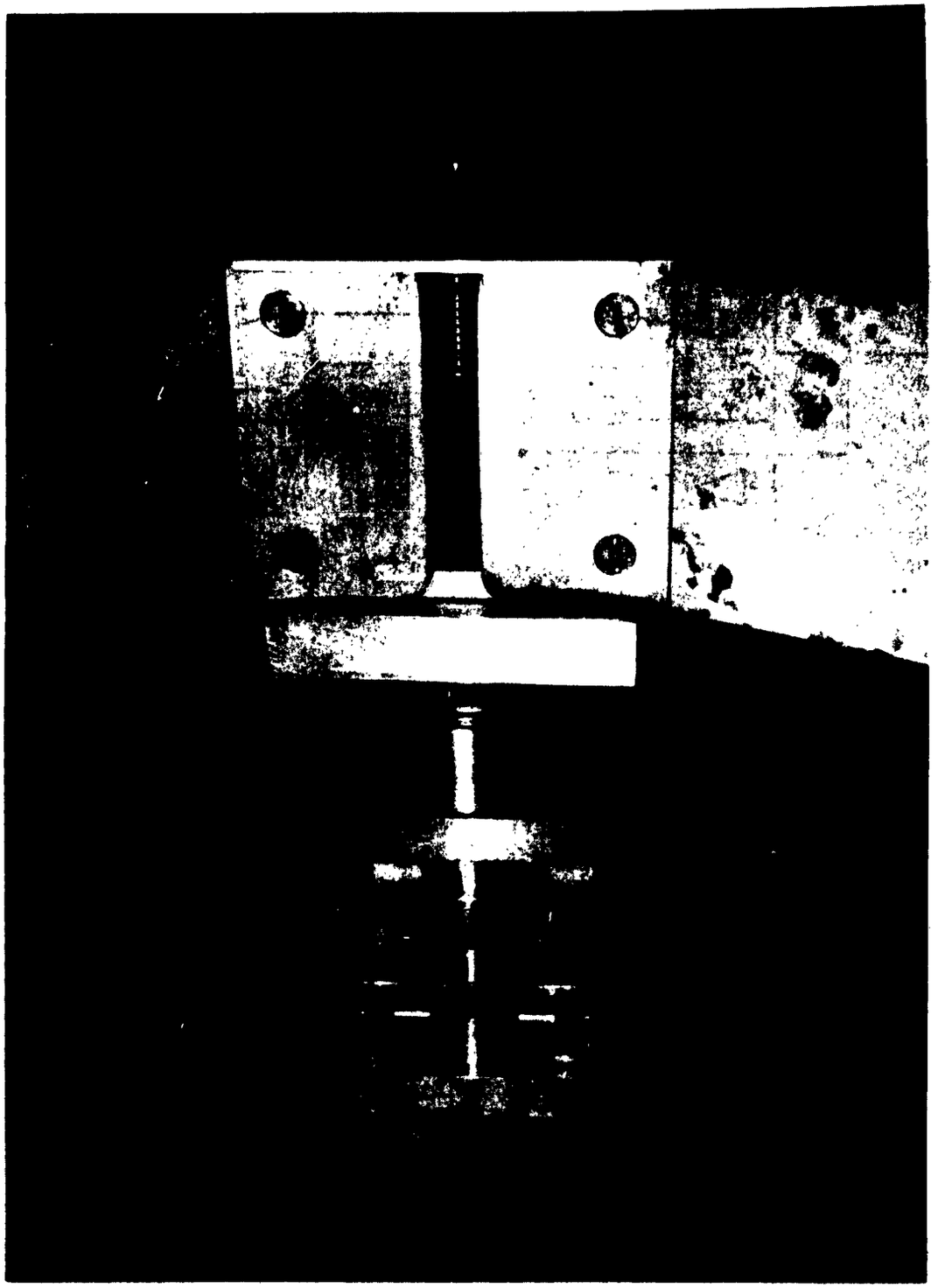

FIGURE 40 FOUR POINT FLEXURAL TEST FIXTURE

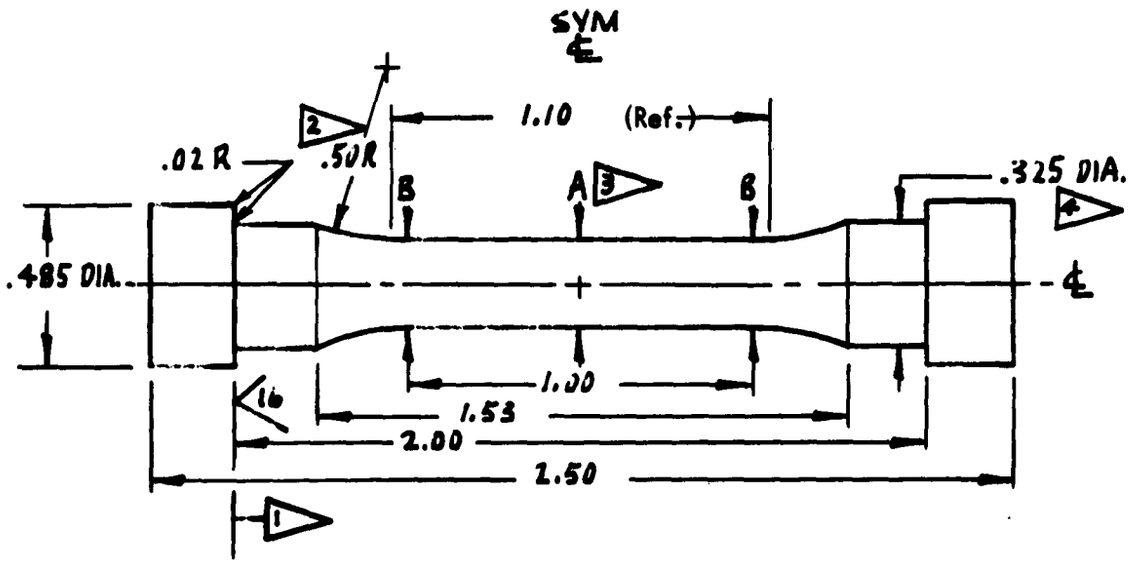

MATERIAL PER SHOP ORDER
TOL NOT NOTED ± .03

4 THESE SURFACES TO BE CONCENTRIC TO LONGITUDINAL & WITHIN .0005 T.I.R.

3 B DIA TO DECREASE UNIFORMLY INTO A DIA

A .250 MAX. .247 MIN.
B A + .003 TO + .005

2 FILLET RADIUS TO FAIR SMOOTHLY INTO REDUCED SECT.

1 THESE SURFACES TO BE PARALLEL TO EACH OTHER AND ⊥ TO LONGITUDINAL & WITHIN .001 T.I.R.

FIGURE 41 - BUTTON HEAD TENSILE TEST SPECIMEN

Distribution List - Contract NOw 64-0194-f

1 Bureau of Naval Weapons
Department of the Navy
Washington, D C 20025
Attn: DLI-31 For internal distribution as follows:
DLI - 31 (14 copies)
RRMA-23 (3 copies plus remainder after distribution)
RAPP-14 (1 copy)

2. Bureau of Ships
Department of the Navy
Washington, D. C. 20025
Attn: Code 342B

3. Office of Naval Research
Department of the Navy
Washington, D. C. 20025
Attn: Code 423

4. Naval Air Engineering Center
Aeronautical Materials Laboratory
Philadelphia, Pennsylvania 19112

5. Air Force Materials Laboratory
Wright-Patterson Air Force Base, Ohio 45433
Attn: Code MANC (1 copy)
MAMP (1 copy)
MAMC (Mr. Clarence Pratt Jr.) (1 copy)

6 National Aeronautics and Space Administration
1520 H Street N.W
Washington, D C. 20025
Attn: OART Code RRM

7 Technical Information Service Extension
U S. Atomic Energy Commission
P O. Box 62
Oak Ridge, Tennessee 37830

8. Director
National Bureau of Standards
Washington, D C. 20025

9. Commanding Officer
Office of Ordnance Research
Box CM, Duke Station
Durham, North Carolina 27706

10. Army Materials Research Agency
Watertown Arsenal
Watertown, Massachusetts 02172

11. U. S. Atomic Energy Commission
Document Library
Germantown, Maryland 20767

12. Battelle Memorial Institute
505 King Avenue
Columbus, Ohio 43201
Attn: Defense Metals Information Center

13. Army Material Command
Washington, D. C. 20025
Attn: OR-TB

14. U S. Naval Research Laboratory
Washington, D. C. 20025

15. U S. Naval Ordnance Laboratory
White Oak, Silver Spring
Maryland 20900
Attn: WM Division

16. U.S.A. Transportation Research Command
Ft. Eustace, Virginia 23604
Attn: Mr. John W. White, Aeronautical Propulsion Group

17. Advanced Engine & Technology Department
General Electric Co.
Cincinnati 15, Ohio
Attn: L. P. Jahnke, Manager, Materials Development Laboratory

18. National Aeronautics and Space Administration
Langley Research Center
Langley Station
Hampton, Virginia 23365
Attn: Technical Library

19. P. R. Mallory Co., Inc.
Indianapolis 6, Indiana
Attn: A. S. Doty

20. State University of New York
College of Ceramics
Alfred University
Alfred, New York

21. W. J. Knapp
Professor of Engineering
University of California
Los Angeles, California

22. Commanding Officer
U. S. Naval Air Development Center
Johnsville, Pennsylvania
Attn: ELCH

23. National Aeronautics and Space Administration
Lewis Research Center
21000 Brookpark Road
Cleveland, Ohio 44135
Attn: Library